UNIVERSITÀ DEGLI STUDI DI MILANO
Dipartimento di Bioscienze

SCUOLA DI DOTTORATO

TERRA, AMBIENTE E BIODIVERSITÀ

Dottorato di Ricerca in Biologia Animale
Ciclo XXVI

Coordination phenomena in the marine demosponge *Chondrosia reniformis*:

physiological, morphological, biomechanical and biochemical aspects.

PhD Thesis

Fassini Dario
R08981

PhD tutors: **Prof. Francesco Bonasoro**

Prof.ssa Maria Daniela Candia Carnevali

PhD coordinator: **Prof. Marco Ferraguti**

Academic Year

2012-2013

Index

Abstract

Although sponges (phylum Porifera) are still often considered to be simple, inactive animals, both larvae and adults of different species show clear coordination phenomena triggered by both extrinsic and intrinsic stimuli. Moreover although sponges lack a nervous system, they show a range of behavioural responses that are affected by exogenously applied neuroactive compounds. *Chondrosia reniformis* (Nardo, 1847), a common Mediterranean demosponge, lacks both endogenous siliceous spicules and reinforcing spongin fibers and has a very conspicuous collagenous mesohyl mainly composed of collagen. This sponge can react to different stimuli by changing its tensile state: it can rapidly stiffen after mechanical or chemical stimulation or destiffen and, following accidental detachment of the substrate, produce long slender outgrowths.

These phenomena involve different responses induced by different external events, but both have been attributed to alteration, under cellular control, of the interactions between the collagen fibrils of the mesohyl. The ability to regulate the viscoelastic properties of the connective tissue matrix is a well-investigated phenomenon in other animal phyla, particularly the Echinodermata in which the mechanical, morphological and molecular aspects of mutable collagenous tissues (MCTs) have been extensively analysed.

The present work was intended to investigate the coordinated phenomena of the sponge *C. reniformis* with an integrated approach that includes: physiology, histology, biomechanics and biochemistry. We focused our attention on different aspects: namely, 1) the reaction to mechanical stimulation; 2) the mesohyl mechanical properties; 3) the possible presence of contraction/expansion events; 4) the role of γ-amino butyric acid and glutamate; 5) the presumptive factor(s) that regulates the sponge tensility.

Our results demonstrate that the stiffening reaction that follows mechanical stimulation consists of a passive shrinkage and an active stiffening of the mesohyl given by modification of the ECM mechanical properties and possibly involving the contraction of the canal system. In fact our experiments reveal that the passive compression involves mainly the canal system and the volume recovery occurs when the stiffening effect fade. A significant tensility difference is present between undisturbed and stimulated sponges and evidences on the presence of signal transmission that requires a continuous exopinacoderm (outer epithelium) are reported.

This thesis provides information on different mechanical parameters: namely, viscosity, stiffness, breaking strain and breaking stress. As far as recovery process is concerned we suggest that the sponge shape and volume recovery are given by the striking mechanical behaviour of its mesohyl that shows unusual elastic properties.

By means of digital time lapses movie we confirm the presence and describe the pattern of contraction/expansion cycles occurring in *C. reniformis*. Contrary to other species our animal model does not display stereotypical contractions and lacks a clear contraction periodicity.

Both glutamate (Glu) and γ-amino butyric acid (GABA) are present in different cell phenotypes. Different experiments suggest that, despite the capability of the two substances to slightly increase sponge viscosity, both GABA and Glu seem to be not involved in the regulation of the stiffening phenomenon and in the recovery process that allows the sponge to return to its original shape and volume. On the other hand the two substances, as demonstrated in other sponges, are able to induce contraction events. There are no differences between the two molecules when comparing the contraction magnitude; however our biomechanical approach highlights significant differences in the forces generated during the contractions, in particular Glu generates higher force than GABA. We hypothesize that the two molecules act on different effectors that produced similar effects though different mechanisms.

Finally we demonstrate that at least one protein is responsible of the stiffening of the sponge mesohyl by interacting with collagen fibrils.

Introduction

The poriferans, commonly named sponges, are generally regarded as rather simple multicellular organisms; these animals live in different freshwater and seawater environments and are still considered the most ancient metazoan phylum. In the last years the interest in sponge biology has suddenly increased due to the discovery of numerous molecules with interesting applied pharmacological effects (Faulkner, 2000; Laport et al., 2009), the complete sequencing of *Amphimedon qeenslandica* genome (Srivastava et al., 2010) and the application of new genetic tools for phylogenetic researches.

A more specialistic, but nevertheless very intriguing, hot topic is related to new data concerning the coordinated phenomena modulated by neuro-active compounds (see Nickel, 2010 for a detailed review).

Indeed, the widespread idea that sponges, due to their apparent structural simplicity, are not able to react to external stimuli has been contradicted by numerous evidences (Ellwanger & Nickel, 2006; Leys & Meech, 2009).

Aim of the present work is to explore the complex aspect of the coordinated phenomena displayed by the marine sponge *Chondrosia reniformis* (Nardo, 1847).

1.1 Overview on sponges

Poriferans are the oldest metazoans, early separated from the other metazoans groups (eumetazoans). Sponges occupy different marine and freshwater ecosystems being present in all seas and in many lakes and rivers. Most of the species live on the continental platforms, however some species live on the abyssal plane at more than 6000 m depth (Simpson, 1984).

The general anatomy of filter-feeding sponges is characterized by the presence of a complex network of canals, called aquiferous system. Though the canals a flow of water and food, mainly composed of bacteria and small organic particles, guarantees the food intake and the elimination of catabolites. Specialized cells, the choanocytes, generate and efficiently maintain the water flow and are responsible for the capture of the food particles. The inner water flow is also important in term of oxygen supply, gametes capture and spawning. Sponge can filter water with high efficiency and in some specific environment they can change the nanoplancton composition or be responsible for the changes in the water column chemical composition. In fact large sponges can filter their own volume of water every 10/20 seconds (Brusca & Brusca, 2002) and some species can trap roughly 90% of all the bacteria and remove from the water an average of 10% of the dissolved organic carbon (DOC) in a single passage through the water canal system (Yahel et al., 2003; Milanese et al., 2003).

In the polar ecosystems sponges can constitute most of the sessile animal biomass; in these peculiar environments sponges create a suitable substrate or shelter for many other vertebrates and

invertebrates species (Simpson, 1984). On the other hand sponges of the *Clionidae* family have and important role in the shaping of coral reefs (Barnes & Hughes, 1990).

A wide range of shapes, colours and size are present in the Porifera phylum. This variability is often found within the same species according to the environmental conditions; namely, water current speed and direction, turbidity and light exposure. If the shape is mainly given by the water current direction and intensity, colours vary according to the presence/absence of light that regulates the production of melanic pigments and the presence/absence of symbiotic algae and/or autotrophic bacteria. Size of specimens can vary from few mm in the *Clionidae* family to more than one meter as in the case of the genus *Xestospongia* (McMurray et al., 2010).

Adult specimens are sessile and live all their life on the same substrate. On the other hand during the larval stage the sponges can swim or crawl in order to increase the dispersion or to found their suitable substrate for growing (Bond & Harris, 1988; Bond, 1992; Pronzato, 2004).

Sponges are generally dioecious but can there are also hermaphrodites; although sexual reproduction occurs in most species, reproduction can be also assured by asexual events through budding events, formation of gemmules, or sponge fragmentation (Sara & Vacelet, 1973). During sexual reproduction male gametes are released in the aquiferous system and released from the osculum; fecundation generally occurs internally to another specimen: here sperm is captured by a choanocyte that evolves into an amebocyte and then transfers the captured gamete to the egg cell. To avoid self-fecundation the gametes production, in the hermaphroditic species, does not occur simultaneously.

Except for the free-swimming larval stage, which can actively moves by cilia, most sponges spend their whole adult life anchored to an appropriate substratum.

The body plan of sponges is organized around the aquiferous system that can assume three different conformations: asconoid, syconoid and leuconoid.

Asconoid sponges are tubular in shape, with a single, wide central chamber (spongocoel). The beating of choanocyte flagella forces water into the spongocoel through inhalant pores in the body wall. Choanocytes line all the spongocoel and filter the water capturing the nutrients. This conformation is the simplest models and is characterized by a low filtering efficiency. Asconoid sponges are smaller than other sponges and have a low filtering surface/body volume ratio.

Syconoid sponges are rather similar to asconoids. They have a tubular body with a single osculum, but the body wall is thicker and more complex than that of asconoids and contains choanocyte-lined radial canals that empty into the spongocoel. Water enters through a number of external ostia into incurrent canals and then passes through tiny openings (prosopyles) into the radial canals. Syconoids do not usually form highly branched colonies as asconoids do. The first stage of their development is chacterized by an asconoid stage.

Leuconoid sponges lack a significant spongocoel, their body wall being very thick and complex an containing a number of choanocytes chambers. Water enters through numerous inhalant canals leading to the choanocyte chambers where filtering occurs. The filtered water is then actively pumped outside through many exhalant canals that merge together before to reach the osculum. This leuconoid organization is the most efficient and common.

Many sponges have an internal endoskeleton composed of mineral and/or organic elements with reinforcing functions. The inorganic skeletal elements can be composed of calcium carbonate or silicon dioxide; the organic elements consist of spongin and/or different type of collagen. The composition and the shape of the mineral elements (spicules) are still often used for ascertain the species, but in the last years the genetic tools have acquired more and more popularity.

If it is sometimes difficult to determine the species of one sponge, it could be even more difficult to recognize or define a single individual due to the possible occurrence of fusion events at early stage or to the great capability of sponges to incur fragmentation/regeneration phenomena. In this work we assume that an individual organism can be defined as follows: "all is lined by a continuous pinacoderm" (Borojevic, 1966).

1.1.2 History and taxonomy hints

As expected on the basis of their ancient origin, fossil sponges are among the oldest known metazoan fossils, dating since the late Precambrian. During the Palaeozoic and the Mesozoic sponges created huge reefs, exceeding in term of biomass all the other benthic animals (Storch & Welsch, 2008). Most of the living species appeared 150 millions years ago and many characters present in the fossil records are still maintained unchanged. Nowadays poriferans are divided into the subphyla Cellularia and Symplasia; there are 4 classes: Hexactinellida, Calcarea, Demospongiae and Homoscleromorpha; 5 subclasses, 28 orders, 232 families and 977 genera. Approximately 8000 species of extant sponges have been described, but it is likely that 15000 species do exist (Hooper et al., 2000; Borchiellini et al., 2004). Demospongia class is the largest class with more than 90% of the overall described species.

The subphylum Cellularia includes the Demospongiae, the Calcarea, the Homoscleromorpha and, with some contrasting opinions, the extinct Archaeocyatha. On the other hand the subphylum Symplasma includes only the Hexactinellida.

The shape and the mineral composition of the spicules vary among the different classes: in the Demospongiae can have mono or tetraxons siliceous spicules that are often associated with spongin fibres and/or collagen; in the Hexactinellida only siliceous triaxon spicules are present; in the Calcarea, as expected from the name of the class, spicules are composed of calcium carbonate. Homoscleromorpha, which has been recently proposed as a separate class mainly on the basis of molecular data, have generally small siliceous or no spicules (Gazave et al., 2010, 2012).

Sponge systematic is controversial and still in evolution; some authors on the base of genetic evidences suggest that the Phylum is paraphyletic (Borchiellini et al., 2004); however the old classification is still prevalent. Most of the data reported here are derived from the book "Systema Porifera" (Van Soest & Hooper, 2002) and "Fauna d'Italia Porifera" (Pansini et al., 2011).

The animal model used in our experiments is the marine demonsponge *Chondrosia reniformis* (Nardo, 1847), subclass Tetractinomorpha, ordine Hadromerida, family Chondrillidae (Lazosky et al., 2001).

1.1.3 Sponge cell phenotypes

In this paragraph we provide an overall view of the most represented and widespread sponge cell phenotypes (we exclude the class Homoscleromorpha due to its peculiarity). A more detailed description of *C. reniformis* cell phenotypes will be provided in paragraph 1.2.1.

Classifying sponge cell phenotypes can be a difficult task because of their ability to change location and function as well as their morphology (Lévi, 1970; Pansini et al., 2011). According to literature cells can be divided into cells that line surface and cells that are constituents of the mesohyl. The latter group is divided into: totipotent cells, cells that secrete the skeleton, cells with contractile elements, cells with inclusions (Pansini et al., 2011).

Cells that lines the surface

The two most common cell phenotypes lining the sponge surfaces are the pinacocytes and the choanocytes (Lévi, 1970). Another cell phenotype, the porocyte, characterized by contractile activity, probably derives from pinacocytes (Pansini et al., 2011).

Pinacocytes are flattened cells that cover the outer surface (exopinacocytes) and also line both the inhalant and exhalant channels (endopinacocytes). They represent the first boundary between the organism and the external environment. Cellular processes belonging to these cells often take contact with other cells present in the inner layers. These cells have an important role in the regenerative process and may play a role in the contraction events thanks to the presence of cytoplasmic actin filaments (Bagby, 1970; Matsuno et al., 1988; Nickel et al., 2011). Some authors suggest that the endopinacocytes may have also a sensory activity due to the presence of primary cilia (Leys et al., 2009, Nickel et al., 2011).

Choanocytes cells are provided by a flagellum sourranded by a collar of 30-40 microvilli. They line the walls of the spongocoel or the choanocyte chambersbut do not form a proper ephytelium due to he lack of an evident basal membrane. The flagellar activity generates the water current through the sponge; the microvillar collar is responsible for the capture and uptake of food particles.

Porocytes are cylindrical, tubular cells that regulate the water flux by modifying the ostial diameters with their contractile activity.

Mesohyl cells phenotypes

Totipotent cells, called *archeocytes*, have amoeboid and phagocytic activity and are responsible for the organisational and functional plasticity of sponges. They can give rise all the other cell phenotypes and, as expected from this sort of "stem cells", their activity is very relevant in the regenerative and asexual reproduction processes (Borojevic, 1966). Moreover these elements are important in the cell turnover by producing new cells and by recycling the old ones (Borojevic, 1966). The term archeocytes is commonly used in sponge biology to indicate all the cells that cannot be well ascribed to other phenotypes on the basis of their morphology. In other words these phenotypes often represent transitory phases of many cells during their differentiation process.

Cells that secrete the skeleton are also called *collencytes*, and include *lophocytes*, *spongocytes* and *sclerocytes*. *Lophocytes* are large and mobile cells with numerous thin cytoplasmic projections; they are responsible for the collagen production and deposition. *Spongocytes* synthetize and secrete spongin, the peri-spicular or fibrous supporting collagen-like protein. On the other hand *sclerocytes* are involved in the production of both calcareous and siliceous spicules.

Cells with contractile elements: also know as *myocytes* these cells are now more properly named *actinocytes* (Boury-Esnault & Rutzler, 1997). The actinocytes look like small smooth-muscle cells: the presence of actin filaments bundles in their cytoplasm was firstly demonstrated by Bagby (1966). This cell type was found in many sponge species and is considered to represent a real contractile effector systems on the basis of its morphological characteristics (Vacelet, 1966). In contrast, neither the presence of myosin or an evident contractile activity have been demonstrated (Nickel, 2010).

Cells with inclusions: cells with cytoplasmic granules and inclusions are an heterogeneous population that derives from archeocytes (Levi, 1970). The chemical nature of the inclusions and the specific function of these cells may vary a lot in poriferans and are often unknown (Vacelet, 1967; Bretting & Königsmann, 1979; Bretting et al., 1983). On the basis of ultrastructural analysis these cells have been roughly distinguished in cells with few large inclusions and cells with numerous and small inclusions (Simpson, 1984). The former are called *spherulous cells* (Garrone 1978; Harrison & De Vos, 1991) whereas the latter include other five types: *the grey cells*, the *microgranular* cells, the *spumous* cells, the *rhabdypherous* cells and the *globopherous* cells (Bergquist, 1978; Pansini et al., 2011).

Grey cells seem to be involved in the glycogen metabolism (Boury-Esnault, 1977) or in collagen and lectins secretion (Garrone, 1974; Diaz, 1979; Sciscioli et al., 2000). On the other hand, the functional role of *microgranular* cells and the specific molecular composition of their granules are still unknown.

1.1.4 Coordination activity in sponges

Although the terms "sponge" and "behaviour" are not frequently associated, reports of sponges contracting or otherwise controlling the flow of water through their bodies can be dated as far back as

Aristotle's *History of Animals* (see Mackie 1979). In defining the Phylum, Grant (1936) concluded that the Porifera lack "*perceptible nervous or muscular filaments or organs of sense; they are animals that simply generate water flow through the body to feed*". The lack of a "true" nervous system was finally demonstrated by Jones (1962) and Pavans de Ceccatty (1974a, b).

Despite these observations, many phenomena involving some well-defined signalling pathways have been described in adult sponges. These phenomena are related to: contractile events; propagation of electrical signals (only in glass sponges); water flow control; response to mechanical stimuli; response to light, response to temperature. In addition, in sponge larvae geotaxis (Warburton, 1966), phototaxis (Warburton, 1966; Maldonado et al., 2003; Elliot et al., 2004; Uriz et al., 2008) and rheotaxis (Maldonado & Young, 1996) have been all well documented.

Although some details on the possible receptors, and signalling pathways have been provided for sponge larvae, the situation in adult specimens is still unclear. Possible mechanisms involve the release of hormones or chemicals, or a mechanical cell-to-cell, all processes similar to signalling mechanisms in non-excitable tissues reported in many metazoans (Mackie 1979; Lawn 1982). Another hypothesis (Ellwanger & Nickel, 2006) involves the release of specific molecules by specialized sensory cells in the canals flow; this could induce a first response of pinacocytes followed by a second response given by the mesohyl cells. The presence of rhythmic contractions, the possibility to induce or modulate such contractions with neuro-active molecules and the observations that sponges react to external stimuli with immediate contractile reaction leave no doubts on the presence of an integrative system (see Nickel, 2010 for a detailed review).

Contractile activity in adult sponges

Many sponges are able to contract the whole body or part of it (oscula, canals, ostia). Contractions events are frequently found in the class Demospongiae (Schmidt, 1866; Marshall, 1885; Pavans de Ceccatty, 1959; Emson, 1966; Vogel, 1977; Nickel, 2004; Elliot and Leys, 2007), in the Calcarea (Minchin, 1900; Bond, 2013) and in the Homoscleromopha (Nickel, 2010). These contractions events have never been found in the glass sponges due to the high abundance of rigid skeletal components (Leys et al., 2007), and in those demosponges also possessing a rigid skeleton that prevents the possibility of body contractions (Nickel, 2010). These contractile behaviours can be induced by mechanical or photic stimuli *in situ* and by chemical or electrical stimuli in laboratory experiments. These stimulations can cause a slow down of the inner water flow possibly due to the contraction of the aquiferous system (ostia, canals and oscula) (Parker, 1910). Although some responses, such as the closure of the oscula (Pavans de Ceccatty, 1959; Emson, 1966) and the reduction in size (Pavans de Ceccatty, 1959; Gaino et al., 1991) remain localized, propagation phenomena have been also described (Mcnair, 1923; Pavans de Ceccatty, 1959; Ellwanger & Nickel, 2006; Nickel, 2006; Elliot & Leys, 2007). The observed contraction waves are thought to travel through the pinacocytes and/or from cell to cell

in the mesohyl where the signal may also be transmitted at short distance through the extracellular matrix (Leys & Meech, 2006).

Historically two hypotheses regarding the effectors of the contraction phenomena were formulated. The first hypothesis implied a mesohyl-mediated response originated from the actinocytes (Schmidt, 1866; Sollas, 1888); the second hypothesis attributed to the pinacoderm the actual effector role (Minchin, 1900; Wilson, 1910; Bidder, 1937; Jones; 1957, Nickel et al., 2011). These two hypotheses were then combined into a more complex model where both the actinocytes and pinacoderm play the effector role (Pavans de Ceccatty, 1981, 1986). Recent evidences confirm this more complex hypothesis: in fact it was demonstrated both the contraction of inner canals, mediated by the pinacocytes (Nickel et al., 2011) which can have tighter and more stable connections than expected (Leys et al., 2009), and contractile activity of the mesohyl (Elliot & Leys, 2007).

1.1.5 Chemicals treatment affecting sponge "behaviour"

Although the presence of different molecules, which are generally associated with signal transmission, have been demonstrated since the past century, the specific effects of these neuro-active molecules have been explored mainly in the last ten years. Some molecules appeared to be able to induce contraction of part of the sponge or to modulate the endogenous rhythmic contractions in some species; in contrast in others species no effects were recorded. A comprehensive table (table 1), provided by Nickel (2010) and shown below summarize very well what is mainly known so far on this matter.

The lack of a well-defined nervous system and the possible humoral paracrine mechanisms, that may involve different signalling molecules at the same time, make really difficult to understand and elucidate the effects of single molecules; indeed Pavans de Ceccatty (1971) found that although neither adrenaline nor acetylcholine alone appeared to affecte the osculum diameter of the genus *Euspongia*, when used in succession they acted in synergy causing its constriction. Actually we do not know if other neuro-active molecules, combined with other ones, can induce coordinated phenomena. It is possible to speculate that the lack in sponges of identifiable and specific nervous paths is balanced by the effect of combined molecules*.

*To better explain this concept we can compare the polyphonic music (coordinated phenomena) played by an orchestra (upper metazoan) or by an harpsichord solo (sponges). In an orchestra each single instrument (nervous path) is able to produce a specific sound that together with the other instruments contributes to the harmony, on the other hand sponges own only an instrument (paracrine signalling) and the harmony is produced by the combination of different keys played at the same times.

Receptor system	Background	References	Evidence in sponges				
			Higher taxon	Species	Physiology	Genomics	References
Acetylcholine	Ligand-gated ion channels (nicotinic receptors); metabotrophic receptors (muscarinic); specific AChE activity in Ach-hydrolyzing cells	Walker et al. (1996), Walker & Holden-Dye (1991)	Calcispongia	*Sycon* sp.	AChE activity (histochemistry)		Lentz (1966, 1968)
				Scypha sp.	No AChE activity (histochemistry)		Bullock & Horridge (1969)
				Leucandra aspera	No AChE activity (histochemistry)		Bacq (1947)
			Demospongiae	*Hippospongia communis*	AChE activity (histochemistry); ACh increased rhythm and intensity of contraction		Pavans de Ceccatty (1971), Thiney (1972)
				Cliona celata	ACh: slight reduction of current and slight closure of oscule; nicotine: current reduced		Emson (1966)
				Spongilla lacustris	No AChE activity (histochemistry)		Mitropolitanskaya (1941)
				Siphonochalina crassa	No AChE activity (histochemistry)		Bacq (1947)
				Tethya wilhelma	AChE activity (histochemistry); ACh: no induction of contraction, but alters frequency; nicotine: no effects		Nickel (2001), Ellwanger & Nickel (2006)
Adenosine	Metabotrophic receptors, linked to ATP-driven energy metabolism, pathway strongly interact with other signaling pathways. Caffeine acts as non-specific antagonist.	Fredholm et al. (2000), Walker et al. (1996)	Demospongiae	*T. wilhelma*	Caffeine: increased endogenous contraction rhythm; attenuated amplitude		Ellwanger & Nickel (2006)
Glycine	Ligand-gated ion channel	Oberdisse et al. (1997), Pierobon et al. (2001)	Demospongiae	*T. wilhelma*	Glycine: stimulates contraction, accelerates endogenous contraction rhythm, attenuates amplitude		Ellwanger & Nickel (2006)
GABA/glutamate	Metabotrophic and ionotrophic receptors	Walker et al. (1996), Walker & Holden-Dye (1991)	Calcispongia	*Clathrina clathrus*	Glutamate induces contraction		Arnold & Nickel unpubl. data; Fig. 1C
			Homoscleromorpha	*Oscarella lobularis*	Glutamate induces contraction		Arnold & Nickel unpubl. data; Fig. 1B
			Demospongiae	*T. wilhelma*	GABA/glutamate induces and modulates contraction		Ellwanger et al. (2007), Ellwanger & Nickel (2006)

				C. celata	GABA: decreased pumping activity		Emson (1966)
				Chondrilla nucula	Immunohistochemical demonstration of $GABA_B$ receptors		Ramoino et al. (2007)
				Geodia cydonium	GABA/glutamate induces intracellular Ca^{2+} release	GABA/ glutamate-like receptor gene	Perovic et al. (1999)
				Amphimedon queenslandica		$GABA_B$ receptor gene	Sakarya et al. (2007)
Adrenergic	G-protein coupled receptor; among others involved in circadian rhythm regulation	Shibata (2004)	Calcispongia	*Sycon* sp.	Adrenaline: slight reduction of pumping rates		Lentz (1966), Lentz (1968)
			Demospongiae	*T. wilhelma*	Adrenalin: disturbes endogenous rhythm		Ellwanger & Nickel (2006)
5-HT	G-protein coupled receptors; ligand-gated ion channels	Hoyer et al. (1994)	Calcispongia	*Sycon* sp.	Serotonin present in cells (histochemistry)		Lentz (1966, 1968)
			Demospongiae	*C. celata*	Serotonine: no effect on currents		Emson (1966)
				Tedania ignis	Serotonine present in larvae (immunohistochemistry)		Weyrer et al. (1999)
				T. wilhelma	Serotonine: induced contractions		Ellwanger & Nickel (2006)
Nitric oxide	Soluble guanylate cyclase	Colasanti & Venturini (1998), Jacklet (1997), Walker et al. (1996)	Demospongiae	*T. wilhelma*	NO: induces contractions, modulates endogenous rhythm and contraction amplitude		Ellwanger & Nickel (2006)
				C. nucula	NO involved in temperature signaling cascade		Zocchi et al. (2001)
				A. queenslandica		NO synthase (NOS) gene	Sakarya et al. (2007)

Table 1 (pp. 8-9). Summary of neuro-active molecules and their effects in sponges. From Nickel, 2010.

1.2 *Chondrosia reniformis*

Figure 1. *Chondrosia reniformis*

Chondrosia reniformis Nardo 1847 (fig. 1) is a common Mediterranean demosponge (Lazoski et al., 2001) that colonizes shaded rocky cliffs or caves at a depth of 1-50 m (Bavestrello et al., 1998a). The shape is generally ellipsoidal or cushion-like with a standard size of about 15 cm long, 10 cm width and 4 cm high. Nevertheless the largest specimens are often composed of different sponges merged together: in this case the sponge appears much more flattened the height remaining stable, i.e. the same of an individual sponge, and the total surface depending on the number of merged specimens (Zanetti, 2002). The sponge colour depends on the presence of melanic pigments that vary according to the light conditions. Sponges that live on illuminated shores are generally brown with some bright spots, whereas samples living in caves are completely white (Pansini & Pronzato, 1982; Corriero et al., 2000) due to the lack of photosynthetic endosymbionts and pigments. In contrast to many other members of the phylum, this species lacks both endogenous opaline spicules and reinforcing spongin fibres (Garrone et al., 1975; Bavestrello et al., 1998a): on the other hand, exogenous siliceous and calcareous material can be actively incorporated by the sponge itself and distributed in the mesohyl according to a specific polarity (Bavestrello et al., 1995; 1998a).

C. reniformis generic name (kidney sponge) is given by the cartilaginous consistency of its thick and dense collagenous mesohyl and for its shape resembling a vertebrate kidney.

This sponge attracted our attention (Bonasoro et al., 2001) because of its striking tissue plasticity and intrinsic possibility to modulate its mechanical properties under cellular control (Wilkie et al., 2006). Indeed the sponge display the capability to modulate the mesohyl tensility according to specific events: in particular the sponge body can acquire a very soft and plastic consistency producing long and slender outgrowth when part of the substrate brake off (creeping phenomena), or become stiff and rigid when repeatedly touched (stiffening phenomena) (Wilkie et al., 2006; Parma et al., 2007).

Creeping phenomena

The outgrowths produced during the so-called creeping phenomenon are generally slender deformation downwards directed, as they are induced by gravity; however some authors reported that also horizontally and obliquely directed extensions can occur in other species (Bond & Harris, 1988; Fell, 1994; Pronzato, 2004). This phenomenon has been described in other demosponges living, as *C.*

reniformis, on exposed cliffs and lacking an organised endoskeleton of either spicules or spongin fibres. The sponges that display similar behaviour are *Pseudocorticium jarrei* (Boury-Esnault et al., 1995); *Oscarella lobularis* (see Sarà and Vacelet, 1973); *Chondrilla nucula* (Gaino and Pronzato, 1983; Sidri et al., 2005); *Plakina weinbergi* (Muricy et al., 1998) and *Clathrina clathrus* (Gaino et al., 1991). These creeping dynamic phenomena have been interpreted in different ways. For instance, they have been regarded as passive responses to mechanical stresses due to environmental changes or rearrangement of the substrata: according to this idea, the whole sponge body could be deformed slowly flattening and sliding under compressive stress (Garrone et al., 1975) or stretching out under tensile stress, this latter condition frequently occurring when the substratum to which the sponge is attached breaks off (Sarà and Vacelet 1973; Parma et al., 2007). According to other authors this phenomenon is correlated to reproductive processes and can be interpreted as a form of opportunistic asexual reproduction (Connes, 1967; Gaino & Pronzato, 1983; Zilberger et al., 2006; Parma et al., 2007). Asexual reproduction events occur by buds formation in some species (see Simpson 1984 for a detailed review) and are sometimes accompanied by the development of long retractile filaments (Fell, 1994). In the natural environment, crumbling of the substratum to which a sponge is anchored is followed by the slow elongation of the related sponge portion under gravity until the eventual separation of a propagule from the still attached parental body; moreover the phenomenon is seasonal and regulated by the water temperature. For all these facts this process can be actually regarded as successfully strategy of opportunistic asexual reproduction (Sarà & Vacelet, 1973; Bonasoro et al., 2001; Parma et al., 2007).

Finally, Bond and Harris (1988) hypothesized that, these dynamic phenomena, could be an atypical form of "localized" locomotion, possibly preceding or related to asexual reproduction. These diverse interpretations are not necessarily in contrast to each other. As stated above, in experimental conditions the whole sponge body or tissue explants can lose their intrinsic stiffness under continuous compression (Garrone et al., 1975; Garrone, 1978). The phenomenon could be easily reproduced both in the field, by detaching some of the sponge anchoring points and applying a tensile stress (downward directed or upward directed), and in laboratory on tissue explants (Parma, 2007, Parma et al., 2007).

Stiffening phenomena

The first clues on the presence of a stiffening phenomenon following mechanical stimulation derive from empirical observations: in fact when an undisturbed specimen, in the sea or in the laboratory aquaria, is repeatedly touched, it results softer the first time than on subsequent tests. On the basis of this behaviour, the possible evidence of contractile activity was explored in laboratory experiments. According to morphological and physiological results the presence of identified contractile elements in the sponge was demonstrated to be not enough to explain this response (Bonasoro et al., 2001); in contrast the stiffening reaction was ascribed to modifications of the interaction of the collagen fibrils in

the ECM under cellular control (Wilkie et al, 2006; Parma et al., 2007). Experiments conducted by Parma (2007) with a basic mechanical apparatus able to stimulate and in the meantime to measure the induced deformation given by a steel rod shaped load, underlined the following points: 1) the procedure of measuring the sponge tensility induced a stiffening response nearby (0.5 mm) the measured/stimulated point; 2) there were no responses at 4 cm distance from the stimulated point; 3) there was a great difference in the deformation values between the specimen before and after a vigorous manipulation that induced the maximum stiffness. In addition, other experiments on isolated tissue samples of both ectosome and choanosome demonstrated that also isolated samples were able to stiffen after mechanical stimulations; in particular ectosome samples seemed to exert a sort of modulation of the response according to the number of the given stimulation (Parma, 2007).

Ionic manipulations that resulted to be able to stiffen partially destiffened isolate samples of ectosome (and often choanosome) were the following: $CaCl_2$ 0.38 M, Mn^{2+} 20mM (in ASW) and deionized water (DW) (Wilkie et al., 2006). Chemicals that induced stiffening of partially destiffened isolate ectosome samples (and often choanosome) were the following: 0.1% triton X; nystatin 0.05%; verapamil and nimodipine 100μM (all in ASW) (Wilkie et al., 2006). These treatments (in particular triton X and nystatin), together with the evident stiffening effect of crude extract leaded to the hypothesis that some stiffening factors are stored in the cells and may be released in the ECM modifying the interactions between the collagen fibrils (Wilkie et al., 2006). On the other hands the role of divalent ions is not yet clear since different treatments that decreased calcium concentration had different results according to the mechanical state of the sponges: different and sometimes opposite effects were obtained when testing maximally stiffened samples or partially destiffened samples (Wilkie et al., 2006).

Destiffening phenomena

As described above, once a sponge or an isolated explant is cut off or mechanically stimulated it reaches its stiffer mechanical state. It was demonstrated experimentally (Wilkie et al., 2006) that isolated samples destiffened progressively over 7-9 h. This process appear to depend on temperature: higher the temperature, higher was the speed of relaxation; an evident significant difference between ectosome and choanosome relaxation could be found at 25°C after 3 h from the cut, ectosome samples showing higher level of destiffening. At 14°C the relaxation was more progressive and generally slower than at 25°C. The destiffening process was strongly inhibited (in some case irreversibly) by a range of treatments causing cell membrane disruption or cell permeabilization (Wilkie et al., 2006). Isolated samples exposed to media that increased $[Ca_{2+}]$ in the ECM or blocked Ca_{2+} channels, generally inhibited the destiffening process, whereas calcium free seawater (CaFSW) accelerated the process. Paradoxically both extra/intracellular calcium chelators had the effect to inhibit the destiffening and at higher concentration EGTA could restiffen partially destiffened samples (Wilkie et al., 2006).

1.2.1 Microscopic anatomy: standard resting condition

The overall structure of *C. reniformis* consists mainly of a complex tridimensional network of canals. The sponge body is covered by an external epithelium composed of a monolayer of polygonal flattened cells called exopinacocytes; on the other hand a monolayer of endopinacocytes lines the inner canals (endopinacoderm) which, along their irregular courses, reach the choanocyte chambers lined by choanocytes. The fragile and intricate network of canals and chambers is protected, supported and held in place by the surrounding organic stroma of the collagenous mesohyl.

Mesohyl

As stated above most of the sponge body is composed by mesohyl, which can be considered a collagenous tissue similar to the connective tissue of typical metazoan taxa. Mesohyl is a dense and compact fibrous tissue consisting of a massive extracellular matrix dominated by collagen bundles and non-fibrillar collagen (the first identified gene of the non fibrillar collagen was called COLch) (Pozzolini et al., 2012) in which an heterogeneous population of scattered cells is found (Garrone, 1978; Harrison and De Vos, 1991).

Sponge sections reveals two different regions: an outer region (ectosome) characterized by the presence of dense and well-organized collagen fibres, and an inner medulla (choanosome) where the collagen fibrils were organized in a looser arrangments.

Ectosome

In sponge sections the ectosome region is 3-4 mm thick and can be easily recognizable macroscopically for its brow/grey colour. This cortical layer, that appears to be poorly irrigated by the small incurrent canals (Bonasoro et al., 2001), is responsible for the protection of the inner body, the selective incorporation of mineral materials and the attachment to the substrata (Bavestrello et al., 1998a).

Histological and ultrastructural analyses of ectosome region revealed the presence of two different sub-region: the outer region is characterized by loose fibre bundles, whereas in the inner region fibres are tightly packed and organised in compact layers (Bonasoro et al., 2001). This difference is only related to fibrillar collagen; indeed COLch, which is highly expressed in the ectosome, appears to be homogeneously distributed (Pozzolini et al., 2012).

Choanosome

The choanosome region constitutes the mesohyl majority. This region looks light yellow and is mainly characterized by the presence of a large number of choanocyte chambers and large exhalant canals (Bavestrello et al., 1998b; Bonasoro et al., 2001). This aspect makes this region less homogeneous than ectosome in terms of tissue structure.

In the choanosome region fibrillar collagen (Bonasoro et al., 2001) and COLch are less abundant than in the ectosome (Pozzolini et al., 2012); on the other hand there are no difference in respect to ectosome in the hydroxyproline amount suggesting that other types of non-fibrillar collagens contribute to form the characteristic looser matrix (Pozzolini et al., 2012). Fibrillar collagen is well organized around the exhalant canals where it forms a sheath of collagenous tissue (canals belt) that is particularly evident around the distal part of the exhalant canal that emerges into the osculum (Pavans de Ceccatty, 1979).

Collagen

As far as we know different collagen families are present in the *C. reniformis* genome (Pozzolini, personal communication). As in all metazoans we could find mainly two types of collagen forms: fibrillar and non-fibrillar collagen. The fibril-forming collagen is organized in fibres that appear as bundles of collagen fibrils showing a constant diameter of about 20 nm. At higher magnifications, fibrils show a poorly defined but regular longitudinal period of about 66 nm, with two separate light bands and one dark band of 22 nm in each period (Bonasoro et al., 2001). Fibrils are generally several microns long, the ratio between length and thickness reaching considerable values (5000:1), comparable to that of fibrillar collagen presents in the spine ligaments of sea urchin nad very different to reassembled fibrils of bovine type I collagen (about 50:1) (Heinemann et al., 2007). Both the amino acid composition and FT-IRAS analyses of *C. reniformis* fibrillar collagen revealed no significant differences between bovine Type I collagen; on the other hand, contrary to calf skin collagen type I, sponge collagen is quite insoluble in acetic acids 0.1 M and is mostly degraded when treated with NaOH 0.1 M (Heinemann et al., 2007). By contrast, treating sponge collagen with a neutral buffer solution (0.1 M Tris-HCl, pH 7.4) results in an homogeneous suspensions (Heinemann et al., 2007).

The molecular characterization of non-fibrillar collagen COLch, which belongs to the short-chain collagens, has been recently published (Pozzolini et al., 2012). The gene is characterized by the presence of four collagen domains linked by three linker peptides, both the N and C terminal having non-collagenous domains. The putative translation product has an estimated M_r of about 72 KDa. COLch is highly expressed during the wound healing process and is also responsible for the attachment of the sponge to the substrata; its expression is also positively regulated by the amount of dissolved silicata. The presence of different glycosylation sites, possibly involved in protein-protein non-covalent interactions, lead to the hypothesis that this collagen can play a role in the stiffening events (Pozzolini et al., 2012).

Cells

Cells that line surface. Also in the sponge *C. reniformis* cells that line the surface are represented by pinacocytes and choanocytes. Pinacocytes could be distinguished according to their position, in exopinacocytes, covering that lay on the sponge surface, and endopynacocytes lining the inner canals.

Choanocytes line the choanocyte chambers; these cell are characterized by the presence of a central flagellum sourranded by 30-40 microvilli.

Cells with contractile elements. Actinocytes (fig. 2) are characterized by the presence of actin filaments. These cells, often found around the terminal region of the exhalant canals (Lévi, 1970; Garrone, 1978), appear to be easily recognizable in the stiffened condition where the membrane seems to be reinforced by densely packed filamentous material (Bonasoro et al., 2001).

Cells with inclusions. Lophocytes (fig. 2), the cells involved in the collagen deposition, are scattered homogeneously in the mesohyl and look like typical fibrocytes. Ultrastructure analyses reveal a marked anterior–posterior polarity defined by the presence of a slender cytoplasmic tail, which protruded into a trail of collagen fibrils held together by a thin filamentous matrix. The cellular anterior end is characterized by large stellate pseudopodial protrusions prolonged into long and thin filopodia; in contrast, the posterior end looks indented by deep grooves alternating with cytoplasmic laminae to form a sort of irregular microvillar border. The presence of a large nucleus displaying a prominent nucleolus, a highly developed rough endoplasmic reticulum (RER), a marked Golgi complex consisting of flattened lamellae and abundant dense-core vesicles, quite numerous lipid droplets and a number of microfilaments and microtubules are characteristic features of these cells. Massive cytoplasmic inclusions containing amorphous or packed fibrillar material can also be frequently observed. In sponge in dynamic conditions lophocytes look closely associated with endopinacytes processes forming junction-like structures (Bonasoro et al., 2001).

Spherulous cells (fig. 2) are easily and clearly recognisable also with light microscopy due to their membrane-bound large inclusions (spherules). As highlighted by ultrastructure analysis, the spherules fill the cytoplasm; the nucleus is frequently anucleolated and deformed by the presence of the huge inclusions, few mitochondria and ribosomes, and sparse RER cisternae are often found (Bonasoro et al., 2001). The spherules look usually homogeneous, but sometimes they present a paracrystalline or microfilamentous undefined content comparable to that described in spherulous cells of *Tethya sp.* (Connes, 1967). Despite variations in their specific content, the morphology of the spherules is always very different from that of other types of inclusions such as phagosomes, making it unlikely an involvement of these cells in phagocytic activity. The spherulous cells are particularly frequent around the canals and in the region between the ectosome and the choanosome.

Numerous differences in the spherules content can be detected during the creeping phenomenon according to the region analysed. In particular, in the parental portion and in the elongation region

these cells appear to take contact with endopinacocytes and lophocytes processes, and the spherules content looks much more heterogeneous showing the presence of irregularly distributed dense-core, rarefied or nearly empty spots. In the transition region the spherulous cells plasmalemma is often disrupted and granules appear partially or totally empty (Bonasoro et al., 2001).

Grey cells (fig. 2) are less abundant that spherulous cells and are rarely detectable. The distinctive feature of these cell types is represented by the presence of many small cytoplasmic granules with a paracrystalline content still to be identified. No significant changes have been detected during the dynamic phenomena (Bonasoro et al., 2001).

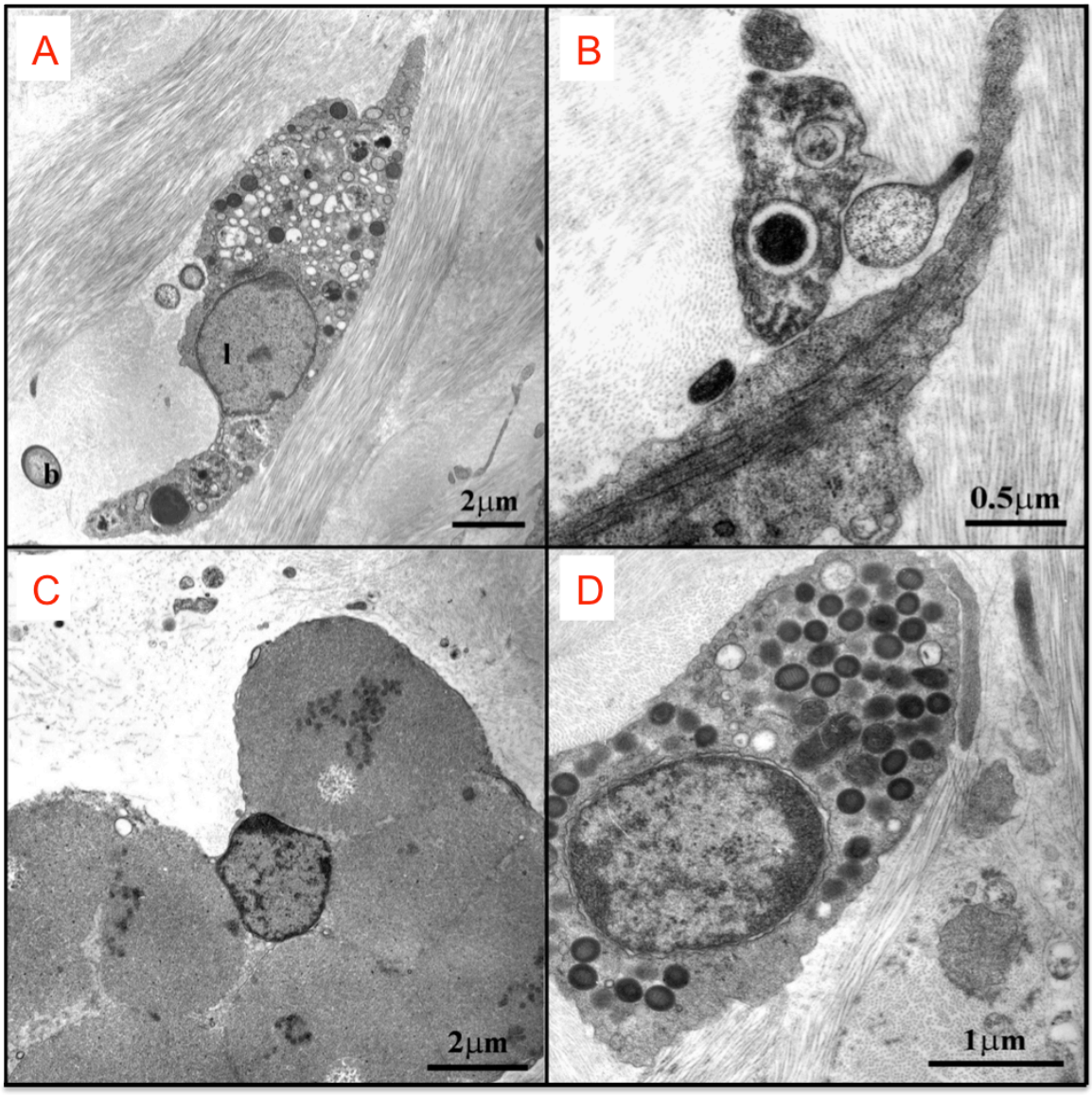

Figure 2. *C. reniformis* cells. A lophocyte; B actinocyte; C spherulous cell; D gray cell. From Bonasoro et al., 2001.

1.3 Dynamic connective tissues

The presence of connective tissues that display analogous dynamic phenomena have been firstly demonstrated and described in echinoderms, in particular in the spine ligaments of sea urchin (Takahashi, 1967). These tissues, called Mutable Collagenous Tissue (MCTs), have been later demonstrated in all the five echinoderms classes in different anatomical structures (see Wilkie 2005 for an extensive review). In echinoderms the dynamic phenomena are regulated by the nervous system and allow these animals to control the mechanical state of the connective tissues by changing the interactions between the collagen fibrils according to specific functional requirements (Wilkie, 2005).

MCTs dynamic phenomena can be reversible or irreversible, this condition resulting in autotomy process (Wilkie, 2005).

MCTs microstructure, physiology, biomechanics and biochemistry have been extensively studied in the last years (Tamori et al., 2010; Yamada et al., 2010; Ribeiro et al., 2011, 2012a, 2012b; Barbaglio et al., 2012). Like all the other connective tissues MCTs consist of an ECM, dominated by collagen fibres, and a cellular component.

The collagen fibres patterns are comparable in variety to what described for vertebrates. We can found parallel fibres arrays (e.g. echinoid spine ligament: Takahashi, 1967; Trotter & Koob 1989), crossed-fibres arrays (e.g. echinoid peristomial membrane: Wilkie et al., 1994) and three-dimensional meshwork of fibres (e.g. holothurian dermis: Motokawa, 1982).

Four cells have been found to be strictly associated with MCTs: fibroblast-like cells, phagocytes, neurons and juxtaligamental cells (Wilkie et al., 2005).

Fibroblast-like cells have extremely long cytoplasmic processes, large amount of multivesicular bodies, and a well evident and developed Golgi apparatus and RER (Tamariz and Grinnell, 2002). These cells are responsible for the collagen biosynthesis and deposition (Myllyharju, 2003); on the other hand collagen is degraded by *phagocytes* that play a role similar to those of fibroclasts (Sugni et al., 2013). Phagocytes are easily recognizable by the presence of a typical intra-nuclear crystalloid structure (Bachmann et al., 1980) and intra-cytoplasmic vesicles containing collagen fibrils. *Neurons* are always found in MCTs structures that are always well innervated (Wilkie, 2005; Sugni et al., 2013). *Juxtaligamental cells (JLCs)* are specific cells of MCTs; they have a presuntive neurosecretory activity (Chapman, 2002) and are thought to be the effector cells of dynamic phenomena. Two kinds of JLCs have been characterized in MCTs structures: type 1 JLC and type 2 JLC. The presence of large intra-cytoplasmic membrane-bounded granules and vesicles characterizes the type 1 JLCs, whereas type 2 JLCs have numerous small electron-dense granules.

The characterization of the collagenous component of MCTs revealed inter and intra-specific differences in the biochemical composition (Exposito et al., 2010) with a consequent difference in extraction efficiency procedures (Trotter and Koob, 1989). Several genes, encoding fibrillar and non-

fibrillar forming collagens, have been described in echinoderms (Saitta et al., 1989; D'Alessio et al., 1990; Exposito et al., 1995; Aouacheria et al., 2004; Cluzel et al., 2004). Some of these collagens showed immunoreactivity to vertebrate type I, II, III and IV collagens (Wessel et al., 1984). Ultrastructural analysis showed a great variability in the collagen fibril D period that ranges from 44 nm (*Strongylocentrotus purpuratus* peristomial membrane: Burke et al., 1989) to 67 nm (holothurian dermis: Matsumura, 1974).

Surprisingly the mutability phenomena involve both the fibrillar forms and the non-fibrillar type collagen (Wilkie et Emson, 1987).

Different ionic manipulations are able to affect MCTs mechanical properties (Wilkie, 2005) although is reported that the same treatment on different structures results in different effects. High $[K^+]$ induced an increase in stiffness in several reversible MCTs (Hidaka and Takahashi, 1983; Wilkie et al., 1992; Hennebert et al., 2010), whereas decreased viscosity in irreversible MCTs (Wilkie, 1983, 1988; Byrne, 1985). These contradictory effects suggest that the response to K^+ is tissue-specific. Furthermore, K^+ is considered not to act directly on the collagenous ECM but via depolarization of neurons controlling effector cells (Wilkie et al., 1994). Increased $[Ca^{2+}]$ caused increased stiffness in numerous anatomical MCT structures (Szulgit and Shadwick, 1994; Trotter and Koob, 1995; Hennebert et al., 2010); on the other hand increased $[Mg^{2+}]$ stiffens holothurian dermis (Byrne, 1985), but decreases the viscous resistance of echinoid spine ligaments (Hidaka, 1983). Contrary to previous hypothesis, known as "fibrils sliding hypothesis", that assigned a direct role of Ca^{2+} in stabilizing ECM cohesion (Wilkie, 1996), it is now thought that these treatments interfere with the nervous system by depolarizing the neural circuits that regulate the mechanical properties. Indeed it has been shown that MCT can stiffen significantly even in the absence of Ca^{2+} ions (Szulgit and Shadwick, 1994).

Although acetylcholine (Hidaka and Takahashi, 1983; Wilkie et al., 1994, 1992; Ribeiro et al., 2011; 2012a; 2012b) and many cholinergic agonists (Birenheide et al., 1998; Wilkie et al., unpublished) has been demonstrated to stiffen most of MCTs models (Hidaka and Takahashi, 1983; Wilkie et al., 1994, 1992; Ribeiro et al., 2011; 2012a; 2012b), the specific neural circuit involved in MCT destiffening is still unclear, mainly due to contrasting results obtained with epinephrine and L-glutamic acid (Hidaka and Takahashi, 1983; Wilkie et al., 2010; Wilkie et al., unpublished).

Molecular bases of mutability

It appears that most MCTs consist of parallel aggregates of discontinuous, spindle-shaped collagen fibrils to which proteoglycans (PGs) and other glycosaminoglycans (GAGs) are attached. It is thought that PGs and GAGs contain specific domains that act as specific binding sites for specific molecules that regulate MCTs mechanical properties. Three molecules, previously characterized in holoturians, have been considered the ideal candidates for this regulative role: stiparin, tensilin and novel stiffening factor (NSF). At present it is quite evident that stiparin, a 350 KDa glycoprotein capable of aggregate

isolated fibrils via weak surface-bonds PGs (Trotter at al., 1996), is a constitutive molecules that is not associated with mechanical change; in contrast tensilin and NSF are really directly involved. Tensilin (Tipper at al., 2003) is a 37 KDa glycoprotein that interacts with collagen fibrils via GAGs forming inter-fibrillar bridges, thus preventing interfibrillar slippage (Tipper et al., 2003; Wilkie, 2005). This molecule is found both in the ECM and inside the type 2 JLCs, and is considered mainly responsible for the restiffening of compliant tissues.

On the other hand NSF, a very small protein (2.4 KDa) can stiffen tissues that are in standard condition but do not affect compliant tissue (Yamada et al., 2010). However the stiffening activity of NSF is not yet demonstrated to act directly on extracellular components and a possible effect on cells must be verified (Yamada et al., 2010).

1.4 Aims of the work

The present work is addressed to explore the presence of coordination phenomena in the demosponge *C. reniformis*.

The thesis is mainly divided into four, partially interactive, parts focusing on the following specific aspects: 1 reaction to mechanical stimuli; 2 characterization of the mesohyl mechanical properties; contraction/expansion events; 4 the presumptive stiffening factors involved in the modulation of the mechanical properties.

1.Reaction to mechanical stimulations

The capability of the sponge *C. reniformis* to react to mechanical stimulation is evident when handling these animals and has already been reported in literature (Garrone et al., 1975; Bonasoro et al., 2001; Wilkie et al., 2004). Sponge tensility has been demonstrated (Wilkie et al., 2006) to be under cellular control. Previous experiments (Parma, 2007) showed that isolated tissues from both ectosome and choanosome react to mechanical stimulation by stiffening. Moreover, Parma (2007) attempted to demonstrate the presence of a possible conduction mechanism causing stiffening of the whole sponge after localized stimulation. The results of this study showed that stiffening involved the nearby-stimulated area, but was not areas more distant than 0.5 cm, leading to the concluson that, at least with the applied protocol, there were no signs of propagation of the stiffening reaction.

In the present work we explored the possibility width of the area involves by the stiffening reaction can depend on the stimulation magnitude and on the time occurring between stimulation and response. In this view the stimulation tests performed were intended to investigate the speed of the stiffening response, the presence of a conduction mechanism and the role of the exopinacoderm in the signal conduction.

Before carrying out appropriate stimulation tests, we also studied the recovery process (i.e. the dimensional changes) that follows the mechanical stimulation both on whole sponges, and on isolated

ectosome and choanosome or sponge slices.

Finally the possible presence of specific machanosensory structures in the exopinacoderm was studied with both scanning and transmission electron microscopy.

2. Characterization of the mesohyl mechanical properties

At present there are no available data on the mechanical properties of the sponge mesohyl. As far as we know this is the first attempt to measure the mechanical parameters of the sponge tissue. Biomechanical tests were performed both in isometric and isotonic condition on both ectosome and choanosome in order to describe the sponge mesohyl mechanical properties.

3. Description of the contraction/expansion events

Rhythmic contraction/expansion events occur in many sponges (De Vos & van de Vyver, 1981; Nickel, 2004; Elliott & Leys, 2007; Bond, 2013). These phenomena can be modulated by neuroactive compounds that can induce or change the contraction rhythm and magnitude (see Nickel 2010 for a review). In particular, our attention was here focused on γ-Amino Butyric Acid (GABA) and glutamate (Glu). In fact while Glu have similar effects on the two most used animal models, *Thethya willelma* and *Ephydatia muelleri*, the effects of GABA are rather controversial since it can induce contraction in *T. willelma* (Ellwanger et al., 2006) or completely inhibit contraction in *E. muelleri* (Elliot & Leys, 2010).

In order to describe eventual contraction/expansion behaviours we employed appropiate time-lapse photography technique. The effects of GABA and Glu were evaluated with an original approach that allowed us to measure at the same time the contractions magnitude and the tensile force generated by the contractions.

4. Presuntive stiffening factors

The possible presence of stiffening factors was firstly hypothesized by Bonasoro and coworkers (2001) and later partially demonstrated by Wilkie and coworkers (2006). Here we focused on the sponge protein fraction. After a rough separation we tested the different fractions of sponge protein on both isolated ectosome samples and collagen fibrils suspension extracted from different organisms.

In view of possible patent the results obtained so far cannot be presented here in detail in order to respect the rules requested by the procedures.

Materials and methods

2.1 Sponge sampling

Specimens of *C. reniformis* were usually collected between October and May by SCUBA divers at two different locations on the Italian Ligurian coast: Bergeggi (44°14'37"N 8°26'40"E) and Paraggi (44°18'40"N 9°12'46"E). We avoid collecting sponges during summer due to the high mortality events often occurring few days after sampling and possibly due to heat shocks. The sponges were detached from the rocky shores by cutting gently their anchoring points with a knife. The sponges were then transferred to 50 l tanks filled with artificial seawater (ASW) and kept at 14-16°C with a photoperiod of 8 h/day. The ASW was prepared by melting a commercial mix of sea salts (Instant Ocean®) and deionized water in order to reach a final density of 1028 g/l. All animals, before being tested, were left undisturbed for at least one night in the aquaria to recover the stress induced by the sampling procedure. All experiments were performed within ten days after collection, since with a prolonged time *C. reniformis* tends to adapt to aquarium conditions by reducing the oscula diameters and changing the inner canals structure (personal observation).

2.2 Rhythmic contraction/expansion recordings

Sponges were gently placed in a small aquarium at room temperature (RT). Single frontal side images were taken every 5' for several hours with a Canon Eos 30D equipped with a Sigma 24-70mm. The single images have been used for creating time-lapse movies with i-Movie© software: several hours were condensed in few seconds. The evaluation of the volume loss was obtained by measuring the thickness of the sponge in 5 different points during the maximum expansion and during the maximum contraction (fig. 3).

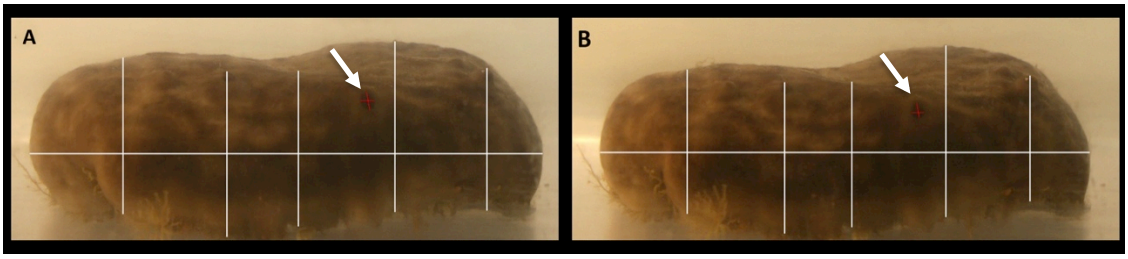

Figure 3. Comparison between sponge during his maximum expansion (**A**) and maximum contraction (**B**). **White lines** indicates the correspondent measured points, **red lines** the correspondent (**white arrows**) diameters of the osculum.

Other movies were produced (with the same technique) in the aquaria where the sponges are usually placed after collection and maintained before the experiments.

2.3 Recovery to resting condition recordings

Whole mount

The recovery process of isolated samples of both ectosome and coanosome to resting condition (RC) state from maximally stiffened condition (MSC) has been previously described by Wilkie and coworkers (2006) by means of mechanical tests. Data related to isolated samples demonstrated that after 4/5 hours at RT (25°) they are almost in RC (Wilkie et al., 2006). In order to describe the process in whole sponges, four specimens, after being manipulated to induce the MSC, were left undisturbed for 7 h. Using a Canon Eos 30D (resolution 2336 X 3506 pixels) with a 24-70 Sigma EX objective, two photographs (frontal and overhead views, fig. 4) of each specimen were taken at intervals of 1 h; the images were then used to measure changes along the three different axes in order to describe volume variations and the recovery pattern during the return to RC. Volume variations that occurred in the passage from MSC to RC were considered indicative of the reverse process.

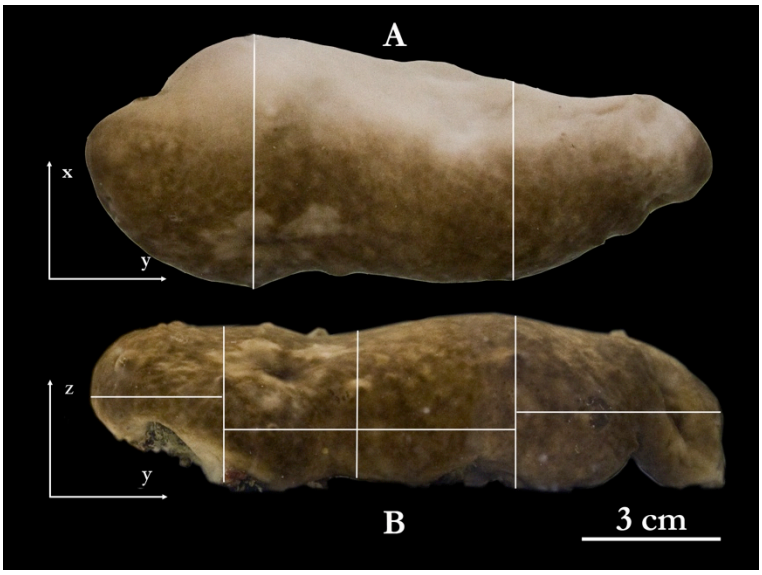

Figure 4. Overhead view (**A**) and frontal view (**B**) of a sponge specimen during the recovery (from MSC to RC) process. **White lines** indicate the measured points.

Isolated tissue samples

In order to determine the main structures/regions affected by the mechanical stimulation, we cut whole sponges vertically into slices of about 2mm in thickness. Each slice was placed in a Petri dish with ASW at RT. Images of the slices where taken soon after the excision and after 4 h using a camera mounted on a stereomicroscope. The images (fig. 5) were used to evaluate dimensional changes of the sponges by appropriate measurements in selected regions using imaging software. In particular we considered changes related to: ectosome (according to x axis); choanosome (according to both x and y axes), small canals (diameter less than 1mm) and large canals. Changes were normalized by expressing

length after 4 h as a proportion of the starting length (length after 4 hours/starting length). Starting lengths were considered in MSC and lengths at 4 h in partially de-stiffened condition (PD).

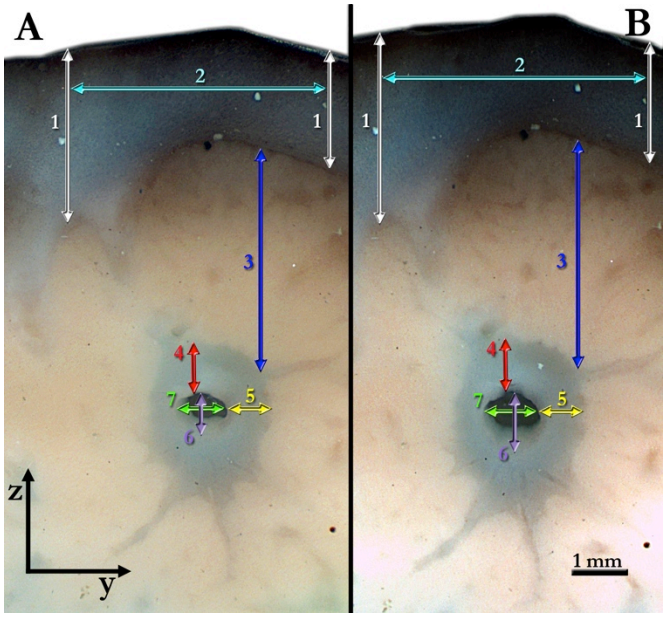

Figure 5. Correspondent images used to evaluate the dimensional changes occurring in different regions. (**A**) condition soon after the cut; (**B**) after 4 h resting in ASW. **1** = ectosome z axis; **2** = ectosome y axis; **3** = choanosome z axis; **4** = canals belt z axis; **5** = canals belt y axis; **6** = canals diameter z axis; **7** = canals diameter y axis.

Isolated ectosome and choanosome samples

Beam-shaped samples, approximately 2x2x10 mm in size, were cut from ectosome (discarding the exopinacoderm) and choanosome regions and soon placed in Petri dishes filled with ASW. Images were obtained using a camera mounted on a stereomicroscope soon after the excision and after 4 h. The images were used to measure, with digital software, changes in sample thickness related to specific and recognizable reference points (fig. 6). One group of ectosome and choanosome samples was placed at 16°C soon after the images acquisition at T0, whereas the other group was kept at RT (26°C).

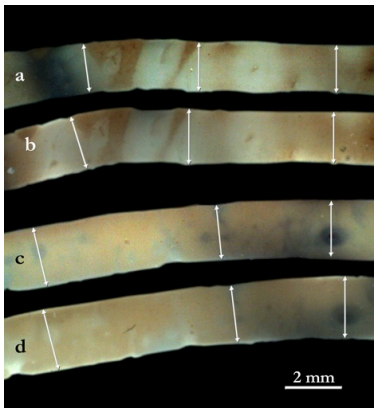

Figure 6. Correspondent isolated beam shaped ectosome (**a**, **b**) and choanosome (**c**, **d**) soon after the cut (**a**, **c**) and after 4 h resting (**b**, **d**). **White lines** show the measured samples references points.

2.4 Methods for morphological analysis

Scanning electron microscopy (SEM)

A sponge specimen was cut in order to obtain a transverse section of a large exhalant canal; a second portion of the sponge was cut horizontally close to the surface in order to obtain about 1 cm^2 of exopinacoderm. Samples have been fixed with (2% glutaraldehyde in filtered ASW) for 4 h at 4°. Fixative has been then removed by washing three times the samples with sodium cacodylate buffer 0.1 M. Then samples have been postfixed in 0.1 M sodium cacodylate buffer + 1% osmium tetroxyde (OsO_4) for 2 h, extensively washed in dH_2O and dehydrated with an ethanol scale before being immersed in hexamethyldisiloxane (HMDSO) for 15 minutes. After two other washes with HMDSO, it has been left to slowly evaporate. Samples have been then attached to aluminium stabs with argentic glue and then a thin (few nanometers) gold layer was deposited over the sample with an electro-sputtering device. Observations have been performed with a LEO 1430 scanning electron microscopy.

Transmission electron microscopy (TEM)

One sponge specimen has been cut in order to obtain samples of both ectosome region and canals. Samples have been fixed in ASW + 2% glutaraldehyde overnight at 4°, washed twice with 0.1M sodium cacodylate for 15 minutes and treated with 1% OsO_4 in 0.1M sodium cacodylate buffer for 2 h at RT. After some wash in dH_2O, samples have been dehydrated with an ethanol scale, washed in propylene oxide and embedded in Epon Araldite© epoxy resin. Samples have been then cut with a Reicher-Ultracut microtome and observed with a Jeol 100SX TEM.

Laser scanning confocal microscopy (LSCM)

Methods of confocal microscopy were employed, namely in order to emphasize the presence of actinocytes elements. Sponges were fixed as described at point 2.4 and embedded in molted paraffin. 20 μm slices where produced by means of a microtome then paraffin have been removed with xylene, slices have been rehydrated and rinsed in 0.1M PBS. 5% normal goat serum (NGS) in PBT (0.1M PBS + Tween 20 0.05%) was added to cover the samples for 1 h in a humid chamber; after five washes in 0.1M PBS rhodamine phalloidin 1.5 mg/ml was added for 30'. After 5 washes in 0.1M PBS the nuclear dye DRAQ5 1 ‰ in 0.1M PBS was added for 1 minute. After some washes in PBS the slices were mounted in PBS-glycerol 80:20 and observed with a Leica TCN-NT laser scanning confocal microscopy. Control samples were treated as treated ones but rhodamine phalloidin was omitted.

2.4.1 Original fixation protocol

Since sponges react to standard fixative protocols by sudden stiffening, an appropriate fixation procedure was requested in order to avoid mesohyl stiffening and compare stiffened condition (SC) with standard resting condition (RC). Six specimens where gently placed in 500 ml beakers with 200 ml ASW and left resting for 3 hour. Sponge mechanical state was then established as described by Parma (2007). Briefly: sponges were placed in a beaker with ASW, then a pressure was generated by a rod shaped weight (contact surface 7.89 mm^2, rod weight 17.5g, generated pressure 21.76KPa), then, after 35 seconds, the deformation was measured on a graduated scale (fig. 7).

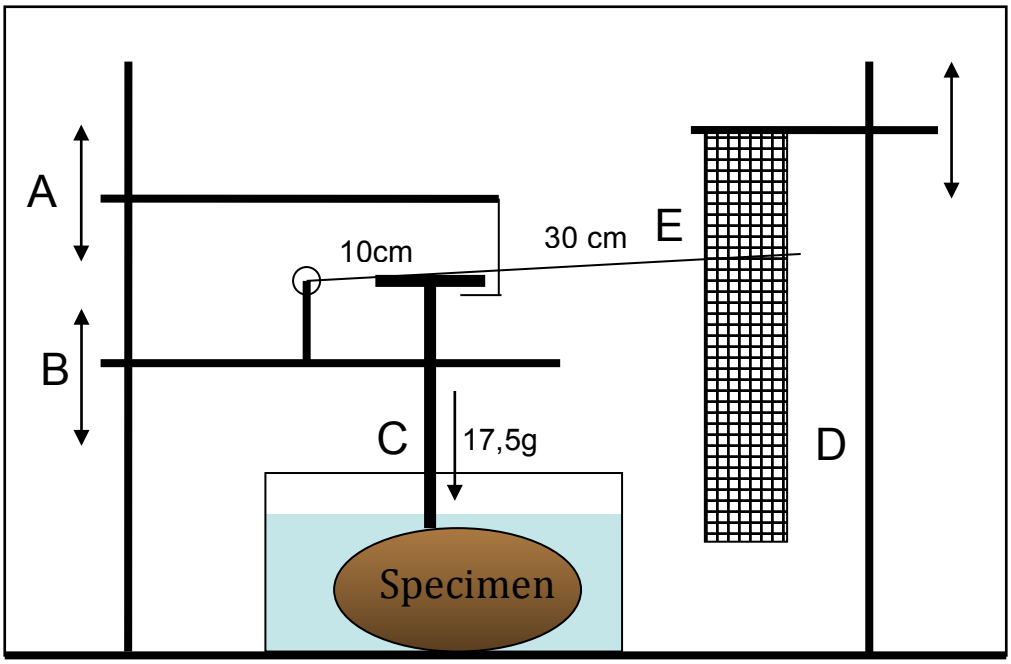

Figure 7. Scheme of the apparatus used by Parma (2007) to evaluate the sponge tensility: **A** = arm used to block the stimulation rod; **B** = arm used to set the starting height; **C** = stimulation rod; **D** = measurement scale; **E** = lever.

After the measurements the six sponges were divided into two groups and left resting for other 3 hours at RT. Sponges to be fixed in MSC were then manually stimulated to induce stiffening while sponge to be fixed in RC were left undisturbed. A solution of 0.4% glutaraldehyde and 8% paraformaldehyde in ASW was then slowly added using a glass pipet according to the following procedure: 2 drops were added near the edge of the beaker every minute until the sponge in RC stop filtering water (it is easy to check on the water surface the flow generated by the oscula). When sponges stop filtering water, 1.5 ml of fixative were added every 2 minutes for 6 times, then the rest of the fixative was added (for each backer 25 ml of fixative solution was used). Sponges were left undisturbed for 1.5 h; after this period all the sponges were transferred into the final fixative solution (0.2% glutaraldehyde and 4% paraformaldehyde in 0.1M Phosphate Buffer Saline, PBS) at 4° overnight. The following day the mechanical properties of the fixed sponges were re-tested as previously described

before cutting and postfixing them with different fixatives according to the method: light microscopy (LM), immunocytochemistry (ICC), transmission electron microscopy (TEM). Possible differences in the tensile state between sponges fixed in RC or SC were evaluated by comparing the total induced deformation obtained before and after the fixative procedures and tested with two-tails t-student test.

2.5 Methods for biomechanical analysis

2.5.1 Standard tests

Beam-shaped samples (2x2x15 mm in size) were cut from both the ectosome (discarding the exopinacoderm) and choanosome regions. Both extremities of each sample were attached to rigid plastic strips using cyanoacrylate cement leaving 10 mm in the middle between the frames. Samples were placed in petri dishes filled with ASW for 4 h before testing them. Samples were subjected to two different experimental conditions: isotonic condition (elongation under constant loads) or isometric condition (forced elongation with different elongation rates).

Isotonic test (creep test)

The lower part of the samples of both ectosome and choanosome were then attached to a fixed hook while the upper part was clamped to the lever of an isotonic force transducer (Harvard apparatus©) connected to an AD Instruments© recording device (fig. 8). On the other side of the lever different loads were attached (i.e, 1, 5, 10 g).

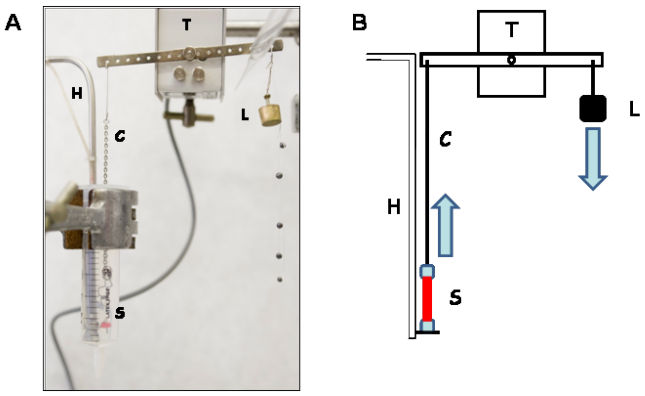

Figure 8. Apparatus set up for calculating sponge viscosity. (**A**) Picture of the system; (**B**) drawing of the system used to record the variation in length of the samples subjected to a constant load. **T –** isotonic transducer, **H –** fixed hook, **S –** sample, **L –** load (1-10 g), **C –** stainless chain

Elongation of the samples was digitally recorded with LabChart© software. During the experiment samples were immersed in ASW. The viscosity was calculated by dividing the rate of elongation in the constant phase by the nominal stress. Three samples of ectosome and three samples of choanosome were prepared from each individual of five sponges. To avoid sampling effects the sequence of the applied loads were conveniently mixed during the experiments.

Isometric test (force-extension)

Beam-shaped samples (0.7x0.7x15 mm in size) were cut and prepared as described in the previous experiments. The smaller size of the samples (compared to creep tests) was chosen since the extension of 2x2x10mm samples generated forces that rapidly exceed the limit of the force transducer. One extremity of the samples was firmly clamped to the isometric transducer by a heart-clip and related stainless steel chain; the other side was then firmly clamped to a hook that could be moved by a micro-manipulator (fig. 9). Through a stereomicroscope it was possible to move the manipulator in order to force the samples to elongate of 0.5mm steps every 2, 5, 10, 15, 20 seconds.

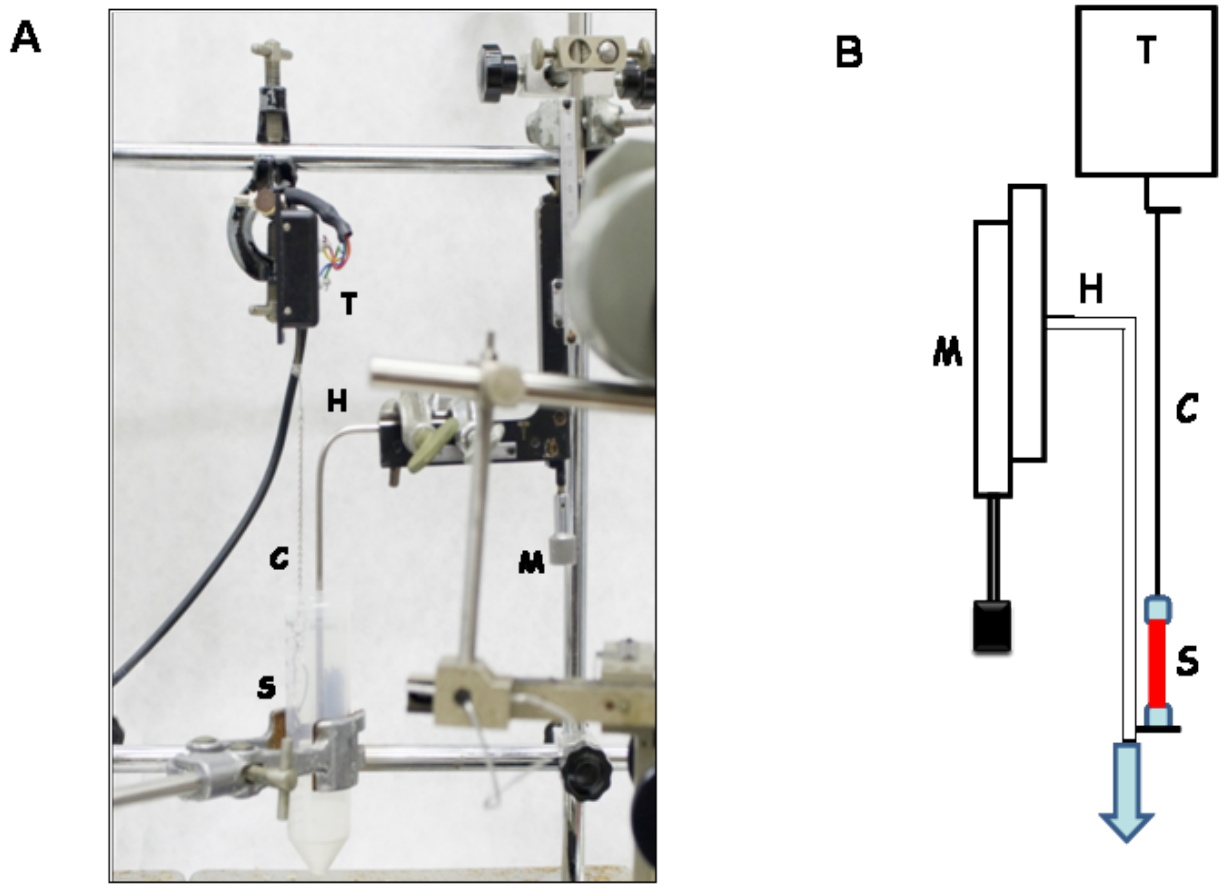

Figure 9. Apparatus set up for the force-extension tests.
A) image of the experimental set up; **B**) schematic drawing of the apparatus.
T = isotonic force transducer, **S** = sample, **H** = fixed hook, **C** = stainless chain, M = manipulator.

When stretched samples resisted to the imposed strain by generating a force that is recorded by the software (fig. 10). Each peak of the force/extension curve was used to generate a stress/strain curve by transforming the force into stress and the extension into strain.

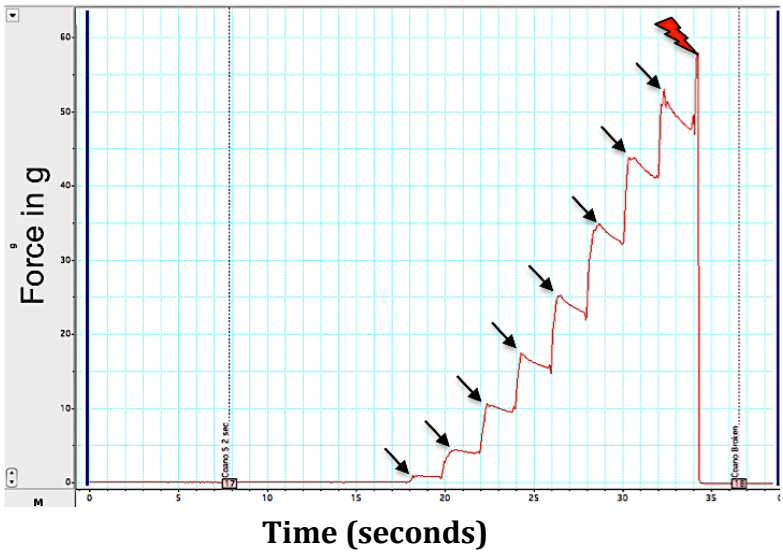

Figure 10. Example of a typical LabChart output during a force-extension test. Each **arrow** indicates the peaks used to build the stress/strain curves. **Red thunderbolt** = samples rupture.

2.5.2 Mechanical stimulation tests

The following experiments were performed by means of a specific experimental set up that allowed us to measure the sponge tensility, producing in the meantime a localized stimulus (fig. 11).

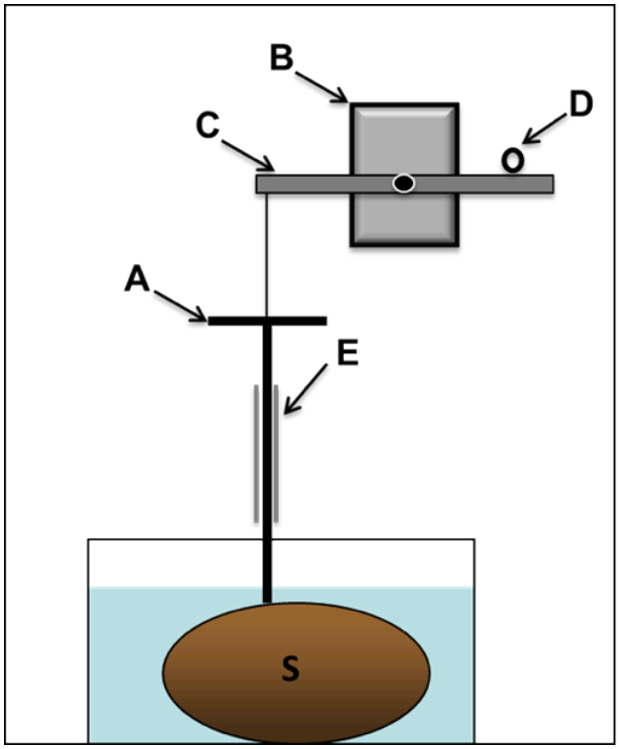

Figure 11. Schematic drawing of the apparatus used to measure sponge tensility and to produce the stimolus. **A** = rod shaped weight; **B** = isotonic transducer; **C** = lever; **D** = blocking device; **E** rails to keep the rod vertical.

This experimental set up was assembled according modifying suitably a previous, more rudimental equipment (see fig. 7) used by Parma (2007) for analogous experiments. The core of the new set up was the introduction of the isotonic force transducer (see paragraph 2.5.1). The concept of the apparatus was to measure the deformation induced by a rod shaped weight (18.9 g, contact surface area 10 mm^2, generated pressure 18.52 KPa) in a fixed time.

Sponge subjected to the pressure generated by the rod underwent a typical deformation curve (fig. 12).

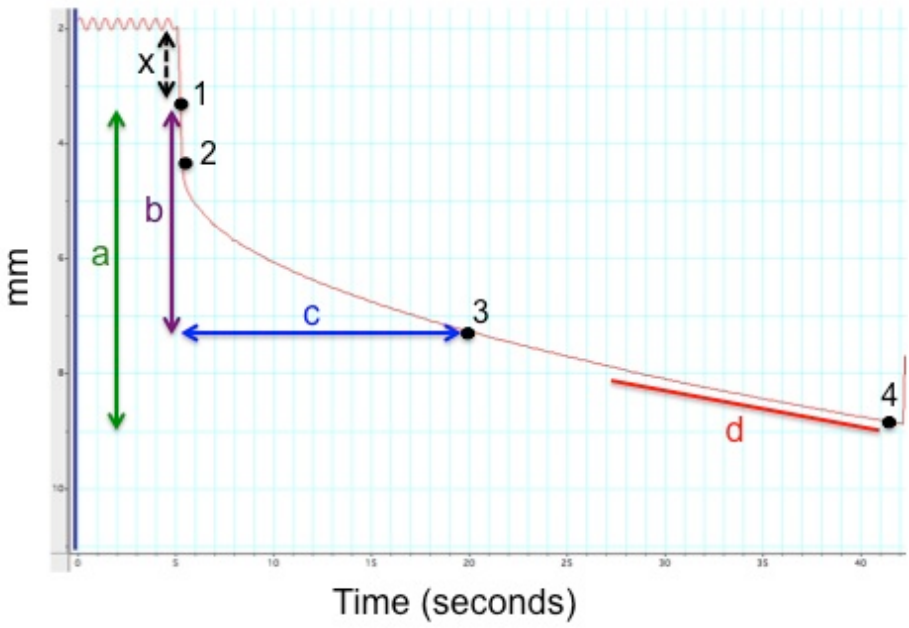

Figure 12. A typical curve obtained in the mechanical test and recorded with LabChart software. After releasing the locking device, the rod reached the sponge surface (**x**). The deformation could be divided into three phases: fast deformation phase (from point **1** to point **2**); decelerating phase (from point **2** to point **3**) and a following period of relative constant deformation speed (from point **3** to point **4**). From the curve it was possible to extract different parameters: (**a**) = total induced deformation (TID), (**b**) = decelerating phase magnitude (DPM), (**c**) = decelerating phase duration (DPD) and (**d**) = constant phase deformation speed (CPS).

After releasing the block device, the rod, kept close to the sponge surface without touching it to prevent stimulations, reached the sponge surface and a first rapid deformation could be observed. Since the speed of deformation in this first phase was often similar to the speed of the free fall of the rod, it is difficult or impossible to distinguish when the rod impacted the sponge surface. After this first phase a decelerating period occurred; at a certain point the speed of deformation reached a rather constant speed. From the deformation curves it was possible to extrapolate four different parameters: the total induced deformation (TID), the magnitude (DPM) and the duration (DPD) of the decelerating phase and the speed of deformation in the constant phase (CPS).

2.5.3 Analysis of the parameters extrapolated from the deformation curves

Ten sponges were placed in small containers filled with ASW and left resting for 4 hours before being tested. Before carrying out the tensility measurements (as described at point 2.5.2), a frontal picture of the specimen was taken in order to obtain the overall thickness of the sponges referred to the point where the tensility measurement was later performed (fig. 13).

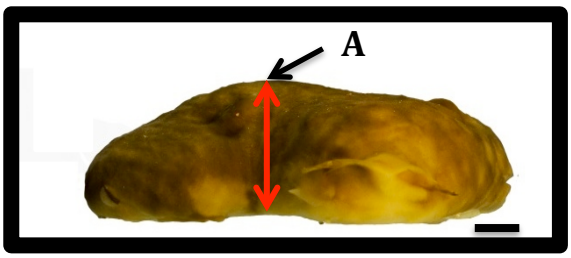

Figure 13. Sponge image immediately before measuring tensility. Overall thickness (**red line**) was calculated in the exact point (**A**) where tensility measurements were later performed. Bar = 1 cm.

These measurements were plotted against the values of the four parameters obtained from the curves in order to check the independence of these latter from the sponge thickness. The statistical analyses (Pearson test) have been performed with Graphpad©. The most independent parameter was the speed of deformation in the constant phase (CPS) (details of the analyses will be provided in paragraph 3.7.1). Sponge stiffness resulted to be inversely proportional to the speed of deformation in the constant phase.

2.5.4 Stiffening response to mechanical stimulations

Twelve sponges were placed in small aquaria and left resting for 4 hours. Sponge were then gently transferred on a desk and subjected to the treatment: treated samples were manually stimulated by leaning on the sponge surface the hand palm for 5 seconds, whereas in control samples the stimulation was omitted. Then sponges were soon transferred into the experimental tank where tensility have been measured as describe above. Measures were done after 20 seconds, 1 minutes or 3 minutes after replacement of the sponge in the tank. The treatments sequence was mixed in order to avoid sampling effects during the three days test.

2.5.5 Stiffening signal transmission

Seven sponges were placed in small tanks containing ASW at RT for 4 h before being tested as described above. A summary of the experiments is given in figure 14. The first measurement (A) was considered to reflect the basal mechanical state of sponges in RC. After the first measurement we subjected the sponge to three impacts (impact speed 0.54 m/s, impact energy 1.44 J) by raising the rod 3 cm above the sponge and allowing it to drop freely. According to this procedure a second

measurement (B) was taken at 1 cm from the first (A). Other three impacts were then applied at the B site, and a third measurement at point (C) 4 cm from B, and a fourth measurement at point (D) equidistant between B and C were performed (fig. 14). To induce a state of maximal stiffness, the animal was then strongly stimulated by pulling it several times, and then a fifth measurement (E) was made at the same point D. Measures A, B, C and D were all performed within 3 minutes.

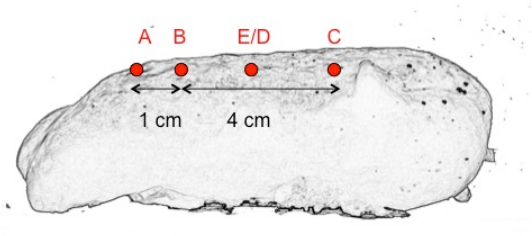

Figure 14. Scheme of the distribution of the stimulation points (**red dots**) on the sponge body.

In addition, in order to explore the possible role of the exopinacoderm in the signal transmission, the following experiments were performed: six sponges were collected from the aquaria and, once obtained the MSC by squeezing them, were left undisturbed for 7 h before being tested in glass container filled with ASW. After the sponges reached the RC we tested the mechanical properties as described above. Figure 15 give a summarized view of the experiment topology. A first reference measurement, representative of the RC value, was performed in a selected point (A); then the same point A was stimulated by 50 g weight (contact surface 0.78 cm^2, generated pressure 6.3 KPa) for 5 seconds; after 20" another measurement was taken at the same point (A') to check the individual stiffening capability of each specimen. Other measurements were taken at 1 cm on the right of the weight edge (B), and at 2 cm on the left of the weight edge (C) (fig. 18).

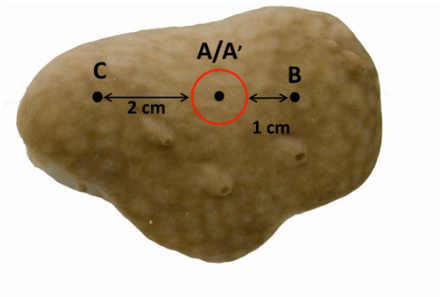

Figure 15. Top view of the distribution of the stimulation points (**black dots**). **Red circle** = edge of the weight used to stimulate the sponge after measuring the tensility at point A.

The following day the same individuals have been used to evaluate the possible role of the exopinacoderm in the conduction mechanism. The sponges were stimulated up to reach the MSC and a

strip of exopinacoderm was removed just around the area where the first measurement was performed (fig. 16). After 7 h the same procedure described in the paragraph above was repeated.

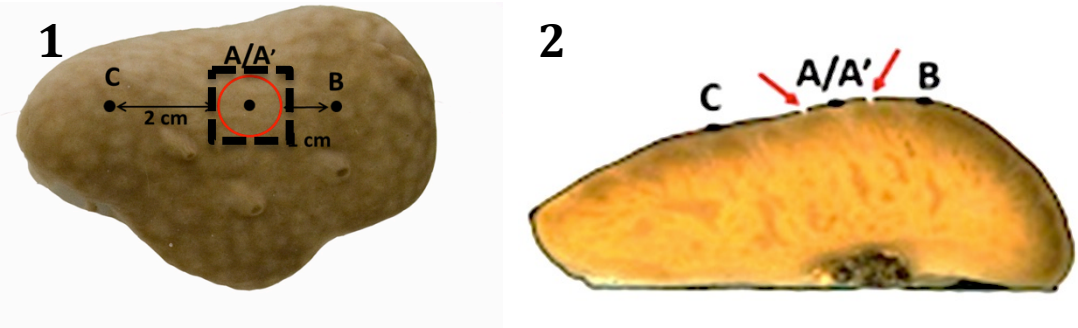

Figure 16. (**1**) top view of the sponge stimulation points. **Black dot** = edge of the rod used to measure sponge tensility. **Red circle** = edge of the weight (50 g) used to stimulate the sponge after measuring the tensility at point **A**. A small strip of ectosome (including exopinacoderm) was cut along the perimeter of the **broken line rectangle**. (**2**) Sponge vertical section highlighting the removal of the exopinacoderm (**red arrows**) and the reference points.

2.6 GABA and Glutamate tests

2.6.1 Immunocytochemistry

Fluorescence methods

Sponge fragments were fixed as describe at 2.4. A special mixture (i.e. 4% paraformaldehyde, 1% glutaraldehyde) was used to postfix samples for glutamate detection due to specific requirement of the primary antibody. Samples were extensively washed in 0.1M PBS, dehydrated and paraffin embedded (melt fusion 56°) in order to cut 15 μm slices with microtome. Paraffin was removed with xylene, slices were then rehydrated and put in 0.1M PBS. 5% normal goat serum (NGS) in PBT (0.1M PBS + Tween-20 0.05%) was added to cover the samples for 1 h in a humid chamber; after five washes in PBS the primary antibodies (Sigma Anti-GABA polyclonal produced in rabbit, Sigma Anti-Glutamate polyclonal produced in rabbit) was added. Anti-GABA antibody was diluted 1:200 in PBT + 5% NGS, Anti-glutamate 1:50 again in PBT + 5% NGS according to the datasheets instructions. After an overnight incubation at 4° and some washes in 0.1M PBS, samples have been covered for 1 h with a 1% solution of bovine serum albumins (BSA) in 0.1M PBS. The secondary antibody (Sigma anti-rabbit IgG-FITC or IgG-TRITC produced in goat) was diluted 1:300 in 1% NGS in PBT and left overnight at 4°C at dark. After several wash in 0.1 M PBS samples have been treated by adding the nuclear staining DRAQ5 1:1000 diluted and mounted in 20% glycerol and 80% 0.1M PBS. Some samples (previously treated with FITC secondary antibodies), before the nuclear staining, have been treated with rhodaminated phalloidin (1,25 mg/ml) for 30' and washed 5 times in 0.1M PBS in order to label actin molecules. Samples have been then observed with a Leica TCN-NT laser scanning confocal

microscopy (LSCM). In control samples the primary antibodies was omitted and used to set the background noise.

Immunogold methods

RC and MSC sponge fragments, prepared as described at paragraph 2.4, after some wash in 0.1M PBS were dehydrated with an ethanol scale and then embedded in LR White© acrylic resin. Thin sections (about 90nm) were produced with a Reicher-Ultracut microtome and placed on gold grids (300 mesh). Thin sections have been then treated for 10 minutes with glycine 0.05M in 0.1M PBS, 20 minutes with PBT supplemented with 2% NGS and 0.2% BSA and washed twice with incubation buffer (PBT + 0.2% BSA + 15mM NaN3, pH 7.4). The primary antibody (Sigma Anti-GABA polyclonal produced in rabbit) was diluted 1:25 in the incubation buffer and added on grids for 1 h at RT in a humid chamber. After six washes with incubating buffer the secondary antibody (Abcam goat anti rabbit IgG-18nm colloidal gold) was dilutes 1:40 in incubation buffer and added for 1 h in a humid chamber; after five washes the slices were post-fixed for 5 minutes with 2% glutaraldehyde in 0.1M PBS. After two fast washes in distilled water the samples were contrasted with a saturated solution of uranyl acetate for 15 minutes, and for 5 minutes with lead citrate solution. Samples were then observed with a LEO 912AB TEM or a Jeol 100SX TEM. In control samples the primary antibody was omitted.

2.6.2 Volume recovery tests on isolated slices

Isolated slices, 2.5 mm thick, were cut vertically. Each slice was then placed in a Petri dish filled with ASW or ASW GABA 2mM or Glu 2mM and a picture was soon taken using a camera mounted on a stereomicroscope. After 4 hours other images of the slices were obtained in order to evaluate any possible expansion occurred in different regions according to the different axes (see fig. 5). The expansion was calculated by comparing the changes on correspondent reference points selected on the base of the "topography" of the slices.

2.6.3 Expansion/contraction tests

Whole mount preliminary experiments

Preliminary experiments for evaluating the effects of 2mM GABA and Glu were carried out by placing three sponge in three 2L tanks filled with ASW, and kept at 16°C, oxygen supply was provided by an aquarium bubble maker during all the experiment. Frontal view images were taken every 5 minutes for about 9 h. After 2 hours three different tests solutions were added into the tanks: the first and the second one contained the amount of GABA and glutamate (both in ASW) needed to reach, once poured in the tanks, a final concentration of 2mM; the third solution was ASW only. After the addition of the test-solutions the sponges were left undisturbed for 4 hours, then all the water of the three tanks

was replaced with new ASW and the sponge were left rest for other 4 hours. The images were used for creating a time-lapse movies: possible dimensional changes induced by the treatments were calculated by means of Photoshop© ruler tool by comparing the images before the treatments and after 15' (see fig. 3). In order to evaluate possible toxic effects of GABA and Glu, the occurrence of contraction/expansion cycles was checked in the hours following the water replacement.

Whole mount: biomechanics experiments

In order to better evaluate the amount of contraction and the force generated during the contraction/expansion cycles we designed a new experimental set up using both isotonic and isometric transducers (fig. 17). Both the force transducers were plugged to an AD instrument recorder device via pre-amplifiers. All the data originated from the mechanical tests were recorded with Labchart 7 software (fig. 18).

Two plastic pieces (1.5 x 1.5 mm) placed at 1 cm distance from one other (fig. 17) were attached to the specimen nearby the osculum using cyanoacrilic cement. Each plastic piece was connected by a cotton thread to one force-transducer. Sponges were then placed in a small aquarium filled with 5 L ASW at 19°C and oxygen provided with a bubble maker. Water temperature was maintained stable during all the experiments. The isometric transducer was lifted with a micromanipulator until the force generated reached a force of 0.15g in order to prevent that the expansion occurring in the beginning could mask part of the force generated during the experiments. Sponges were left undisturbed for 24 hours, then a concentrated solution of GABA or Glu in ASW was added to reach a final concentration of 1mM; in the controls only ASW was added. After the addition of the test solutions sponges were left undisturbed for other 24 hours.

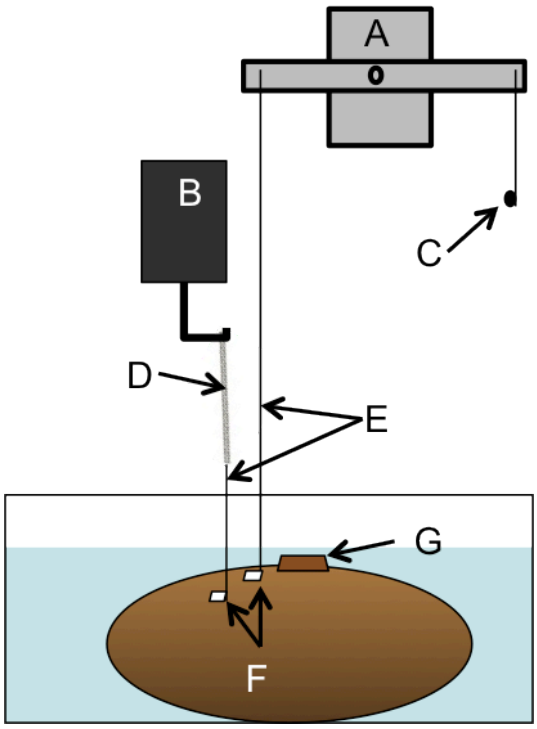

Figure 17. Schematic drawing of the apparatus used to measure the changes in thickness and the force generated by the contraction/expansion cycles. **A** = isotonic transducer; **B** = isometric transducer; **C** = counterbalance weight; **D** = soft spring; **E** = cotton threads; **F** = plastic plates; **G** = osculum.

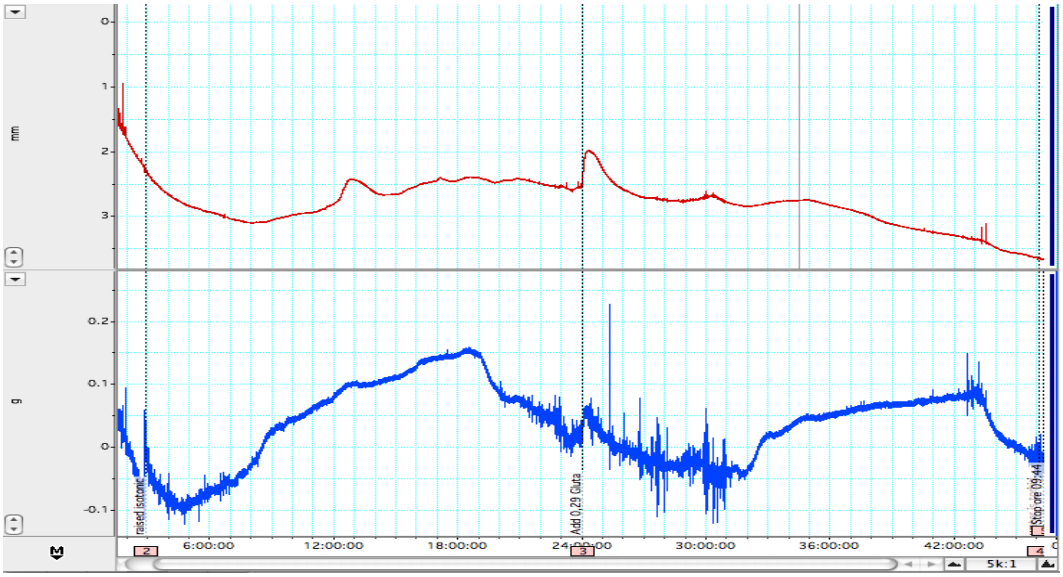

Figure 18. Example of LabChart output during a 48h test with both isotonic (**red line**) and isometric (**blu line**) signals.

2.6.4 Viscosity tests on isolated samples

Isolated samples of both ectosome and chanosome were prepared as describe at point 2.5.1. In these experiments we left the sponge to elongate under a constant load (5 g) for five minutes, then the solution in which the samples were kept during the experiment (ASW) was replaced with ASW only (control), GABA (500µM, 2mM) or glutamate (500µM, 2mM) both in ASW and left free to elongate for

25 minutes. The possible effects of the treatments were evaluated by comparing the elongation speed (inversely proportional to viscosity) before and after the treatments at different endpoints (fig. 19).

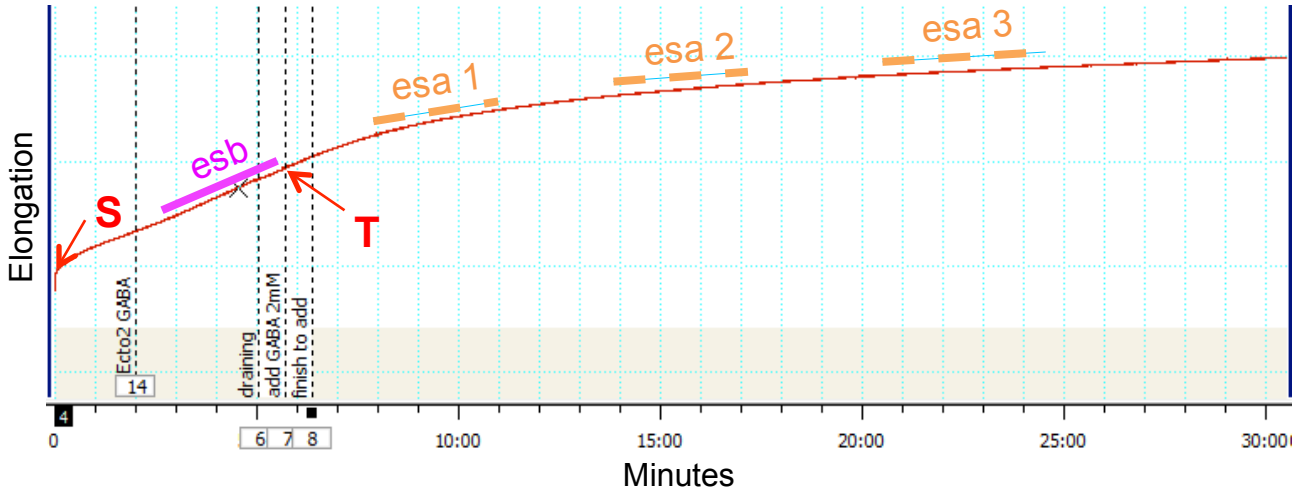

Figure 19. Elongation curve during a 30 minutes creep tests. After the blocking device is released (**S**) samples undergoes elongation. A first measure of the elongation speed (**esb**) was obtained before replacing the solution with the new one (**T**). Subsequent measures of the elongation speed (**esa 1, 2, 3**) were performed at different end points.

2.7 Biochemistry of mesohyl component

2.7.1 Protein fraction extraction

One sponge was collected from the aquaria and rapidly immersed in liquid nitrogen. The sponge was then thawed and weighted; the specimen was cut into small pieces and blended with the addition of EDTA 0.1 % in 0.1M PBS (sponge/medium ratio 1 g : 2 ml). After four freeze (-80°C) and thaw cycles the homogenized solution was centrifuged at 4°C for 30' at 4500rcf in order to eliminate most of the cells and organic materials; the supernatant underwent a second cleaning centrifuge at 16.100rcf for 1h at 4°C and then subjected to a salting out procedure using ammonium sulphate (AS) to roughly separate proteins on the basis of their hydrophilic properties. Briefly: a saturated solution of ammonium sulphate was gradually added to the protein solution to reach 40% of AS; the mix was then centrifuged at 12.100rcf for 10' at 4°C, the pellet (containing both protein precipitated and AS) was resuspended in dH_2O (1/3 of the initial volume was added in order to bring the proteins at the physiological concentration); the supernatant was used to yield protein at 50%, 60%, 70% and 80% with the same procedure described above. Each protein solution, that we call PX (e.g., P40 for proteins yielded at 40% AS, P50 for protein yielded between 40% and 50% AS, and so on) was then dialyzed with a SpectraPore© 4 membrane in dH_2O or ASW. Three dialysis cycles were done: each cycle lasted for 3 hours at 4°C, dialyzing buffer ratio of 1:1000. The dialyzed proteins were then store at -80°C until used. A stock of elution buffer of P80 (both ASW and dH_2O) was stored at -80°C for using it as a control in further experiments.

2.7.2 Testing the protein fraction on isolated ectosome samples

Beam-shaped samples approximately 2 x 2 x 15 mm in size were cut from the ectosome region using parallel-mounted razor blades. In each sample, two opposite long sides were roughly parallel to the external body surface, whereas the other two long lateral sides were orthogonal with respect to the external surface. Samples included no exopinacoderm.

Each sample was fixed to a glass coverslip using cyanoacrylate cement, a 'lateral' surface being in contact with the coverslip and with exactly a 10 mm portion projecting from the edge of the coverslip. This orientation was chosen to minimise variability caused by the slow bending of ectosome samples, which occurred only in a plane orthogonal to the external surface (Parma, 2007).

Tissue extract on RC samples

Ectosome samples were then transferred into Petri dishes containing ASW and left undisturbed for 6 h to reach the RC. A first measurement of sample tensility (T0) was performed by placing the samples horizontally; after 35 seconds a picture was taken, sponge tensility was inversely proportional to the occurred bending. Images were used to measure (with Photoshop© ruler tool) the bending magnitudes (fig. 20).

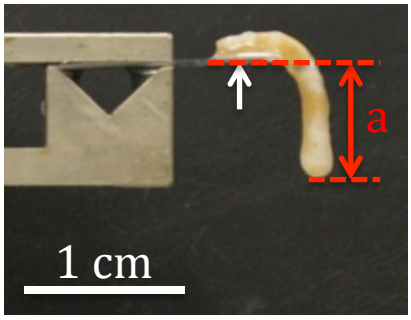

Figure 20. Image of the bending apparatus used to establish the mechanical state of isolated tissue samples. The **white arrow** indicates the glass coverslip where the sample was attached by cyanoacrilic cement. **a** = deflection magnitude.

Samples were transferred to and from test solutions by gripping the coverslip with forceps, never by gripping or touching the tissue itself. After the first measure, each sample was transferred into the different solutions: ASW + dialyzing buffer used for P80, ASW + P40, ASW + P50, ASW + P60, ASW + P70, ASW + P80. The ASW/dialyzing buffer or proteins ratio was 2:1, proteins stocks were all dialyzed in ASW and the final concentration was similar to that of the sponge tissue. A second and a third measure of samples tensility were carried out after 1 and 2 h.

Tissue extract on PD samples

A similar experiment was performed on PD ectosome. Here we left the samples destiffening only for 3 h before transferring them into ASW, ASW + P40 and ASW + P50. Tensility was calculated as describe above. The protein stocks used were dialyzed against ASW and the ratio was the same of the previous experiment. Measurements were carried out 1, 2 and 3 hours after the immersion in the proteins/control solutions.

2.7.3 Collagens extraction

Ectosome and choanosome collagens

Protocol A: 5 grams of extosome/choanosome were cut from a thawed sponge. Collagens were extracted following Matsumura (1974) protocol. Ectosome was cut into small pieces (2 x 2 x 2 mm) and placed in 50 ml of disaggregating solution (DS, 0.1 M Tris-HCl, 0.1 M β-mercaptoethanol, 0.05 M EDTA, 0.05 M NaCl, pH 8.0) for 3 days on a vertical rotor. The collagen suspension (CS) was then filtered with a nylon mesh and then extensively dialyzed (2 dialyzing buffer changes every 3 h and one overnight, collagen solution/dialyzing buffer ratio 1:1000) against dH_2O or ASW. Collagen was then partially cleaned from exogenous materials by centrifuging it for 10 minutes at 1000rcf. A second cleaning step was performed by centrifuging the CS for 30 minutes at 4500rcf, the supernatant (approximately 40 ml) was discarded and the bottom (a dense solution of collagen) diluted by adding 40 ml of ASW/dH_2O. The procedure was repeated three times, then the supernatant was removed and the collagen have been stored at 4°C until used.

Protocol B: 5 grams of sponge were put in acetic acid 1 M (50 ml) for 3 days. The insolubilized pieces were discarded and the supernatant centrifuged at 2000rcf for ten minutes. The supernatant was then discarded and the pellet resuspended with 40 ml of dH_2O. Other two cycles of centrifugation/resuspension were applied then the pellet have been resuspended in dH_2O/ASW and stored at 4° until used.

Echinoderms collagens*

Collagen from the peristomial membrane of the common sea urchin *Paracentrotus lividus* Lamarck, 1816 was extracted according to Matsumura (1974). Briefly: peristomial membranes, that are composed by a collagenous tissue-MCT MCT (Wilkie et al., 1993; Bonasoro et al., 1995), were explanted from the sea urchins, cut into small pieces and put into DS (1.5 ml/peristomial membrane) on vertical rotor for 48 h at RT. The suspension was then filtered with nylon mesh and dialyzed with a SpectraPore© 4 against EDTA 0.5 M for 3 h and after against dH_2O for at least 3 h. The suspension was then dried into silicone molds to obtain collagen biofilms that were stored at -20°C until used.

*Appropriate amount of echinoderm collagen were generously provided by Dr. Cristiano di Benedetto.

Rat uterine cervix collagens

Three uterine cervixes were explanted from dead rats, cut and placed in DS for three days on vertical rotor at RT. The collagen suspension was then dialyzed three times for 3 hours at 4°C (dialyzing buffer/CS 1000:1) with a SpectraPore© 4 and store at 4°C until used.

2.7.4 Collagen aggregation tests with sponge factors

In order to test the capability of P40 to aggregate collagen fibrils, 250 µl of different CS in ASW have been exposed to 250 µl of P40 in dH_2O. In a first control well 250 µl of dH_2O was added to CS; in a second control well 250 µl of P40 were mixed with 250 µl of ASW. Images of the different samples were obtained through a stereomicroscope camera-mounted at different time endpoints. The possible effects of the different treatments were evaluated in terms of collagen fibrils aggregation.

In order to test the possible dose dependent effects of P40 and to verify the nature of the presumptive stiffening factors (SF) (in particular a possible enzymatic activity) we mixed 250 µl of echinoderm CS in ASW (8mg/ml) with different quantity of P40 (400, 200, 100 µl), and with 400 µl of boiled (5 minutes at 100°) P40. Images were obtained before and 1, 10, 60 minutes after adding the proteins. A control wells was prepared by adding 100 µl of dH_2O.

In order to checking the role of different ions in the aggregation phenomena, aggregation tests were performed by mixing 50 µl of sponge ectosome CS in dH_2O with 50 µl of P40 in dH_2O and placing the plate on orbital shaker for 5 minutes at 100 rvm. Then 50µl of 100 mM NaCl, $MgCl_2$ or $CaCl_2$ were added to the plates. In the controls the same amounts of salt solutions was added to a mix of 50 µl of dH_2O with 50 µl of P40 or ectosome CS. After five minutes the plates were gently shaken and the effects were evaluated on the basis of the presence of fibril aggregates. An estimation of the aggregated collagen was obtained by transforming the images into black and white and by analyzing the white density (collagen) with ImageJ Integrated Fluorescence (IF) tool. Control wells were used to calculate the background IF. The IF values were then plotted against the added P40 quantities.

2.7.5 Preliminary biochemical characterization of presumptive stiffening factor(s)

2.7.5.1 SDS-Page of the different fraction obtained via salting-out

The proteins present in the five fractions obtained through the salting-out technique (paragraph 2.7.1) have been visualized by running 16 µl of the different fractions in a 4-20% bis-acrylamide SDS-Page (stained with Brilliant Blue Coomassie).

2.7.5.2 Second purification step

In order to determine the molecular weight (MW) range of the stiffening factor we separate the fraction P40 in three different sub-fractions by means of Millipore Amicon© tubes. We obtained three

proteins stock containing the protein with a MW higher than 50 kDa, between 50 and 30 kDa and smaller than 30 kDa. The three different fractions were resuspended in a same volume of dH_2O. An aggregation assay was used to verify which fractions showed activity. For this test we mixed 50 µl of ectosome CS (2.7.3 protocol A) with 50 µl of each sub-fractions and 50 µl of $CaCl_2$ 100mM. Again the presence of the stiffening factor was verified on the base of the capability of each fraction to induce aggregation. The sub-fraction that demonstrated activity was also run in SDS-Page.

2.7.5.3 Blue Native Page

The proteins present in P40 were run in native conformation in order to separate them and test the bands obtained with the aggregation assay. Blue Native Pages (BNP) were prepared according to Witting and coworkers (2006). Briefly: two 8% Bis-acrylamide pages were prepared in Tris-HCl 1.5M pH 7.4 with two different amount of Triton-X: the first one containing 0.1% and the second one 0.3%. Stalking gels were both prepared in Tris-HCl 0.5M pH 6.8 with respectively 0.1% and 0.3% Triton-X. 400 µl of P40 were mixed with 400 µl of sample buffer 2X (2.5 ml Tris-HCl 0.5M pH 6.8 + 2 ml glycerol + 5.5 ml dH_2O + 80 µl Ponceau S 5%) and 3.2 µl of Coomassie 5%; two different amount of Triton-X were added to reach a final concentration of 0.1% and 0.3%. The running buffer was prepared by mixing 14.4 g of glycine and 3 g of Tris in 1L of dH_2O. Gel was run in ice at constant voltage (170 mV) for 5 h.

The bands obtained from the BNP were cut using a sterile scalpel, washed twice for 10' in dH_2O and then reduced to a mush by means of a sterile iron-steel spatula under a sterile cabin. Each smashed gel was placed into a 2 ml tube and 450 µl of dH_2O were added before placing it on vertical rotor at 37°C for 24 h. The tubes were then centrifuged at 15.000rcf for 10' and the supernatant divided into two tubes one containing about 350 µl and the other one 60 µl.

350 µl of recovered protein solution were then used for an aggregation assay. In a 24 multiwells plate 50 µl of ectosome CS were mixed with 100 µl of $CaCl_2$ 100mM and the supernatant obtained from each band extraction. After 5 minutes on orbital shaker images were obtained with a camera-mounted stereomicroscope.

The rest of the supernatant recovered from the bands (60 µl) was dried in a Speed Vac. The proteins were then resuspended in 25 µl dH_2O, run on 8% SDS-page.

Results

3.1 Rhythmic contraction/expansion

The presence of contraction/expansion cycles was evident when watching the accelerated movies obtained trough digital time-lapse technique (See movie 1, 2, 3). Both the periodicity and the contraction pattern appeared to vary in each individual. During the observation period some specimen exhibited two complete cycles, whereas in other specimens a complete cycle could not be observed (movie 4). Although the contraction events generally involved the entire sponge, it appears that sponges could to contract only half or part of the body (movie 3). The observed "contraction-like" waves that crossed the sponges reduced the sponge thickness of only few millimetres; the comparison between maximally expanded sponges and maximally contracted sponges showed that contraction magnitude vary according to the considered sponge region (fig. 21).

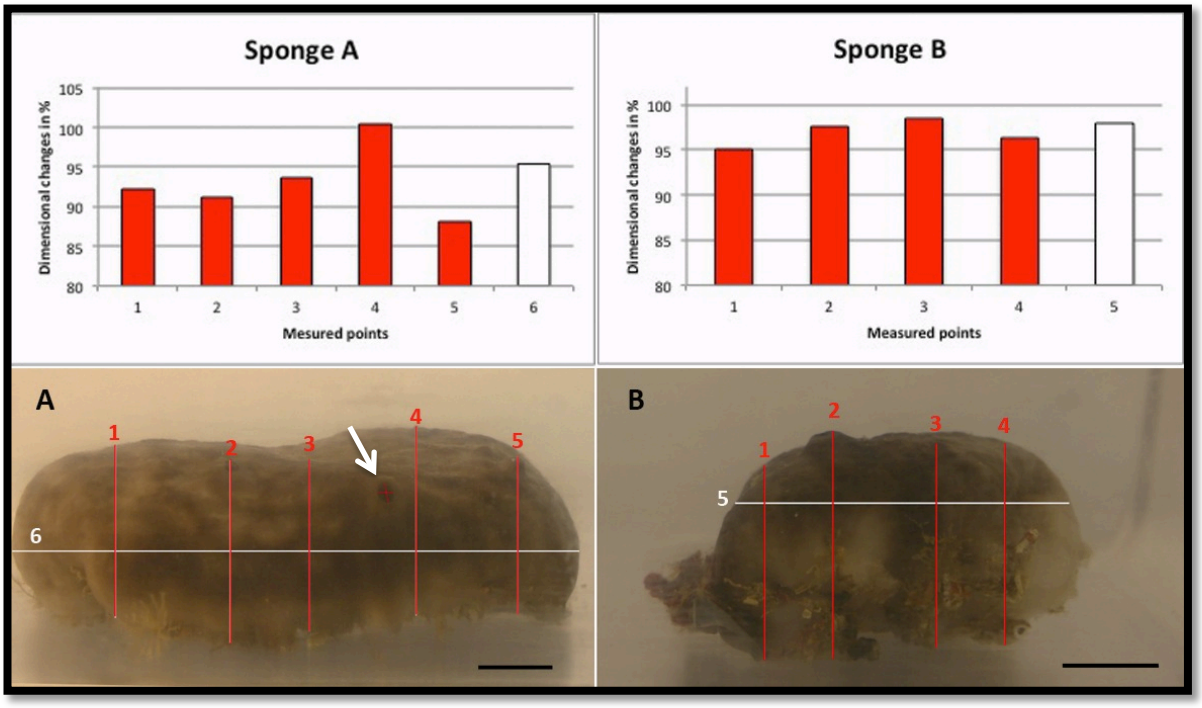

Figure 21. Dimensional changes occurring between maximum expansion/contraction. In the graphs each bar represent the percentage lengths of the selected measured regions (**red** and **white lines A**, **B**). In sponge **A** it was possible to measure the change in the projected area of the osculum (**white arrows**): at the maximum contraction the osculum area was 77% of the maximum value recorded before contraction. Bar = 1 cm.

Occasional observations of simultaneous contraction events of different specimens can be seen in movie 2, 2a and 3.

3.2 Return to RC

Whole mount

One hour after stimulation remarkably dimensional changes were recorded, significant length increases occurred along all the axes (fig. 22). Most of the length and volume increases appeared to occur within the first hour and between the second and the third hour after stimulation (fig. 22, 23).

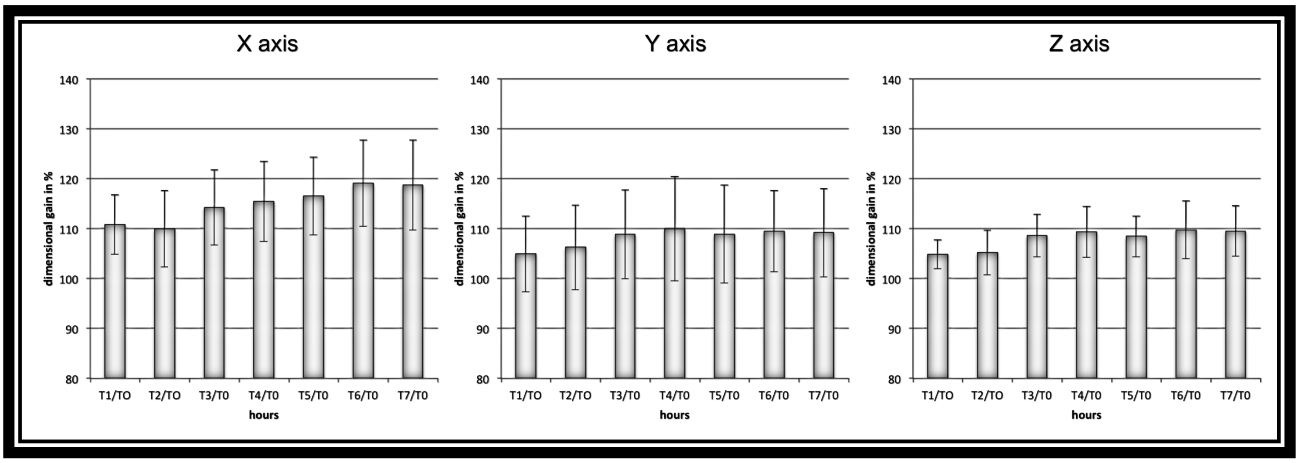

Figure 22. Percentage lengths variations along the three axes during the return from MSC to RC. Except for T1 Y axis ($p<0.05$), all the other endpoints show a highly significant ($p<0.001$) length increase in respect to T0. Statistically significant variation within the endpoints is present between the second and the third hours in the X and Z axes. Statistic test = paired t-student. Bars = standard deviations. N = 9 (X axis); 12 (Y axis); 11 (z axis).

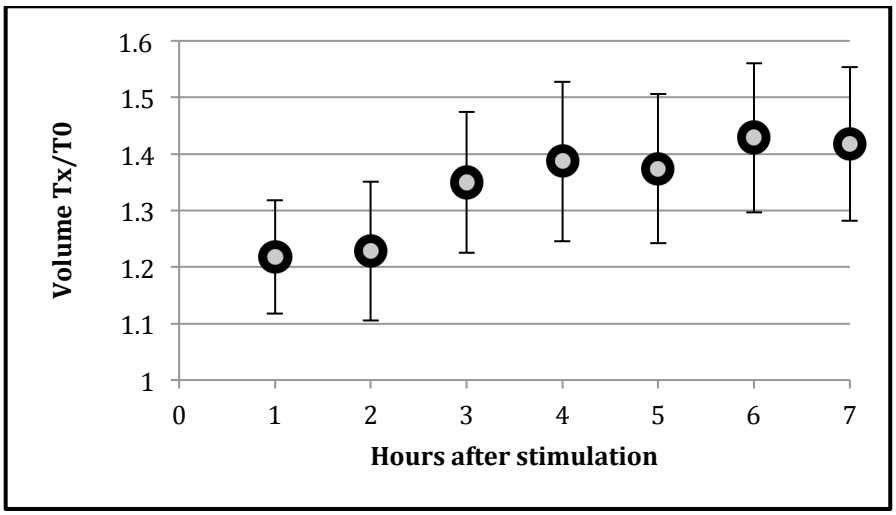

Figure 23. Theoretical relative volume recovery. In respect to T0 all the endpoints are highly significant (paired t-test; $p<0.001$). Most of the volume recovery occurred within the first hour ($p<0.01$, paired t-test) and between the second and the third hour ($p<0.05$, paired t-test).
Bars = standard deviations. N=4.

Most of the volume variations were given to higher length variations occurring along the X-axis that underwent a much more pronounced expansion in respect to Y and Z-axis (fig. 24).

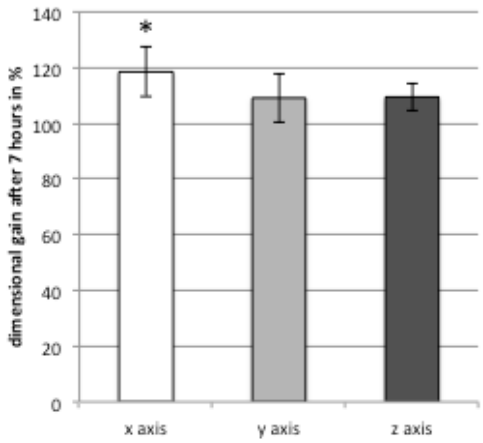

Figure 24. Percentage mean length increases along the three axes after seven hours. X axis recovery is significantly different from that of the other two axes. Two tailed t-test: * = $p<0.05$. Bars = standard deviations. N = 9 (X axis); 12 (Y axis); 11 (z axis).

Isolated tissue samples

Cutting the sponge produced a length reduction of different regions. After four hours significant length variations occurred mostly along the Y-axis (fig. 25). Significant length increases in Y-axis involved the ectosome and the choanosome, and also both small and large canals; there were no significant variations in the canal belts, whereas a significant increase in the X-axis was observed in the large canals.

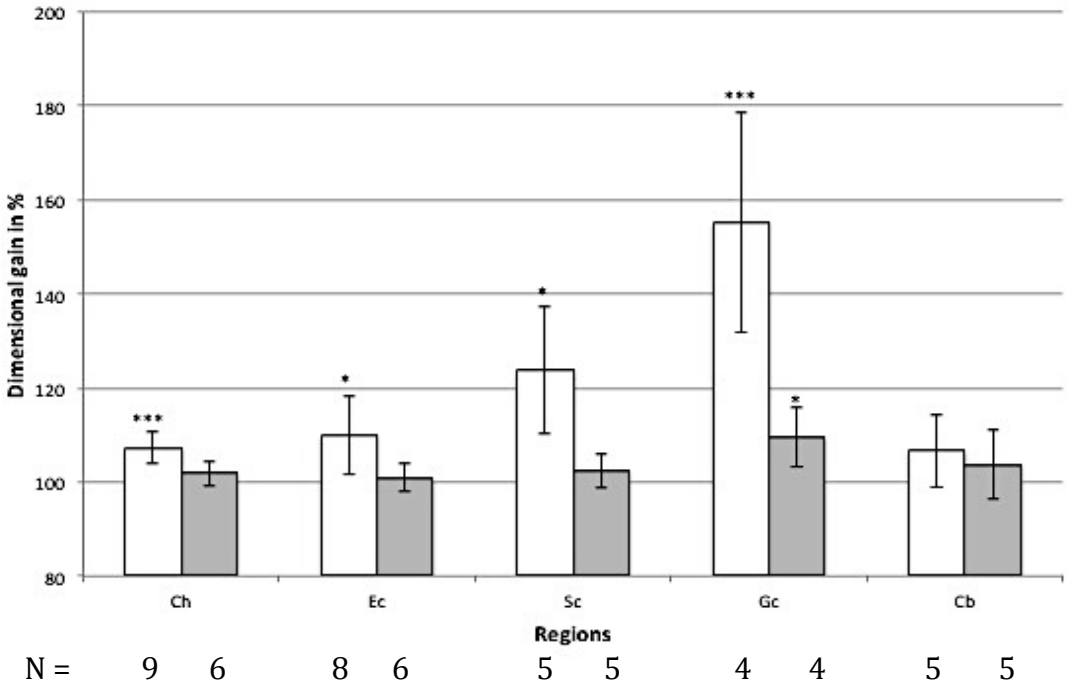

Figure 25. Percentage mean length variations of different sponge regions 4 hours after the cut. **White columns** = Y-axis; **grey columns** = X-axis; **Ch** = choanosome; **Ec** = ectosome; **Sc** = small canals; **Gc** = large canals; **Cb** = canal belts.
Paired t-test: * = $p<0.05$; *** = $p<0.001$. Bars = standard deviations.

Isolated ectosome and choanosome samples

As also shown in our recent pubblication (Sugni et al., 2013) both ectosome and choanosome increased their size after the cut when left undisturbed for 4 hours at 26° in ASW (fig. 26, 27). Samples left resting at 16° showed different responses, only choanosome samples significantly increasing their size (fig. 26, 27).

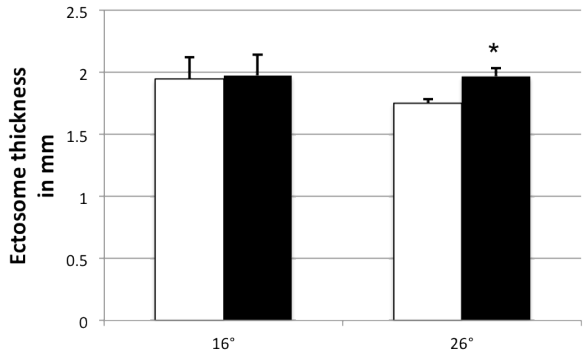

Figure 26. Ectosome thickness soon after the cut (**white columns**) and after 4 hours (**black columns**) in ASW at 16° or 26°. Paired t-student test: * = $p<0.05$; N = 5.

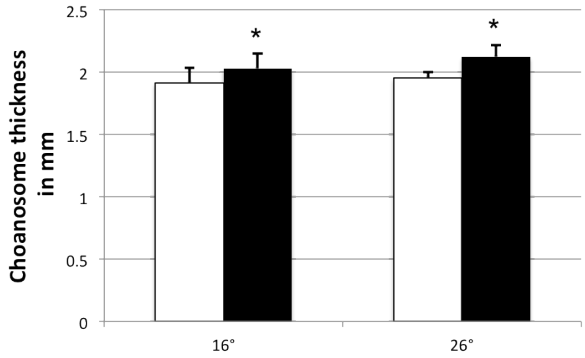

Figure 27. Choanosome thickness soon after the cut (white columns) and after 4 hours (**black columns**) in ASW at 16° or 26 degrees. Paired t-student test: * = $p<0.05$; N = 5.

3.3 Establishing a new fixation method to avoid mesohyl stiffening

The original protocol developed to obtain sponge in resting condition was not completely effective in maintaining the sponge in a real RC condition (fig. 28) since the total induced deformation measured after the fixation was statistically different if compared with the values obtained before the fixation. On the other hand this protocol resulted to be able to fix sponges in a less stiff condition (fig. 28): in fact when compared with the second protocol, the induced deformation values were statistically different (fig. 28).

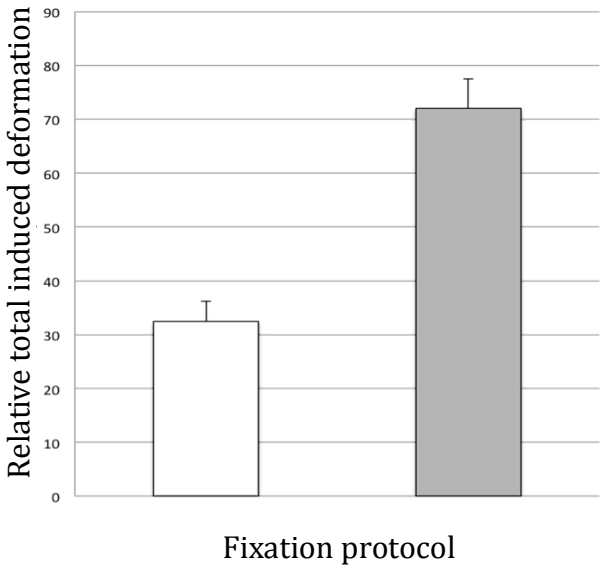

Figure 28. Percentage relative total induced deformation of sponges fixed in MSC (**white column**) and RC (**grey column**). Both the protocols induced significant stiffening (paired t-test: $p<0.001$ for SC samples; $p<0.05$ for RC sponges). Sponges in SC are significantly stiffer than sponges in RC (two tailed t-test: $p<0.01$). Bars = standard deviations. N=3.

3.4 Mechanical parameters

Isotonic test

Isolated beam shaped samples underwent elongation when subjected to a constant tensile stress (fig. 29). Samples showed three different elongation patterns during the test (fig. 29). All samples underwent a first primary phase where the elongation speed gradually decreased; the magnitude and the duration of this phase varying a lot. The simplest pattern (fig. 29, a) was characterized by a rather constant elongation speed that followed a quite long and wide primary phase. In other cases, after the primary phase, it was possible to observe a constant phase period that preceded another temporary increase of the speed; thus was followed by a second decelerating phase that ended in another constant phase (fig. 29, b). The last observed pattern generally began with a fast and small primary phase, then a very low and constant elongation speed followed; after a while the speed increased dramatically and entered in a new rather constant phase (fig. 29, c).

Part of the results was recently reported by Sugni and coworkers (2013).

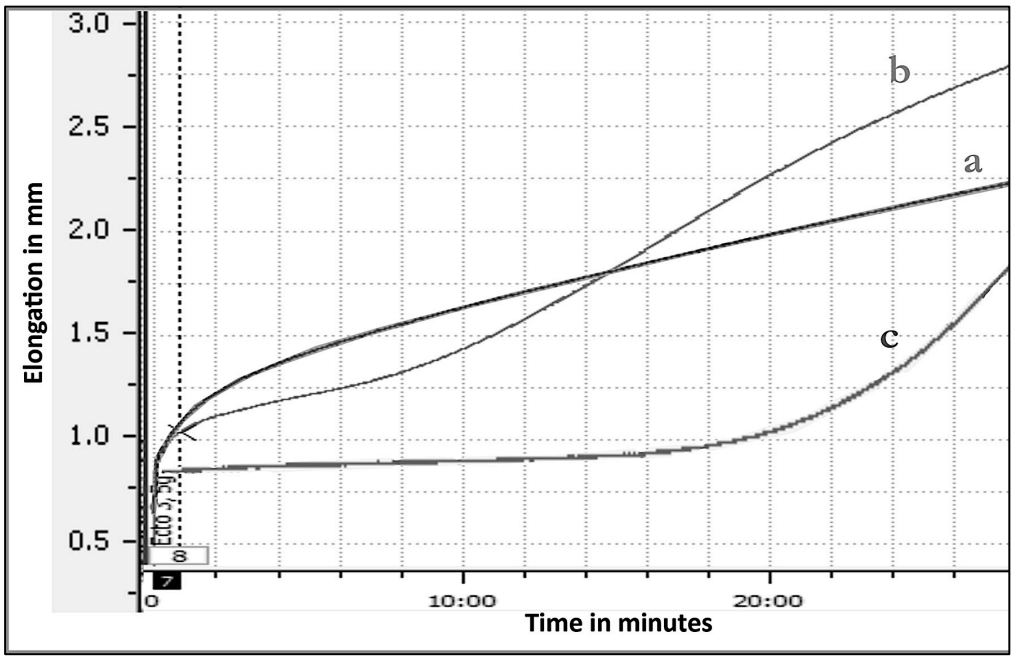

Figure 29. Three elongation curves, representative of the three observed patterns (**a**, **b**, **c**), are merged to highlight the different elongation patterns.

As shown in figure 30 there were frequency differences in the elongation patterns: in particular there was an evident asymmetry (Agostino skewnees test: $p<0.05$) in the distribution of the elongation pattern "a" occurring with higher probability when the samples were subjected to 10 g.

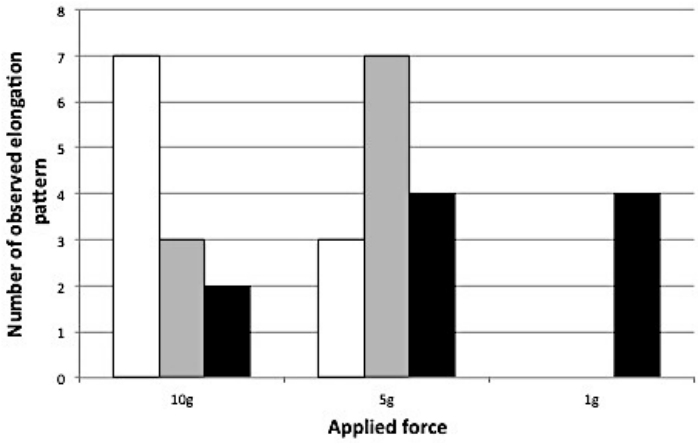

Figure 30. Frequency of the elongation patterns observed in the ectosome and in the choanosome samples when stressed with different loads. **White columns** = pattern a; **grey columns** =pattern b; **black columns** = pattern c.

In the elongation tests the viscosity could be calculated when the elongation speed was constant. Generally other collagenous tissues undergo a typical curve consisting of a primary decelerating phase and a subsequent secondary phase where the elongation speed is constant. As previously described

both choansome and especially ectosome often displayed more than one constant speed phase. For this reason in many ectosome samples it was possible to measure two different viscosity values (fig. 31).

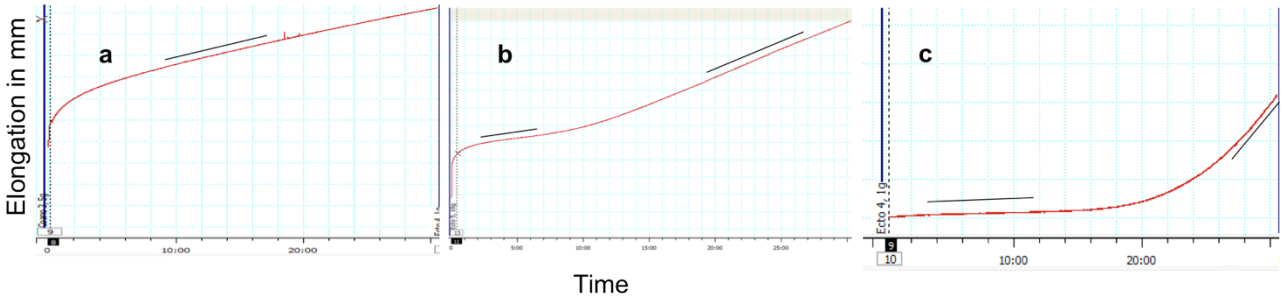

Figure 31. Elongation test curves. Except for the elongation pattern **a**, in pattern **b** and **c** it was possible to measure two viscosity values when the elongation speed was constant (**black lines**).

The ectosome viscosity values (fig. 32 A), calculated in the first constant phase, were independent from the applied stress and showed great variability like in echinoderm MCTs. A very different response to the applied stress was, on the other hand, observed in the viscosity values of the second constant phase (fig. 32 B). The "secondary" viscosity values depend on the applied stress (fig. 33, table 2). Mean ectosome viscosity values are summarized in table 3.

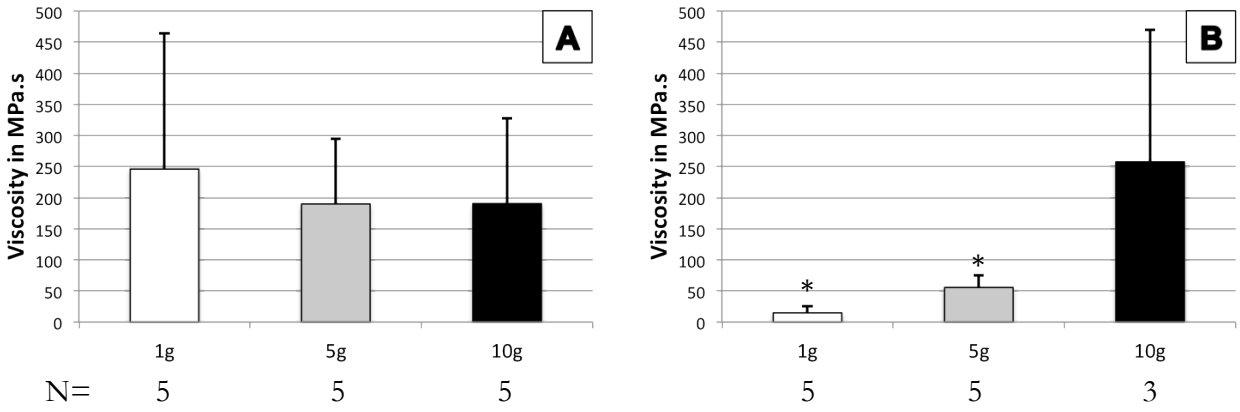

Figure 32. Mean "primary" (**A**) and "secondary" (**B**) viscosity values obtained from ectosome samples subjected to different loads. There were no differences in the primary viscosity values obtained with different loads; on the other hand there was a statistical difference between the secondary viscosity values obtained with 10g and the ones obtained with 1 and 5g.
Two tailed t-test: * = $p<0.05$. Bars = standard deviations.

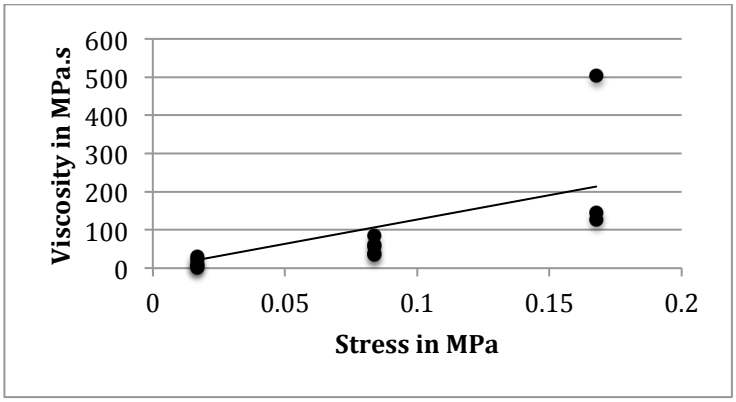

Fig 33. Scatter plot showing the relation between the stress and the viscosity. There is a positive relationship between the applied stress and the viscosity (see table below).

Regression statistics	
R	0.7
R^2	0.5
Fitted R^2	0.45
S	98.37
Tot	13

viscosity =- 34.1632 + 1558.6323 * nominal stress

ANOVA

	d.f.	*SS*	*MS*	*F*	*p-value*
Regression	1.	104'587.86	104'587.86	10.81	0.01
Var	11.	106'435.76	9'675.98		
Tot	12.	211'023.62			

	Coefficients	*Standard Errors*	*LCL*	*UCL*	*t Stat*	*p-value*	*H0 (5%)*
Segment	-34.16	45.73	-134.8	66.48	-0.75	0.47	*No*
nominal stress	1'558.63	474.08	515.19	2'602.07	3.29	0.01	*Yes*

Table 2. Statistical linear regression summary.

As far as choanosome samples are concerned we could only calculate the primary viscosity since most of samples elongated with pattern (a) and there were no sufficient data for statistical analysis. As well as in the ectosome a relevant variability in the primary viscosity values was found in the choanosome (fig. 34). There were again no differences in the primary viscosity values. Mean choanosome viscosity values are summarized in table 3.

As at present we do not know any chemical that could prevent stiffening reactions once the samples were tested, we should consider both ectosomes and choanosome to be in stiffened condition.

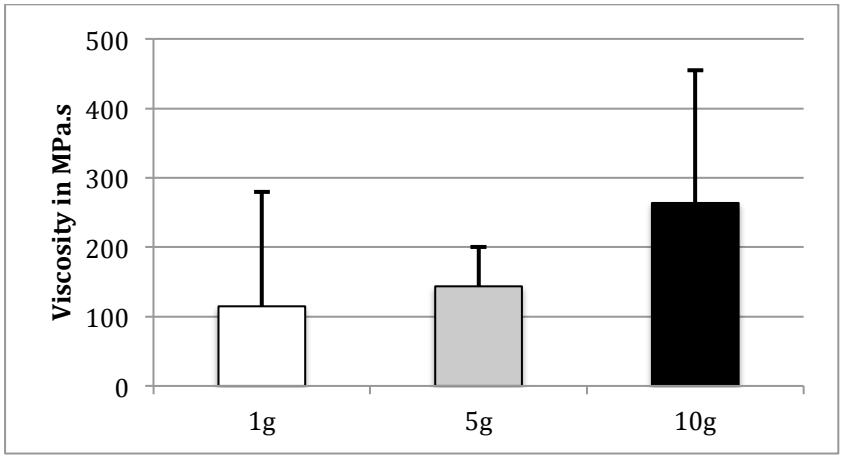

Figure 34. Mean choanosome primary viscosity values obtained with different applied loads. There were no differences between values obtained with different stresses.
Two tailed t-test. Bars = standard deviations. N = 5.

		mean	ST. DV	min	max
ectosome	primary	208.70	151.59	5.28	586.96
	secondary	86.48	132.61	2.72	503.11
choanosome	primary	174.00	153.38	3.59	574.98

Table 3. Summery of *C. reniformis* viscosity values (in MPa.s).

Isometric test

Since our isometric force transducer had a force-limit of 110g, 28/30 ectosomes samples did not break their rupture requiring a force overtaking this limit; this means that it was not possible to measure both the breaking strain and breaking stress values. Although we could not be sure of the behaviour of the samples at higher strains we can be quite confident that the calculated stiffness values were close to the real values (at least lower than the real values).

Choanosome samples always underwent rupture before the limit of the force transducer was reached, thus we could calculate the breaking strain, the breaking stress and the real stiffness values.

The breaking stress and the breaking strain values were obtained from the stress/strain curves when samples underwent rupture. Stiffness values were calculated in the steepest region of the stress/strain curves (fig. 35), stiffness is Δstress/Δstrain.

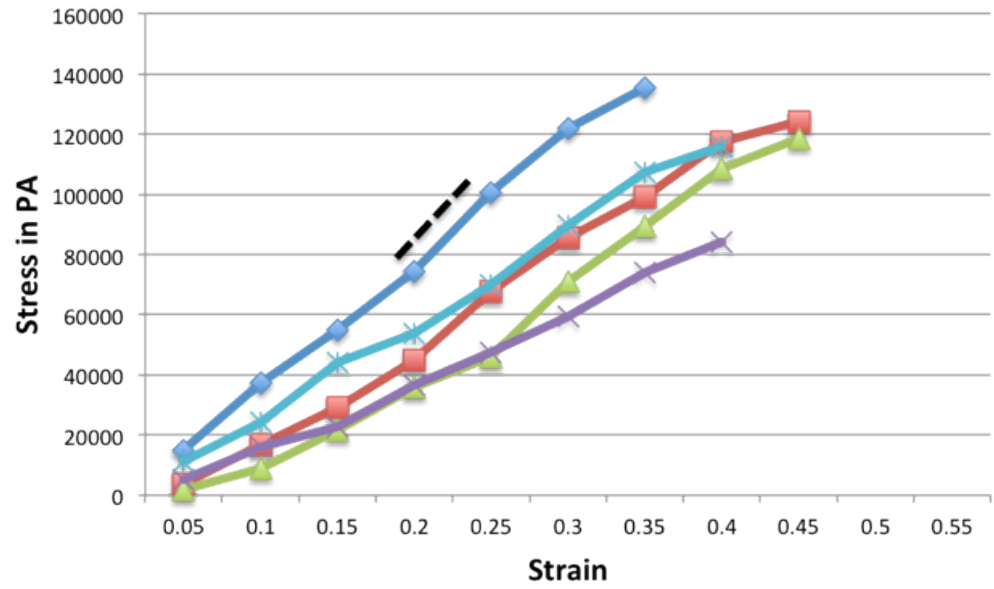

Figure 35. Stress strain curves of choanosome samples subjected to an elongation rate of 0.025mm/sec. Stiffness was calculated in the steepest part of each curve (**broken line**).

Choanosomes

The behaviour of the samples, when subjected to different extension rates, did not vary (fig. 36); no differences were found between the mean stiffness values obtained at different strain rates (fig. 37).

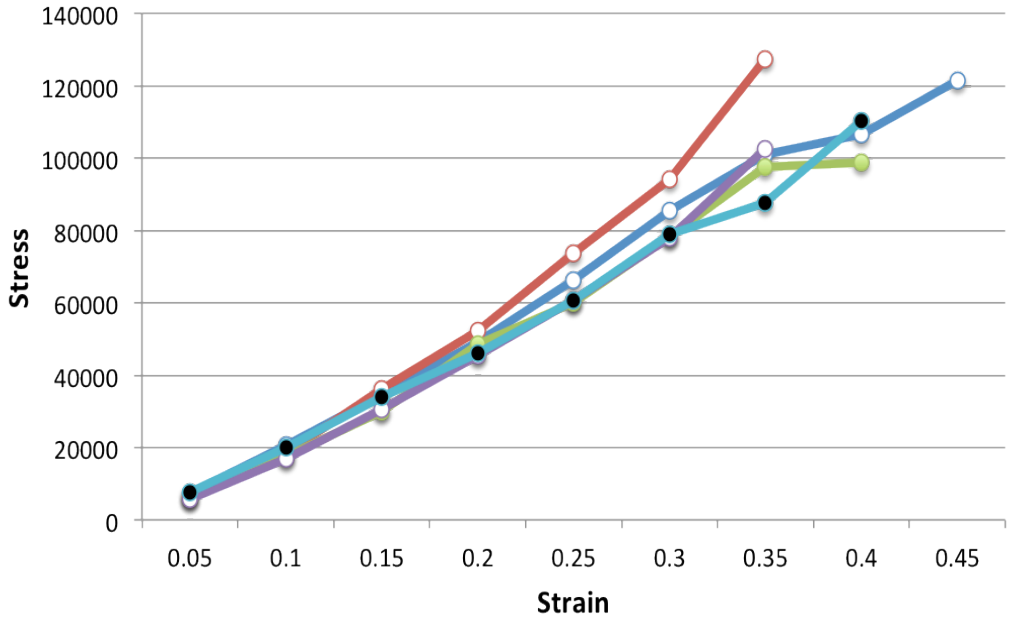

Figure 36. Mean stress values obtained from choanosome samples subjected to different strain rates. It is possible to notice that the pattern is really similar. Standard deviation bars were omitted to make the graph more readable. Strain rates: **deep blue line** = 0.025; **red line** = 0.01; **green line** = 0.005; **violet line** = 0.0033; **blue line** = 0.0025.

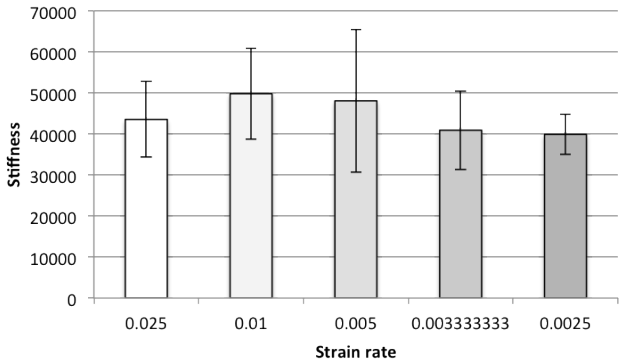

Figure 37. Mean stiffness (in Pa) values obtained from choanosome samples subjected to different strain rates. There are no differences between mean stiffness values; ANOVA. Bars = standard deviations.
N = 5 (4 for 0.01mm/sec).

In the range of elongation speeds tested there was no correlation between the elongation rate and the stiffness (fig. 38; table 4). Stiffness range was 0.029-0.079 MPa.

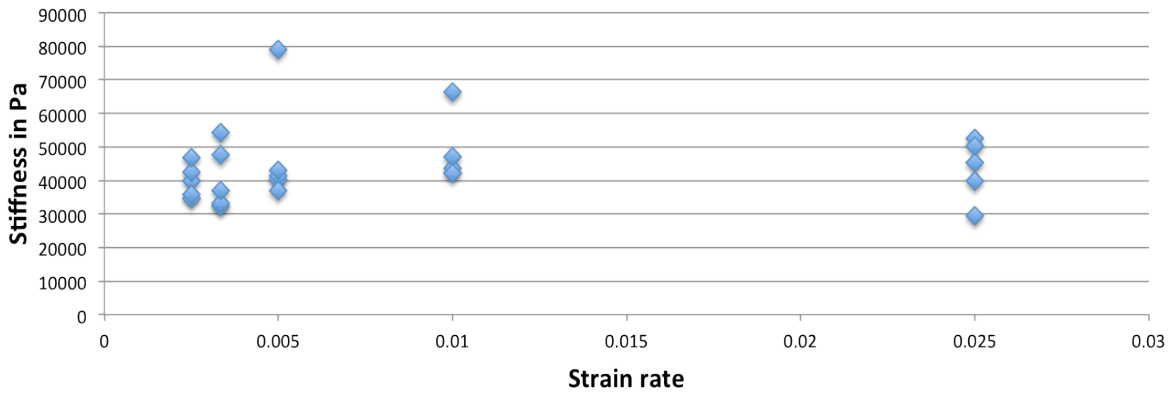

Figure 38. Scatter plot of choanosome stiffness/strain rate. It is evident that there are no relationships between the two parameters.

Coefficents matrix			
Samples number		*24 Critical Value (5%)*	2.07
		strain rate	*stiffness*
strain rate	**Pearson Coefficent**	*1.*	
	R Generic Error		
	t		
	p Value		
	H0 (5%)		
stiffness	**Pearson Coefficent**	*0.06*	*1.*
	R Generic Error	*0.05*	
	t	*0.27*	
	p Value	***0.79***	
	H0 (5%)	*accepted*	

R		
Serie vs. Serie	*R*	
stiffness vs. strain rate	**0.06**	

Table 4. Summary table of the stiffness/strain rate correlation statistics. There is no correlation between the two parameters (Pearson test).

No differences were present in both the breaking stress and breaking strain values (fig. 39) obtained from samples subjected to different extension rates.

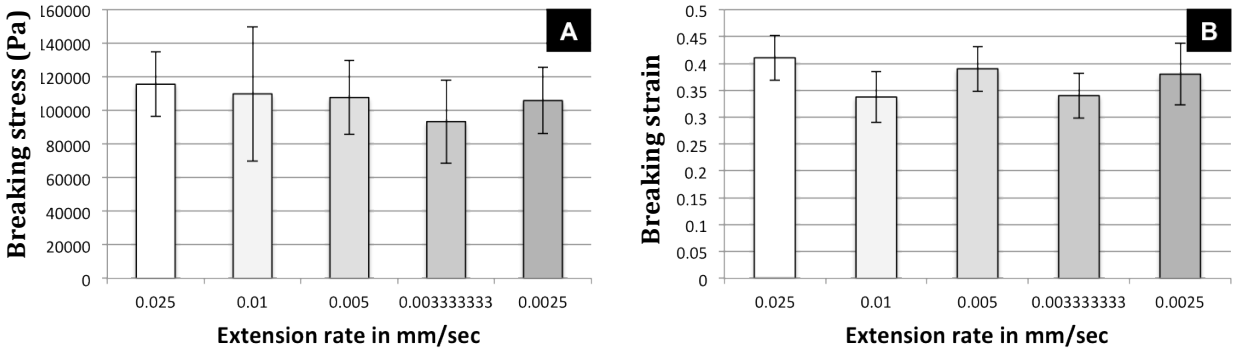

Figure 39. Breaking stress (**A**) and breaking strain (**B**) means obtained from samples subjected to different extension rates. There are no differences. ANOVA. Bars = standard deviations. N = 5 (4 for 0.01mm/sec).

Ectosomes

Also the ectosome samples, when subjected to different extension rate, showed similar behaviours (fig. 40); there were no differences between the mean stiffness values obtained at different strain rates (fig. 41).

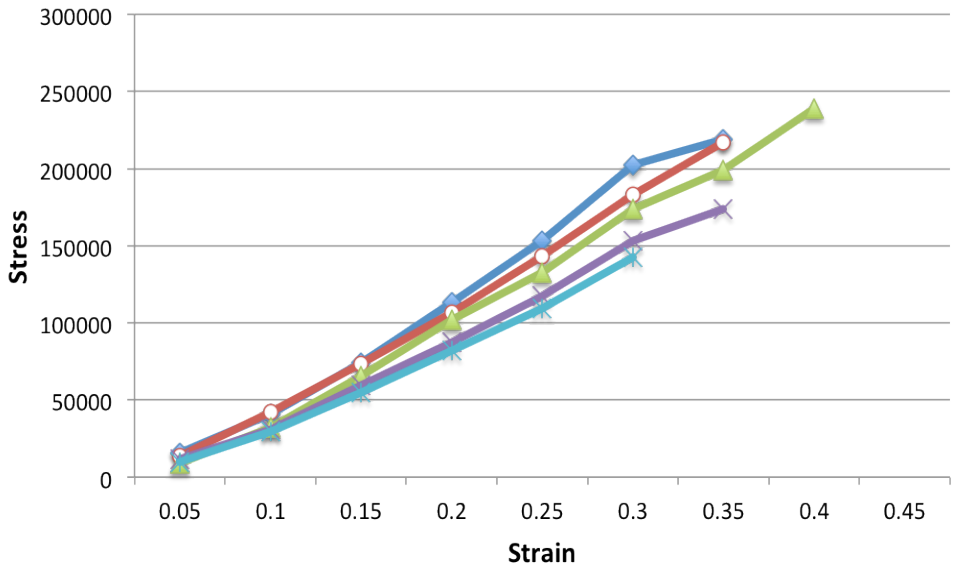

Figure 40. Mean stress values obtained from ectosome samples subjected to different strain rates. It is evident that the pattern is really similar. Although not statistically significant at 0.3 strain, the stress seems to depend on the strain rate. Standard deviation bars have been omitted to make the graph more readable. Strain rates: **deep blue line** = 0.025; **red line** = 0.01; **green line** = 0.005; **violet line** = 0.0033; **blue line** = 0.0025.

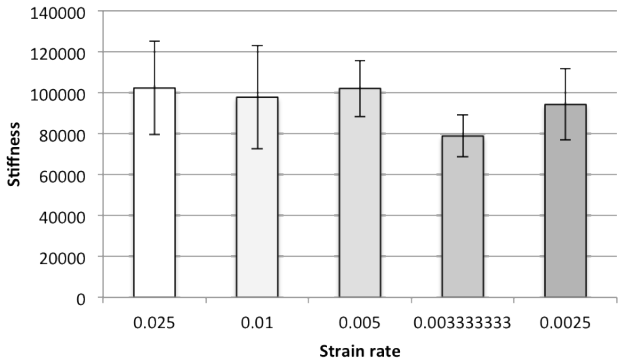

Figure 41. Mean stiffness (in Pa) values obtained from ectosome samples subjected to different strain rates. There are no differences between mean stiffness values; ANOVA. Bars = standard deviations. N = 5.

In the range of elongation speeds tested there was no correlation between the elongation rate and the stiffness (fig. 42; table 5). Stiffness range was 0.06-0.13 MPa

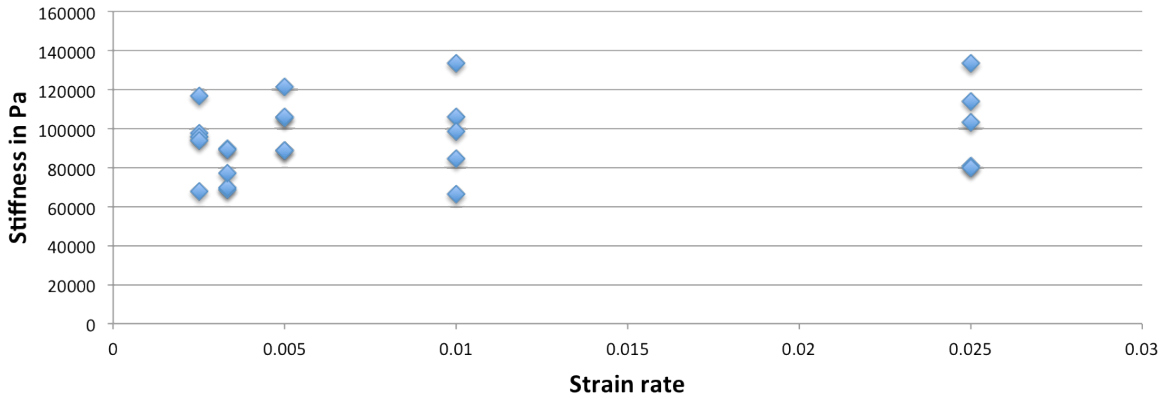

Figure 42. Scatter plot of ectosome stiffness/strain rate. It is evident that there are no relationships between the two parameters.

Correlation Coefficients			
Sample Number		*25 Critical Value (5%)*	2.07
		speeds mm/sec	*stiffness*
speeds mm/sec	**Pearson Coefficient**	*1.*	
	R Generic Error		
	t		
	p Value		
	H0 (5%)		
stiffness	**Pearson Coefficient**	*0.24*	*1.*
	R Generic Error	*0.04*	
	t	*1.18*	
	p Value	*0.25*	
	H0 (5%)	*accepted*	

R

Series vs. Series	*R*
stiffness vs. speeds mm/sec	0.24

Table 5. Summary table of the stiffness/strain rate correlation statistics. There is no correlation between the two parameters (Pearson test).

Ectosome/choanosome stiffness comparison

On the whole, when compared, ectosome stiffness is significantly higher then that of choanosome (fig. 43).

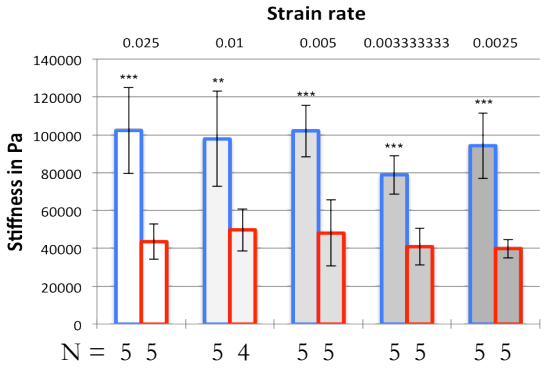

Figure 43. Mean stiffness values obtained from ectosome samples (blue lined columns) and choanosome samples (red lined columns) subjected to different strain rates. There are differences between mean stiffness values; ANOVA: *** = $p<0.001$; ** = $p<0.01$. Bars = standard deviations.

3.5 Exploring the presence of mechanosensors

In order to explore the sponge sensory system and pathway and understand how the sponge can actually sense the mechanical stimulations, we carried out a detailed investigation on the sponge surface by means of SEM and TEM methods. A preliminary investigation has been also conducted on the exhalant canals where recent papers demonstrated the presence of primary cilia possibly involved in the water flow regulation.

Scanning electron microscope

Sponge surface appear to be covered by a thin layer of exopinacocytes, the shape of these cells being much more irregular than expected: some exopynacocytes were hexagonal, whereas others have no defined shape (fig. 44 A). Many exopinacocytes showed digitiform processes overlapping on adjacent cells; sometimes parts of the cells were partially covered by irregular lobes of the nearby cells (fig. 44 A, B). Some exopinacocytes were also characterized by the presence of cell processes that, arising from their surface, were protruded vertically: again some of these processes showed a digitiform shapes (fig. 44 C), whereas others had irregular profiles (fig. 44 D).

The occasional detachment of some exopinacocyte revealed a basal network of exopinacocytis extensions just under the pinacoderm that formed many contacts between different cells processes (fig. 44 E).

In term of presence of primary cilia, our data are still controversial. Actually some elongated and slender protrusions recalling the structure of primary cilia could be seen in the exhalant canals (fig. 44

F); on the other hand, these structures were never identified with TEM analysis and therefore may be artefacts produced during the SEM preparation.

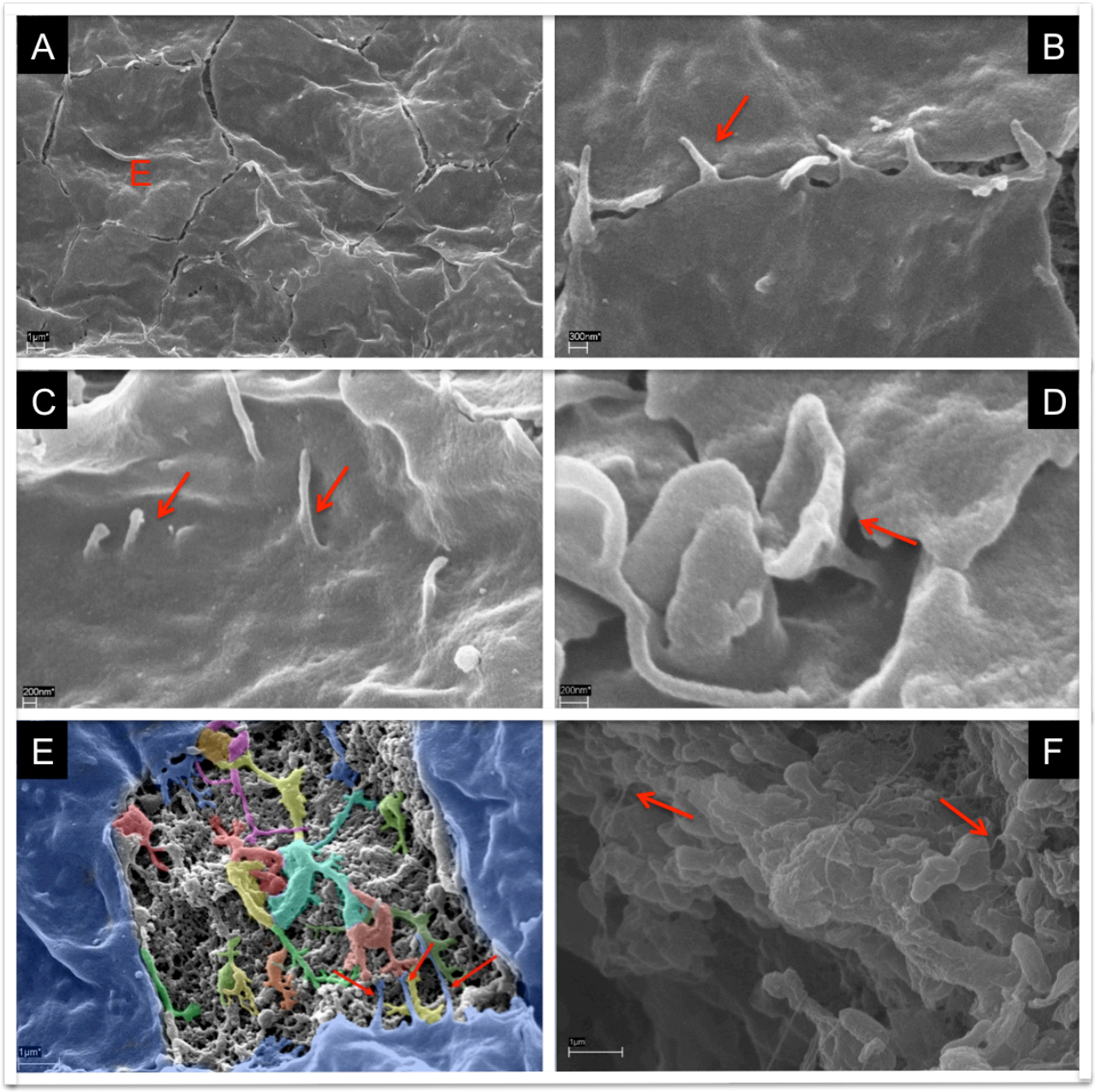

Figure 44. Surface (A-E) and inner canals (F) scanning electron micrographs. **A** overview of the sponge surface; **E** = exopinacocyte. **B** Detail of the digitiform cell processes (**red arrow**) that overlap adjacent cells. **C** Details of digitiform cell processes (**red arrows**) on exopinacoderm surface. **D** Detail of a cup-shaped cell process (**red arrow**) emerging from the exopinacoderm surface. **E** Overview of the cell processes network under an exopinacocytes. The image has been artificially coloured to highlight different cell phenotypes and processes. **Blue** = exopinacocytes; **other colours** = cellular processes belonging to different cells; **red arrows** = exopinacoderm processes contacting other cell processes in the ectosome. **F** Inner view of a great sponge canals. **Red arrows** = presumptive primary cilia.

Transmission electron microscope

The images confirmed what seen at SEM. In particular some exopinacocytes have digitiform projections overlapping on adjacent cells (fig. 45 A). At higher magnification it was possible to observe

how the membranes of these precess were connected to those of adjacent exopinacocytesby means of presumptive cell junctions (fig. 45 B). All the observed exopinacocytes showed slender cellular process penetrating into the deeper layer and taking contact with other granular cells (fig. 45 A, C). These long processes often display the presence of vacuoles, vesicle, microtubules and filaments (fig. 45 E). The presence of multivesicular bodies was also observed in few exopinacocytes (fig. 45 D).

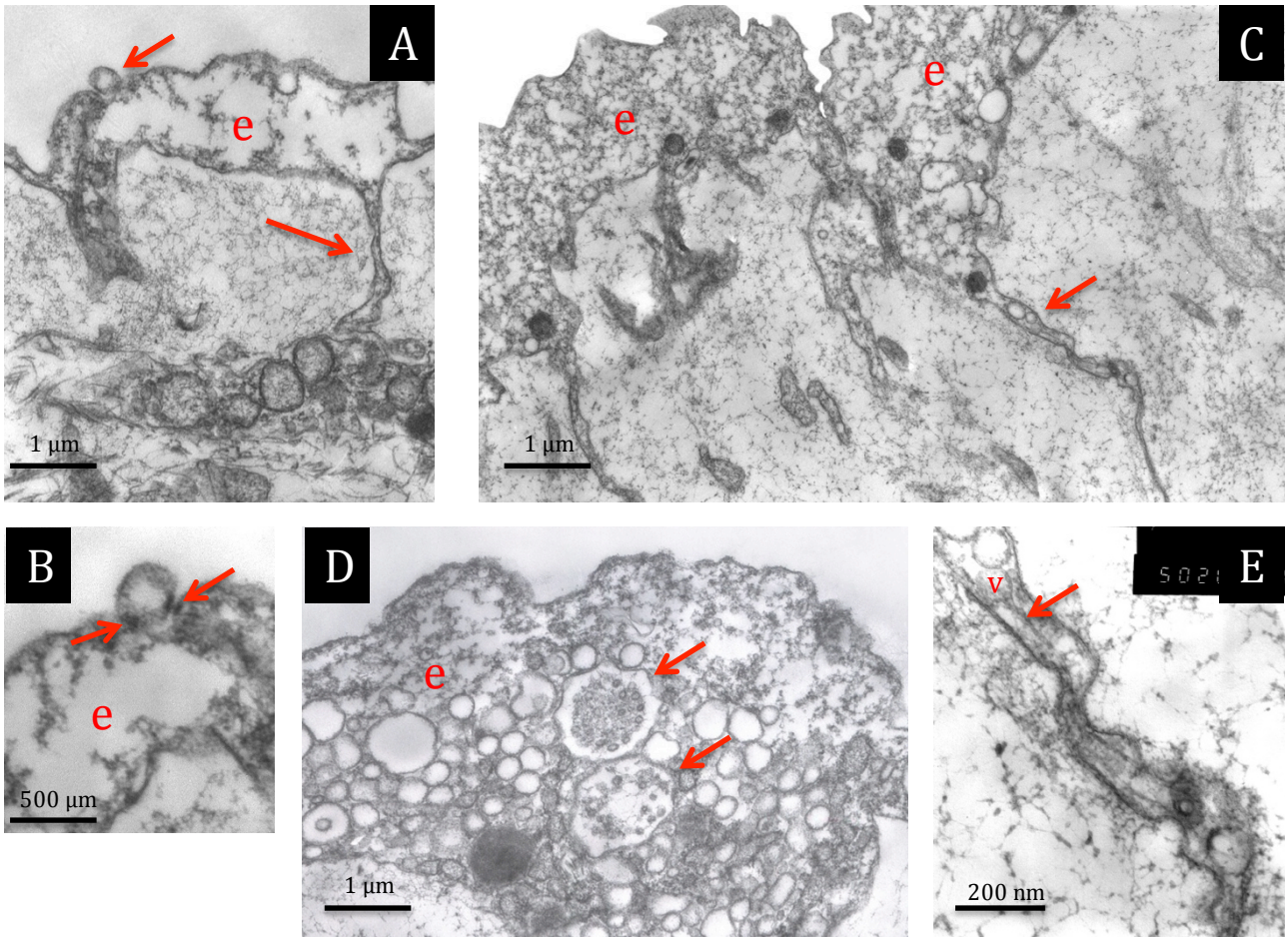

Figure 45. Exopinacocytes transmission electron micrographs.
A vertical section through the sponge surface. **e** = exopinacocyte; **small red arrow** = digitiform process; **long red arrow** = cell process downward directed that contacts a granular cell. **B** Detail of the digitiform process; **red arrows** = presumptive cell junctions. **C** lateral overview of sponge surface. **e** = exopinacocyte; **red arrow** = cell process downward directed. **D** exopinacocyte detail showing multivesicular bodies (**red arrows**). **E** Detail of a cell process downward directed containing vesicles (**v**), filaments and microtubules (**red arrow**).

3.6 GABA and Glutamate

3.6.1 Evaluating the presence of GABA and Glu

Fluorescence: GABA

Overall GABA was found in large amount in the sponge cortical region (fig. 47 A, B, C), around the excurrent canals (fig. 48 D), in the choanocyte chambers (fig. 47 E) and in the actinocytes regions that surround the exhalant canals in the oscular region (fig. 47 F). The same distribution was found in both RC and SC sponges.

Our data revealed a great variability in the observed signal that seemed independent from the mechanical state of the sponges (compare fig. 47 F - 48 A, C; 48 D-E). At higher magnification it was possible to notice a different distribution pattern inside different cell phenotypes.

GABA was found in many cells in different regions of the sponges (fig. 46, 47). More in detail, many cell phenotypes in the mesohyl were not well distinguishable with LSCM; however some cell phenotypes could be easily identified by their localization or on the basis of their particular morphology. GABA was observed in the exopinacocytes (fig. 47 A, B, E); in the endopinacocytes of both incurrent/excurrent canals (fig. 47 A, C, D, E, F); in the spherolous cells (fig. 48 B) and in the actinocytes (fig 47 F; 48 C, D, E) as well as in other unidentified cells.

Both exo/endopynacocytes, when labelled, revealed an homogeneous distribution of the signal inside the cells and their processes; on the other hand in the actinocytes GABA was often found in high concentration just inside the cell membranes (fig. 48 C, D, E). In the spherolous cells the signal was distributed homogeneously in the inner side of the cell membrane (fig. 48 B). Other unidentified cells showed a high signal in their cell bodies and its associated processes that often seemed to connect the endopinacocytes with other mesohyl cells (fig. 48 B).

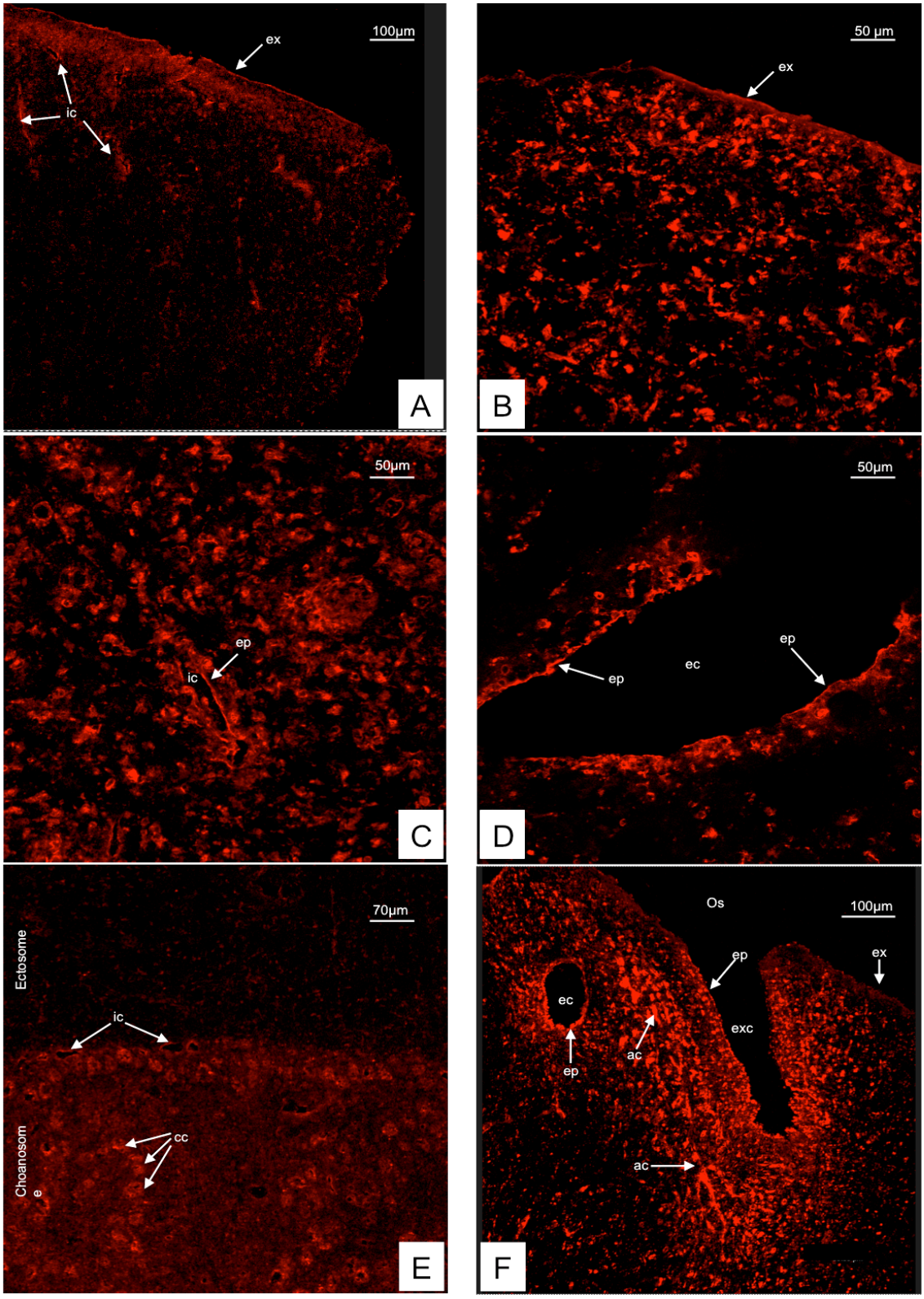

Figure 47. Immunocytochemistry for GABA (**red**). Laser scanning confocal microscopy images highlighting GABA presence. All the images were obtained from sponge in RC. **A** ectosome overview. **B** vertical section showing a detail of the sponge surface and the different cells layers. **C** detail of the transition region (between ectosome and choanosome) where is possible to notice a small incurrent canal. **D** detail of a large excurrent canal. **E** detail of the transition region between the ectosome and the choanosome region. **F** Lateral view of the oscular region. Legend: **ex** = exopinacoderm; **ic** = incurrent canals; **ec** = excurrent canals; **cc** = choanocyte chamber; **exc** = exhalant canal; **Os** = osculum; **ac** = presumptive actinocyte.

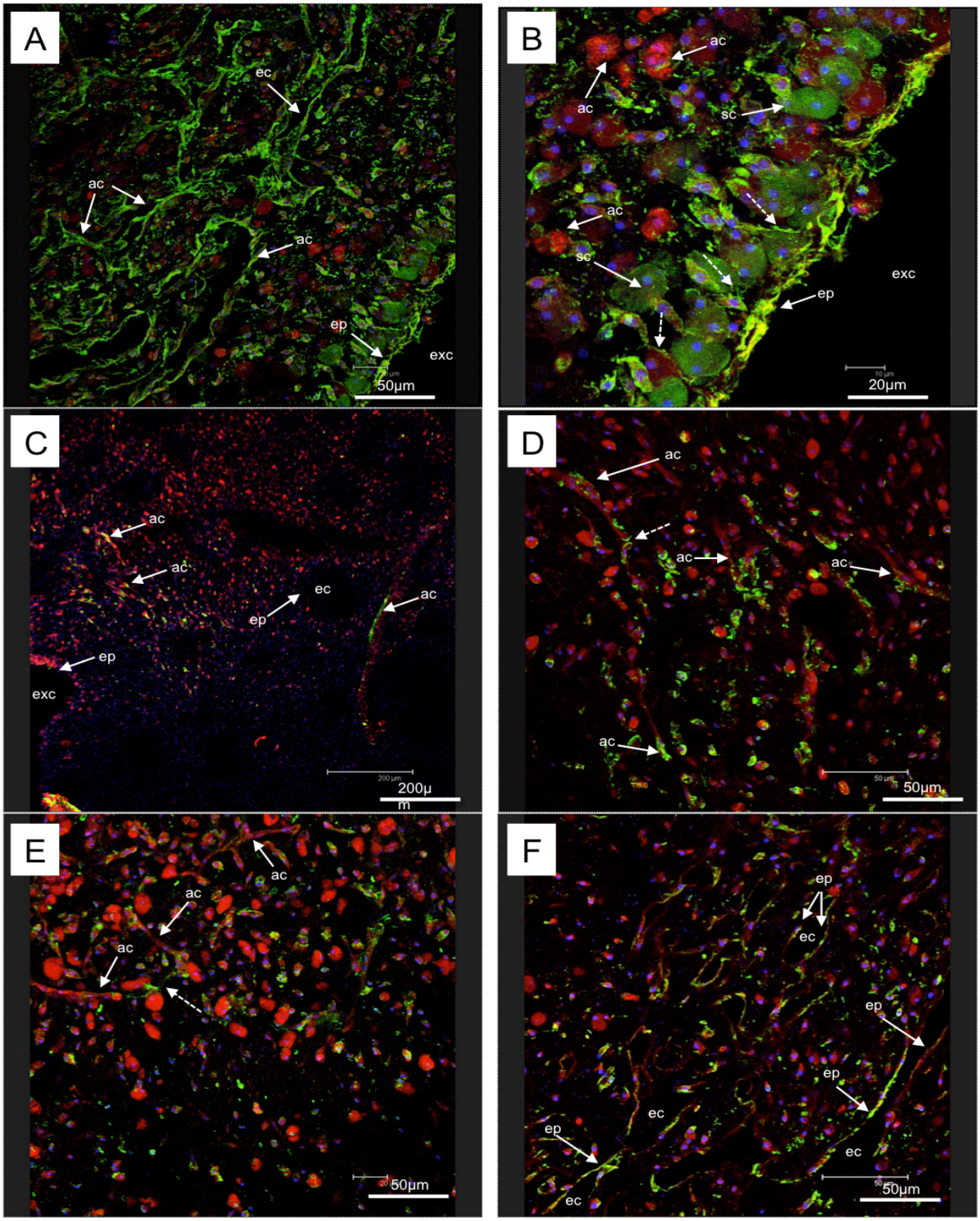

Figure 48. Immunicytochemistry for GABA and Actin. Laser scanning confocal microscopy images highlighting the presence of GABA (green), actin (red), nuclei (blue), GABA + actin co-localized (yellow). **A**, **B**, **F** were obtained from sponge in SC; **C**, **D**, **E** from RC sponges. **A** transversal section of the oscular region. **B** detail of the oscular region. **C** transversal overview of the oscular region. **D** detail of the actinocytes rich region around the exhalant canal. It is possible to notice a dense GABA signal between two adjacent cells (broken line arrow) **E** detail of the actinocytes rich region around the exhalant canal. It is possible to see one labelled cell that connects two actinocytes (broken line arrow). **F** excurrent canals near the oscular region. Legend: **ec** = excurrent canal; **ep** = endopinacocyte; **exc** exhalant canal; **sc** = presumptive spherolous cell; **ac** = actinocytes.

Fluorescence: Glu

Glu was mainly found in the pinacoderm, in some presumptive spherolous cells (fig. 49 B) and in other unidentified cells (fig. 49). Glu was found in both exopinacocytes (fig. 49 A) and endopinacocytes (fig. 45 B, C, D) and in a few presumptive spherulous cells (fig. 49 B, C). There was no apparent difference both in the presence and in the distribution between sponges in RC and sponges in SC except for the exopinacoderm where a few signals were detected only in RC sponges (fig. 49 A).

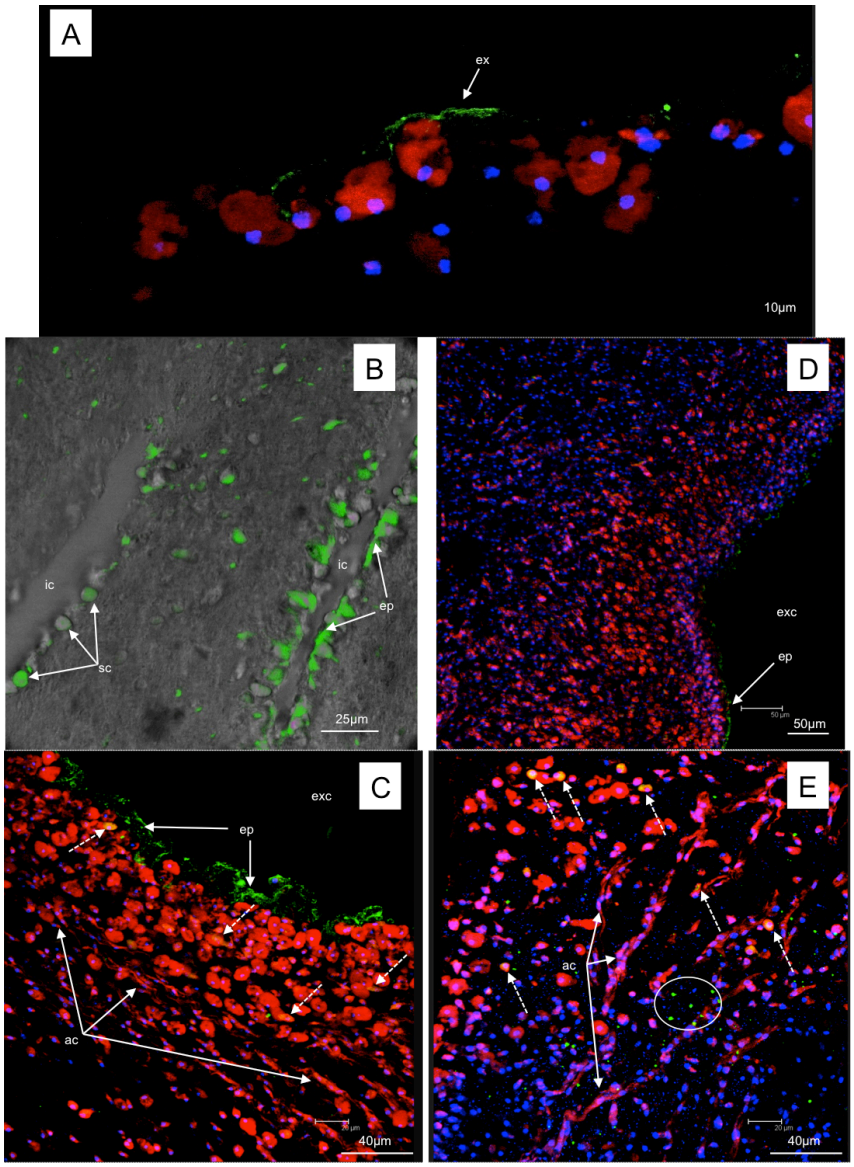

Figure 49. Immunocytochemistry for Glu. Laser scanning confocal microscopy images highlighting the presence of Glu (green), actin (red), nuclei (blue). **A** lateral view of the sponge external surface. **B** merged fluorescent and bright field of ectosome region where is possible to see some incurrent canals. **C** transverse section of the oscular region. **D** transverse section of the oscular region. **E** detail of the circular array of actinocytes around the exhalant canal. Images **A**, **B**, **C** were obtained from RC samples; **D**, **E** from SC samples. Legend: **ex** = exopinacocyte; **ic** = incurrent canal; **ep** = endopinacocyte; **sc** = presumptive sperolous cell; **ac** = actinocyte; **exc** = exhalant canal. **Broken line arrows** = Glu signal in unidentified cell; **white circle** = noise.

Immunogold: GABA

There were very few gold particles in the control samples (fig. 50).

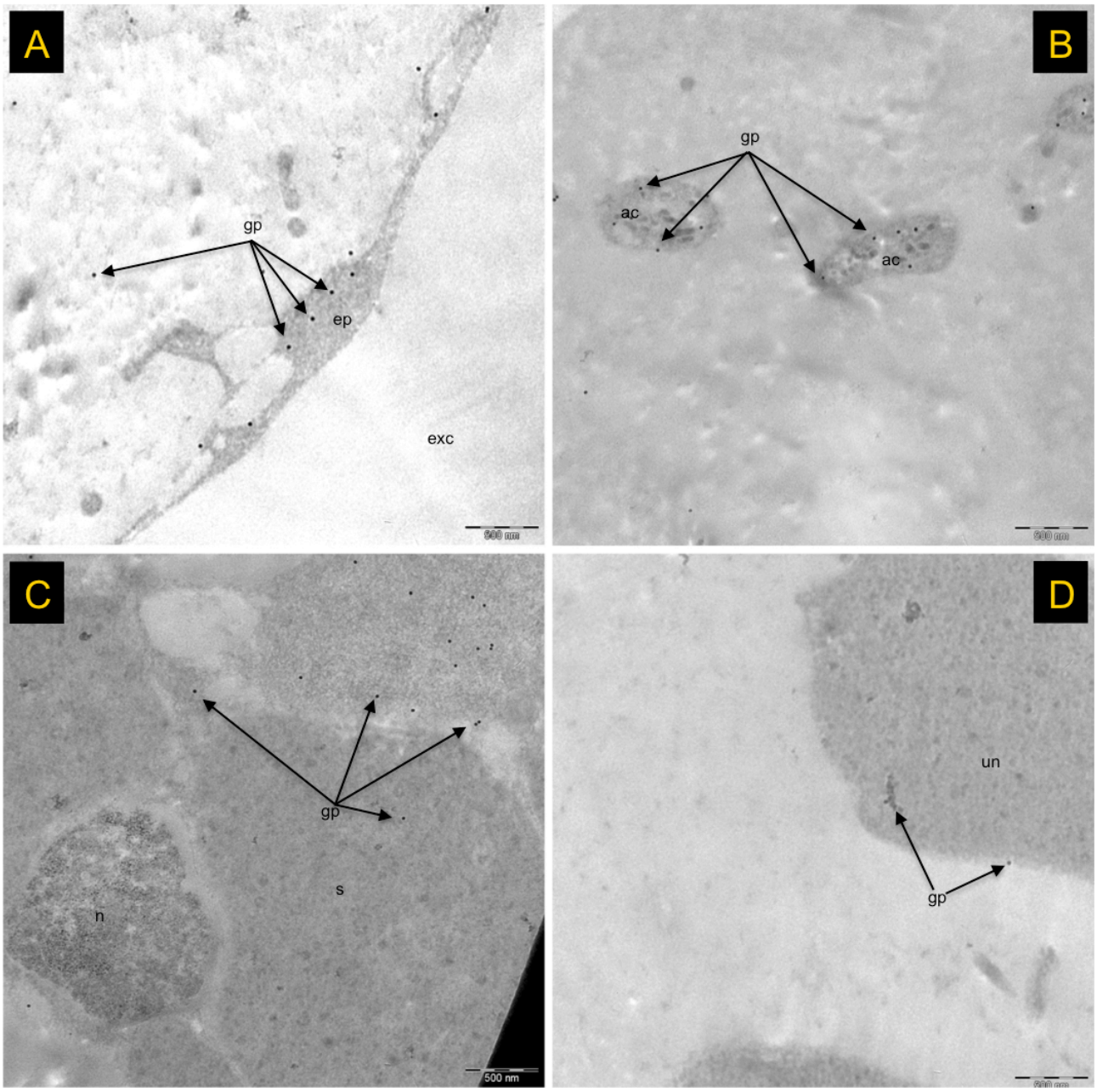

Figure 50. Transmission electron micrographs of immunogold control samples. There was no significant signal; only a few gold particles were detectable. **A** transverse section of the oscular region. **B** actinocytes region. **C** detail of a spherulous cell. **D** unidentified cell in the ectosome.
Legend: **gp** = gold particle; **ep** = endopinacocyte; **exc** = exhalant canal; **ac** = actinocyte; **s** = spherule; **n** = nucleus; **un** = unidentified cell. Gold particles = 17 nm. Bar = 500 nm.

By employing TEM immunogold technique we could confirm definitively the presence of GABA in some specific cell phenotypes; namely, pinacocytes, spherolous cells, lophocytes and choanocytes (fig. 51 B, D; 52 B, D, E). There were again no evident differences in the GABA distribution/quantity between RC and SC samples.

Pynacocytes: GABA was homogeneously distributed in the cytoplasm of many cells; both in the zones lining the canals and in the cell processes protruding in the mesohyl. These processes often took contact with spherolous cells and other unidentified cells.

Spherolous cells: GABA was found in all the sponges with different distribution and localization. Most of the GABA was found in the nuclei or sparse in the cytoplasm although some reaction was found inside the spherules.

Lophocytes: both the cytoplasm of the main body and the cytoplasmic tails were rich in GABA.

Choanocytes: most of GABA was localized in the basal and apical regions of the cells; some signal was also present in the nuclei.

Unidentified cells: many cell phenotypes that could not be identified displayed a huge amount of GABA in some specific cell compartment or sparse in the cell cytoplasm. Often their many long cell processes were very rich in GABA.

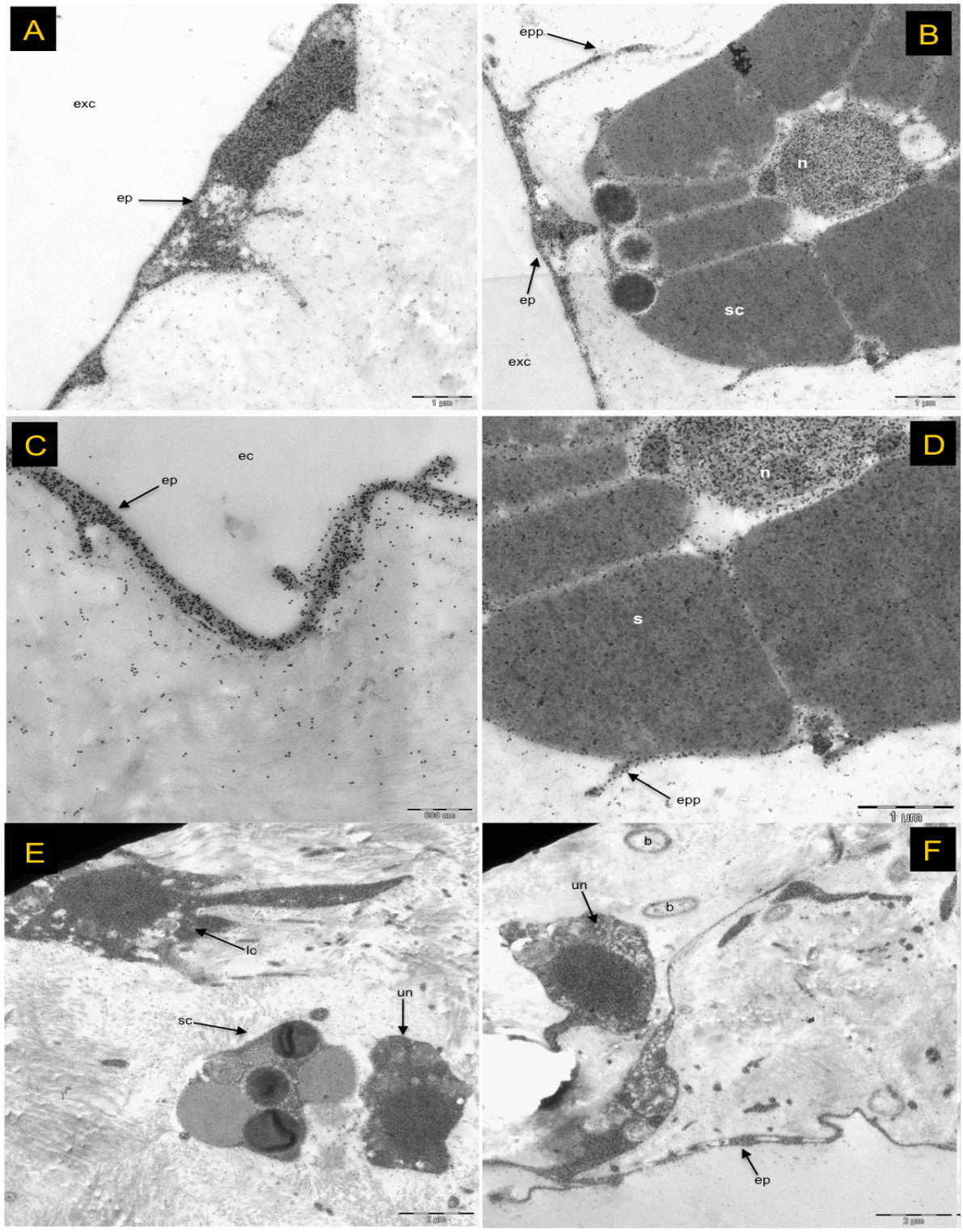

Figure 51. Transmission electron micrographs of RC thin sections immunolabelled for GABA. **A**, **B** oscular region; **C** detail of an endopinacocytes lining an excurrent canal; **D** detail of a spherolous cell; **E** scattered cells in the ectosome; **F** oscular region.
Legend: **ep** = endopinacocyte; **exc** = exhalant canal; **epp** = endopinacocyte process; **n** = nucleus; **s** = spherule; **un** = unidentified cell; **sc** = spherolous cell; **lc** = lophocytes; **b** = bacterium. Gold particles = 17nm.

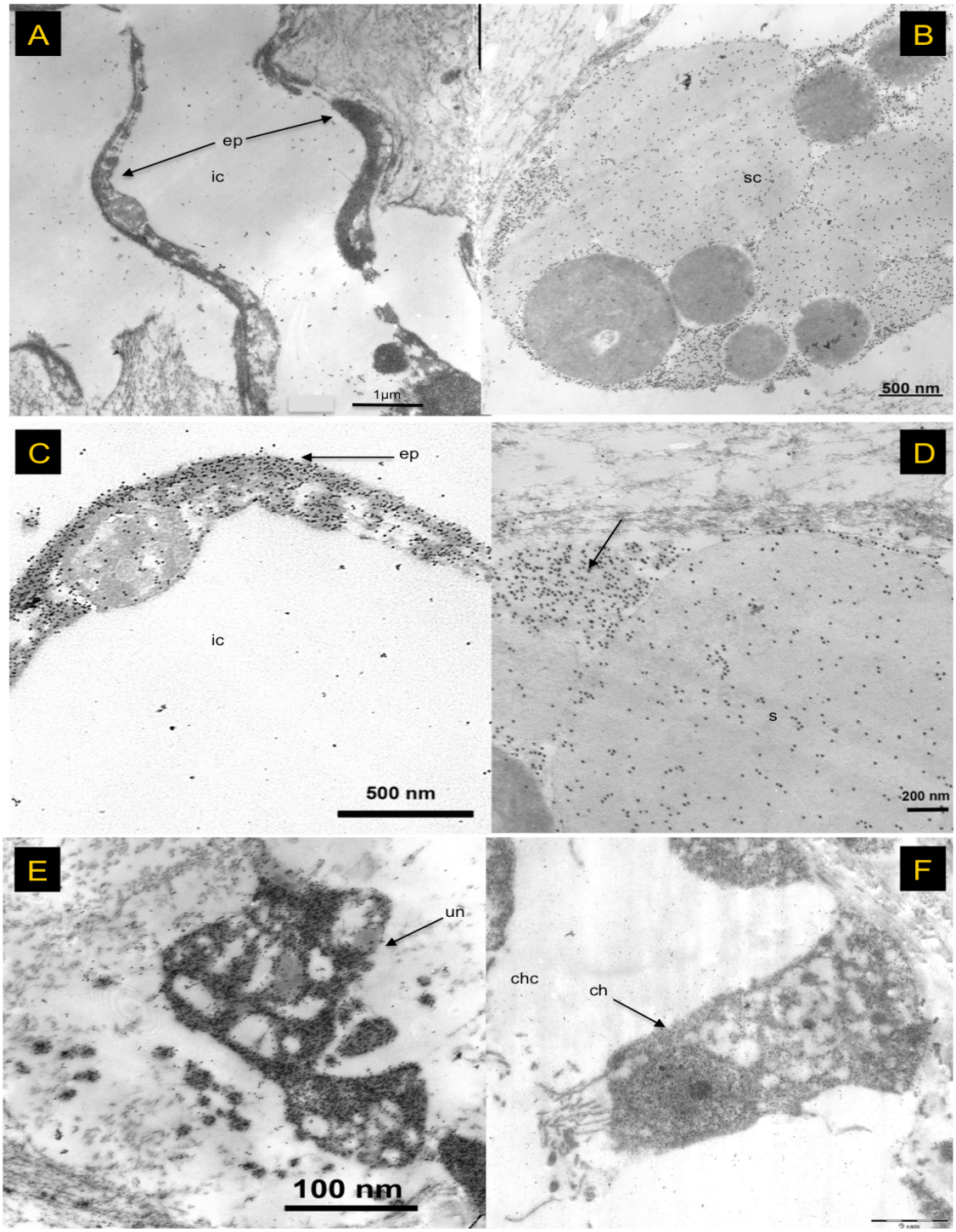

Figure 52. Transmission electron micrographs of SC thin sections immunolabelled for GABA. **A** detail of an incurrent canal in the ectosome; **B** spherulous cell in the choanosome; **C** detail of the endopinacocytes lining an incurrent canal; **D** detail of the spherolous cell in the choanosome, signal is more evident in the cytoplasm (arrow); **E** unidentified cell in the ectosome; **F** detail of a choanocytes. Bar = 500 nm.

Legend: **ep** = endopinacocyte; **ic** = incurrent canal; **sc** = spherolous cell; **s** = spherule; **n** = nucleus; **un** = unidentified cell; **chc** = choanocyte chamber. Gold particles = 17nm.

3.6.2 Effects on volume recovery of isolated tissue

Both 1mM GABA and Glu did not influence the dimensional recovery of isolated tissue samples after 4 hours from the cutting. There were no statistical differences in all the examined structure/regions (fig. 53).

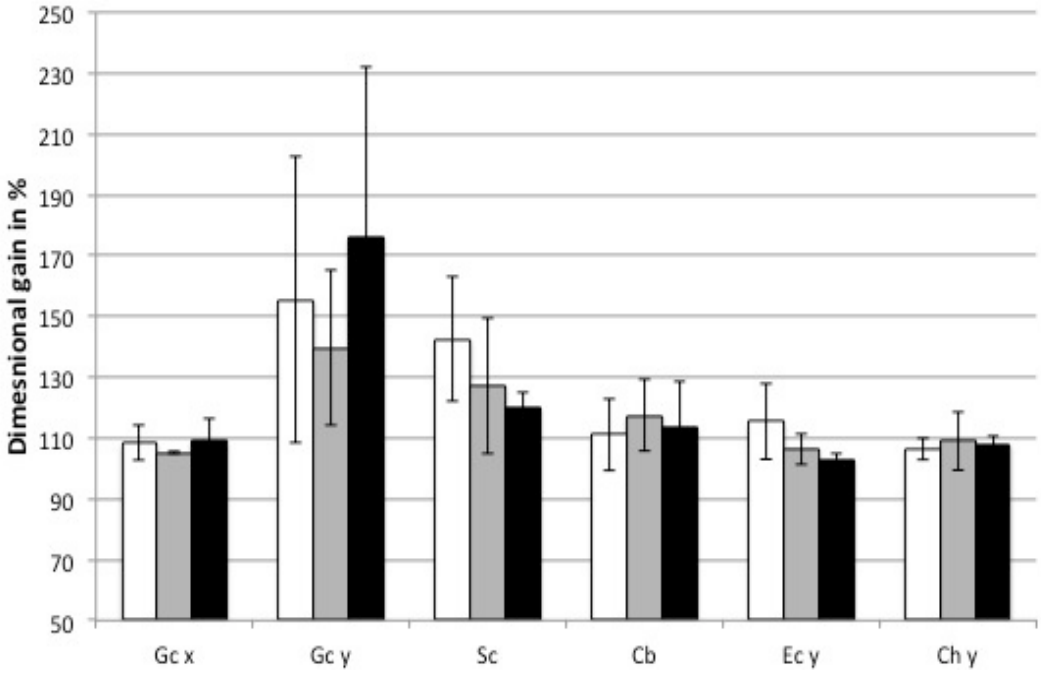

Figure 53. Mean percentage dimensional changes of different sponge regions after 4 hours in ASW (white colums), GABA 1mM in ASW (grey columns), Glutamate 1mM in ASW (black columns). Both chemicals did not induce any changes in the recovery process (ANOVA).
Gc x = great canals x axis; **Gc y** = great canals y axis; **Sc** = small canals; **Cb** = canal belts. **Ec** y = ectosome y axis; **Ch y** = choanosome y axis. Bars = standard deviations. N = 5.

3.6.3 Effects on contraction/expansion cycles

Whole mount: preliminary experiment

Adding GABA and Glu till to reach a final concentration of 2mM induced a significant contraction (movie 5, 6, 7; fig. 54). There were statistical differences between the two treatments and the control, whereas no differences were detected between GABA and Glu. The induced contraction was quite homogeneous and there were no differences between the two considered reference axes (fig. 54). The contractions appeared to fade within 30-45 minutes when the sponge started to expand slowly; no other contraction events were recorded following the exposure to the two molecules. On the other hand after replacing the solution with ASW, the contraction events started to appear again suggesting that after the removal of the chemicals the sponges fully recovered their physiological state (see movie 5, 6).

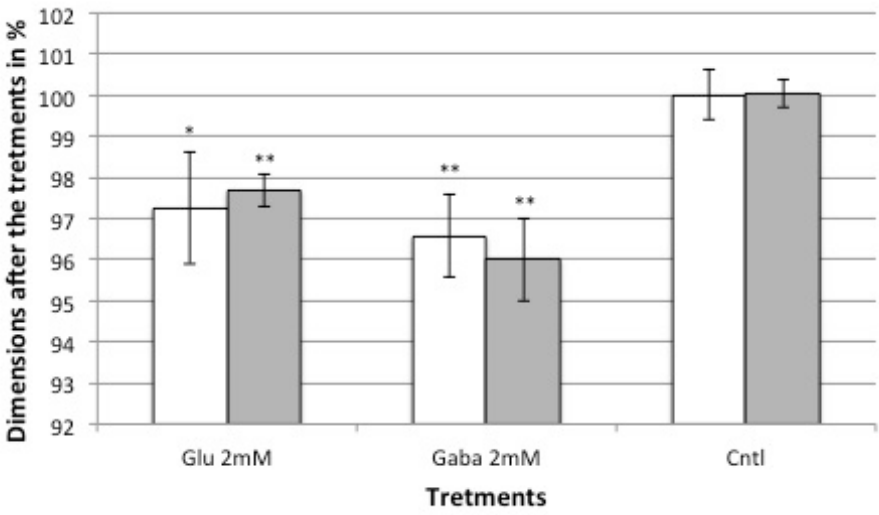

Figure 54. Percentage dimensional changes induced by different treatments. 15 minutes after the addition of GABA (2mM) or Glu (2mM) both y axes (white columns) and x axes (grey columns) were statistically different from the controls.
Two tailed t-test: * = $p<0.05$; ** = $p<0.01$. Bars = standard deviations. N = 3.

Interestly the removal of the water induced itself a rapid collapse of the sponge that affect mainly the y axes (fig. 55).

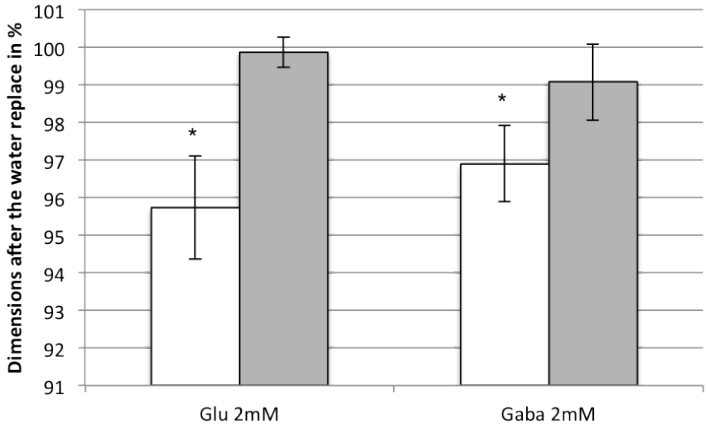

Figure 55. Percentage dimensional changes induced by the water replacement procedure of sponges previously subjected to an exposition of Glu or GABA 2mM. There was a statistical difference only for y axes (white columns); no statistical differences were found in the x axis (grey columns).
Paired t-test: * = $p<0.05$. Bars = standard deviations. N = 3.

In terms of deformation extent, the "contractions" induced by the water removal appear to be significantly lower than those observed when sponges were exposed to the two neurotransmitter only as far as the x axes are concerned, whereas were comparable for the y axes (fig. 56).

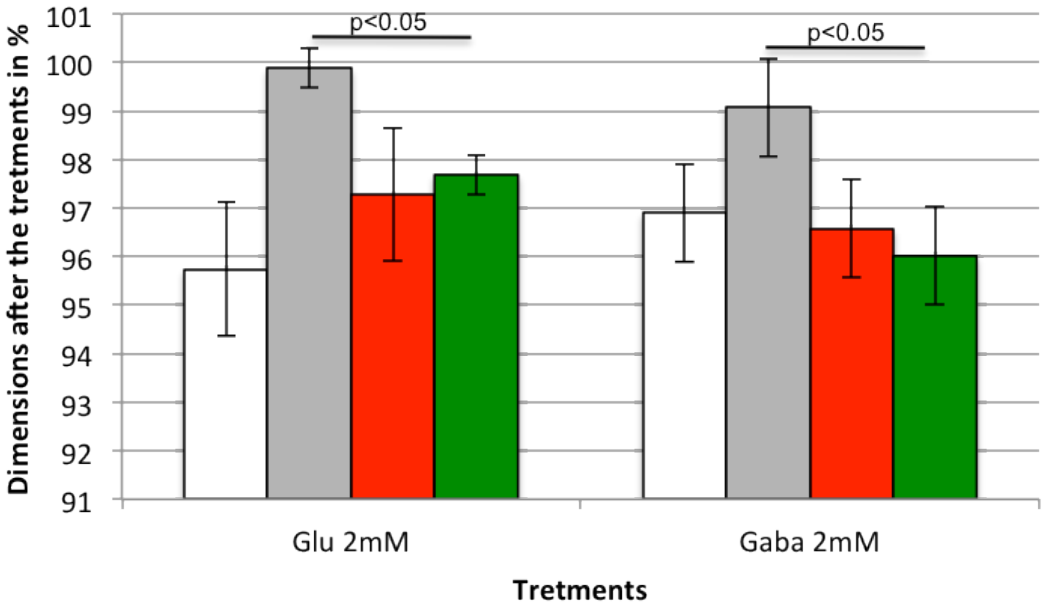

Figure 56. Mean percentage dimensional changes induced by the neurotransmitter exposure (NE) and the subsequent water replacement procedure (WR). **White columns** = y axis WR; **grey columns** = x axis WR; **red columns** = y axis NE; **green columns** = x axis NE. Two tailed t-test: $p<0.05$. Bars = standard deviations. N = 3.

Whole mount: biomechanical experiments

By means of the biomechanical apparatus (fig. 17) it was possible to better analyse the contraction events triggered by an addition of glutamate (1mM) or GABA (1mM). With our set-up we could measure both the contraction magnitude and the force generated by those contraction. All the data presented in this chapter are referred to changes in the y axes (according to figure 4).

Regarding the contraction magnitudes induced by 1 mM Glu it is possible to remark that the molecule induced contraction wave that started soon after the addition of the chemical (although not statistically different, the contractions were really evident also 5 minutes after the addition) (fig. 57); the contraction seemed to reach its maximum intensity after 15 minutes, then remained stable for other 15 minutes before fading slowly (this behaviour was exactly comparable o that observed in the previous experiments, see movie 6).

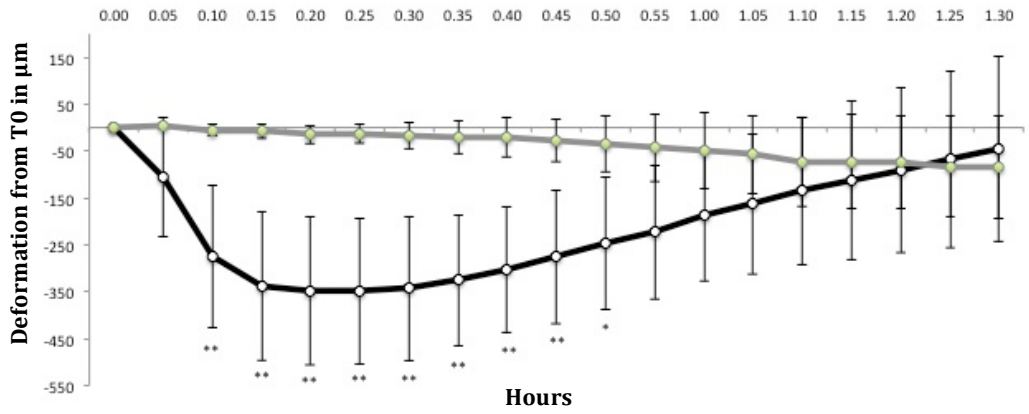

Figure 57. Mean dimensional changes (according to z axis, see fig. 4) of sponges exposed to 1mM Glu (**black & white dots**) or ASW only as controls (**green dots**). One way ANOVA: * = $p<0.05$; ** = $p<0.01$.
Bars = standard deviations. N = 5.

The contraction induced by 1mM GABA (fig. 58) also started few minutes after the addition, but became statistically significant after 15 minutes. Although the responses showed high variations, the curve pattern seemed to indicate the following phases: contraction, subsequent plateaux and slow volume recovery.

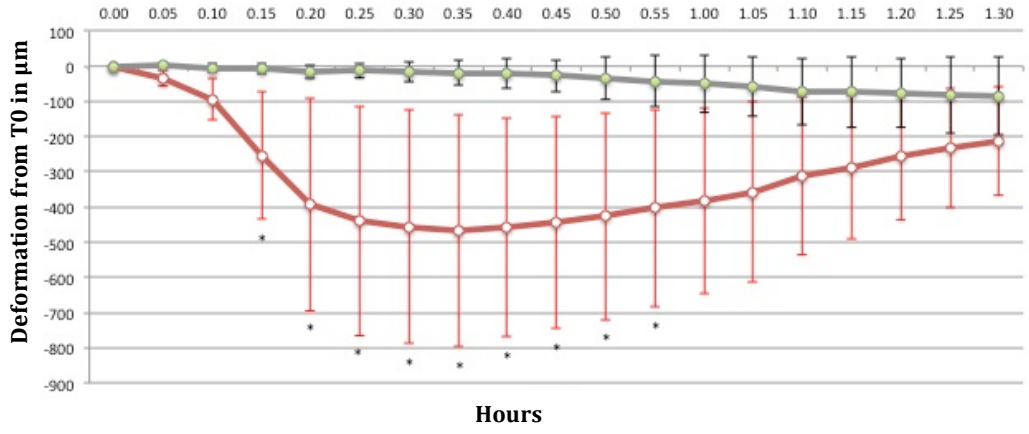

Figure 58. Mean dimensional changes of sponges exposed to 1mM GABA (**red & white dots**) or ASW only as controls (**green dots**). One way ANOVA: * = $p<0.01$. Bars = standard deviations. N = 5.

There were no significant difference in the contraction waves induced by the two neurochemical compounds (fig. 59). Moreover Glu seemed to induce a much more rapid contraction with respect to GABA that, on the other hand, was able to induce higher contractions (maximum contraction induced by GABA was 770 µm high vs 570 µm induce by Glu).

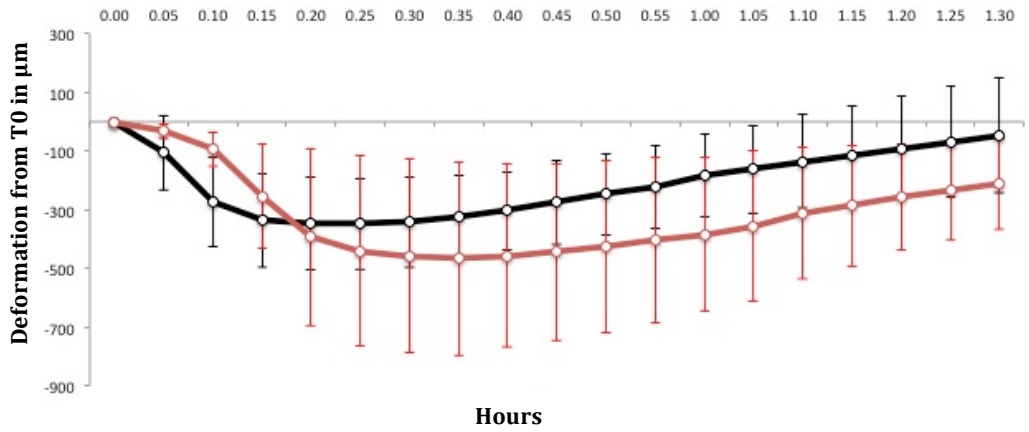

Figure 59. Mean dimensional changes of sponges exposed to 1mM Glu (**black & white dots**) or 1mM GABA (**red & white dots**). There are no statistic differences. One way ANOVA. Bars = standard deviations. N = 5.

The force generated by the application of 1mM Glu reached its maximum values after 15-20 minutes and started to decrease after 25-30 minutes (fig. 60). The range of the maximum contractions was comprised between 200 and 700 mg.

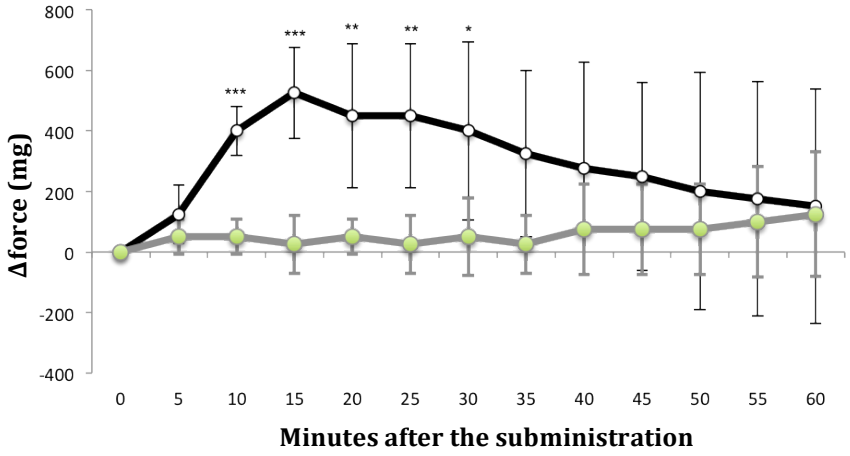

Figure 60. Means of the relative (Tx-T0) tension recorded after the addition of 1mM Glu. **Black & white dots** = 1mM Glu; **green dots** = controls. ANOVA: * = $p<0.05$; ** = $p<0.01$; *** = $p<0.001$. Bars = standard deviations. N = 5.

In contrast to what observed for the contraction magnitude, the forces generated by the application of 1mM GABA showed very low variations. After 15 minutes the sponges generated a force of 200-210 mg; these values were maintained for other 15 minutes before starting to decrease (fig. 61).

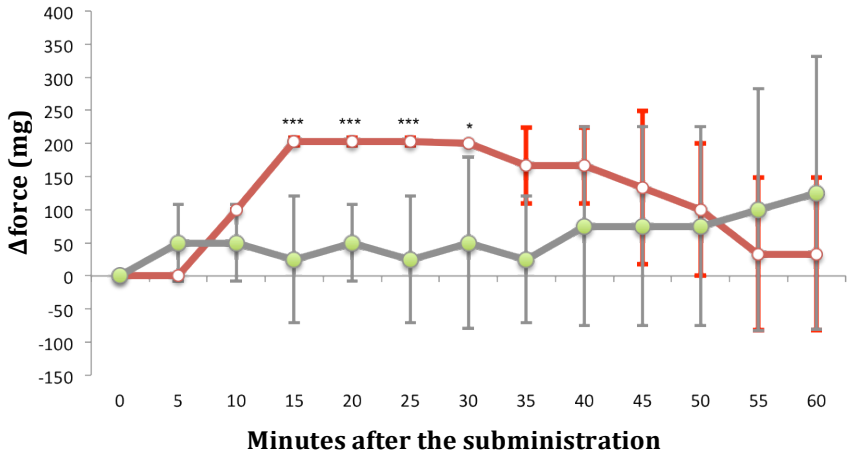

Figure 61. Means of the relative (Tx-T0) tension recorded after the addition of 1mM GABA **Red & white dots** = 1mM GABA; **green dots** = controls. ANOVA: * = p<0.05; ** = p<0.01; *** = p<0.001. Bars = standard deviations. N = 5.

By comparing the forces generated by Glu and GABA (both 1mM) it was possible to demonstrate that Glu induced higher contractile forces between 10 and 15 minutes (fig. 62). Although non-statistically significant the force appeared to be higher from 5 minutes to 30 minutes after the treatment (fig. 62).

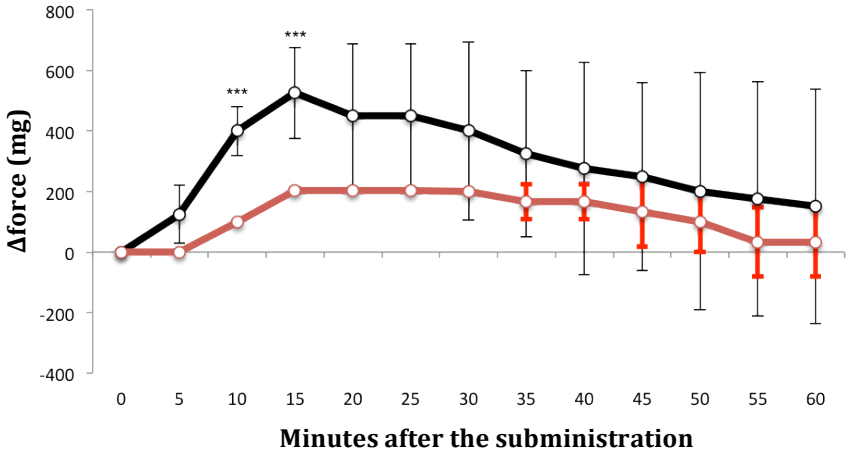

Figure 62. Means of the relative (Tx-T0) tension recorded from sponges exposed to 1mM Glu (**black & white dots**) or 1mM GABA (**red & white dots**). ANOVA: *** = p<0.001. Bars = standard deviations. N = 5.

3.6.4 Evaluation of the effects on viscosity

Exposing isolated ectosome samples to 0.5 or 2 mM GABA concentration did not induce any significant stiffening effect when compared with the controls (fig. 63). Only 2mM Glu induce a significant increase of viscosity (which is inversely proportional to the relative speed), when compared with the controls, between 25 and 30 minutes.

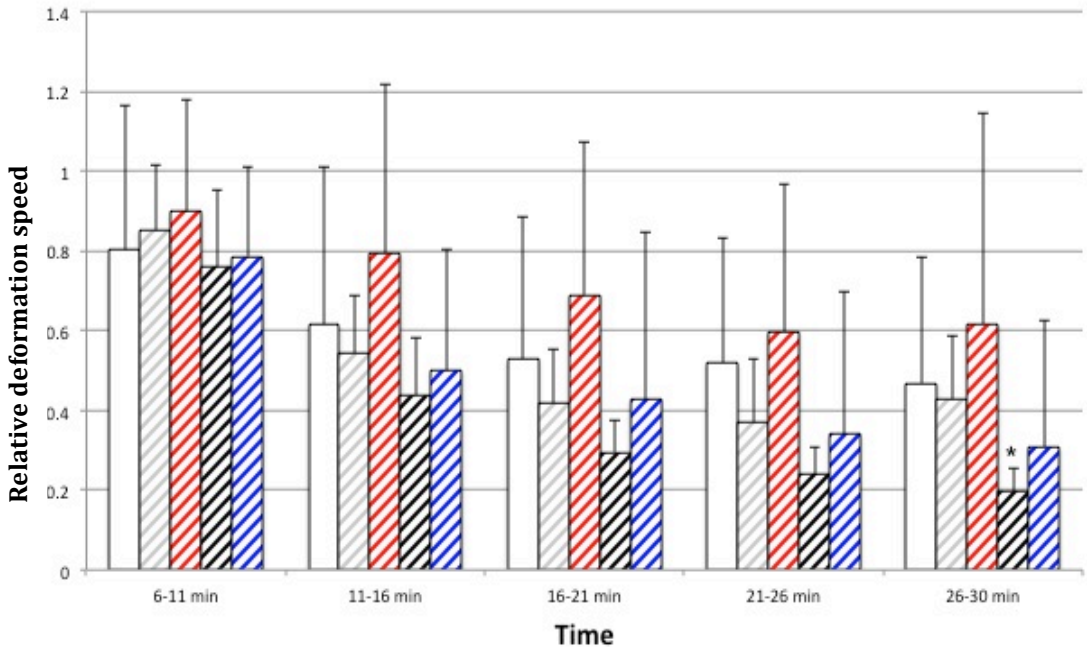

Figure 63. Isolated ectosome samples mean relative deformation speed speed (inversely proportional to viscosity) measured at different endpoints. **White columns** = ASW; **grey striped columns** = Glu 0.5mM; **red striped columns** = GABA 0.5mM; **black striped columns** = Glu 2mM; **blue striped columns** = GABA 2mM. ANOVA: * = $p<0.05$. Bars = standard deviations. N = 10/8.

On the other hand if we consider the absolute viscosities values 10/15 minutes after the addition of the chemical, when both GABA and Glu reach the force peak (see fig. 62), statistical differences could be observed between ASW and 2mM GABA samples, and between ASW and 2mM Glu samples (fig. 64).

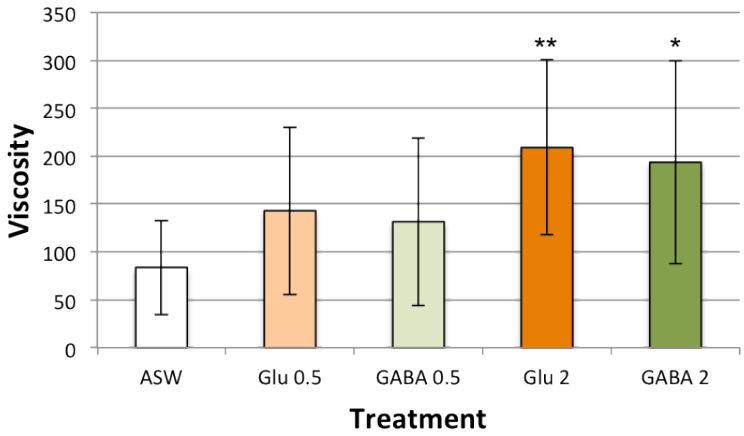

Figure 64. Mean viscosity values between 10/15 minutes after the addition of the chemicals. There are statistical differences between ASW and 2mM GABA, and between ASW and 2mM Glu. Two tailed t-test. * =$p<0.05$; ** = $p<0.025$. Bars = standard deviations. N = 10/8.

The addiction of GABA and Glu (both at 0.5mM concentration) to isolated choanosome samples did not induce any significant viscosity changes when compared with the controls (fig. 65).

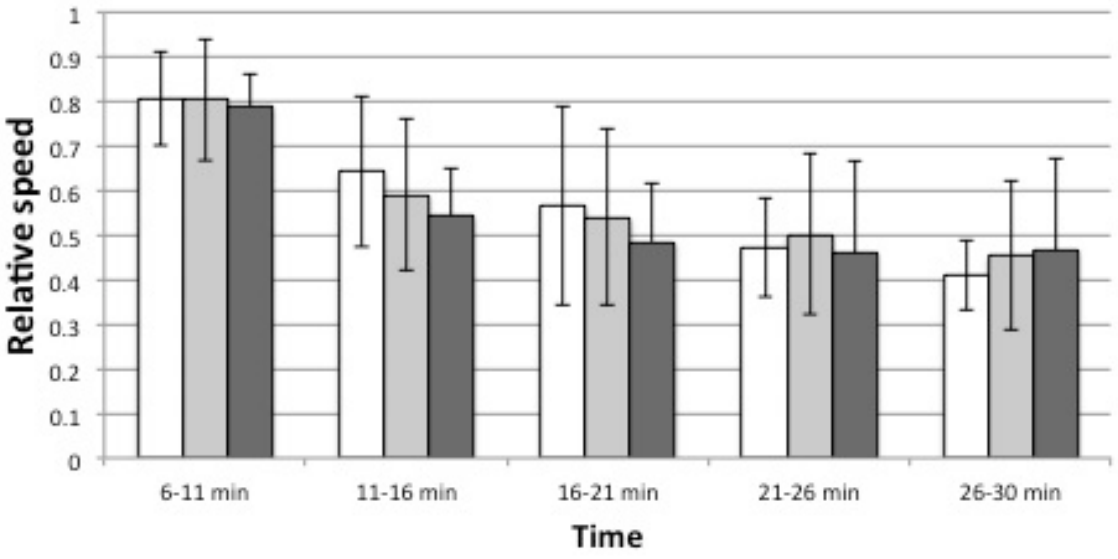

Figure 65. Isolated choanosome samples. Mean relative viscosity (inversely proportional to viscosity) measured at different endpoints. **White columns** = ASW; **light grey columns** = GABA 0.5mM; **dark grey columns** = Glu 0.5mM. ANOVA. Bars = standard deviations. N = 10.

3.7 Survey on actinocytes elements

LSCM

Although actinocytes they can be rarely found in other mesohyl regions, they are very frequently found around the exhalant canals (fig. 66 1). In this area on the basis of the actinocytes orientation and arrangement it was possible to distinguish three different and well-defined regions. In ad luminal region they are orthogonally (longitudinally to canals) directed (fig. 66 2 C), in the intermediate region actinocytes have a radial orientation (fig. 66 2 B), in the ad luminal region actinocytes were arranged in a circular pattern (fig. 66 2 A).

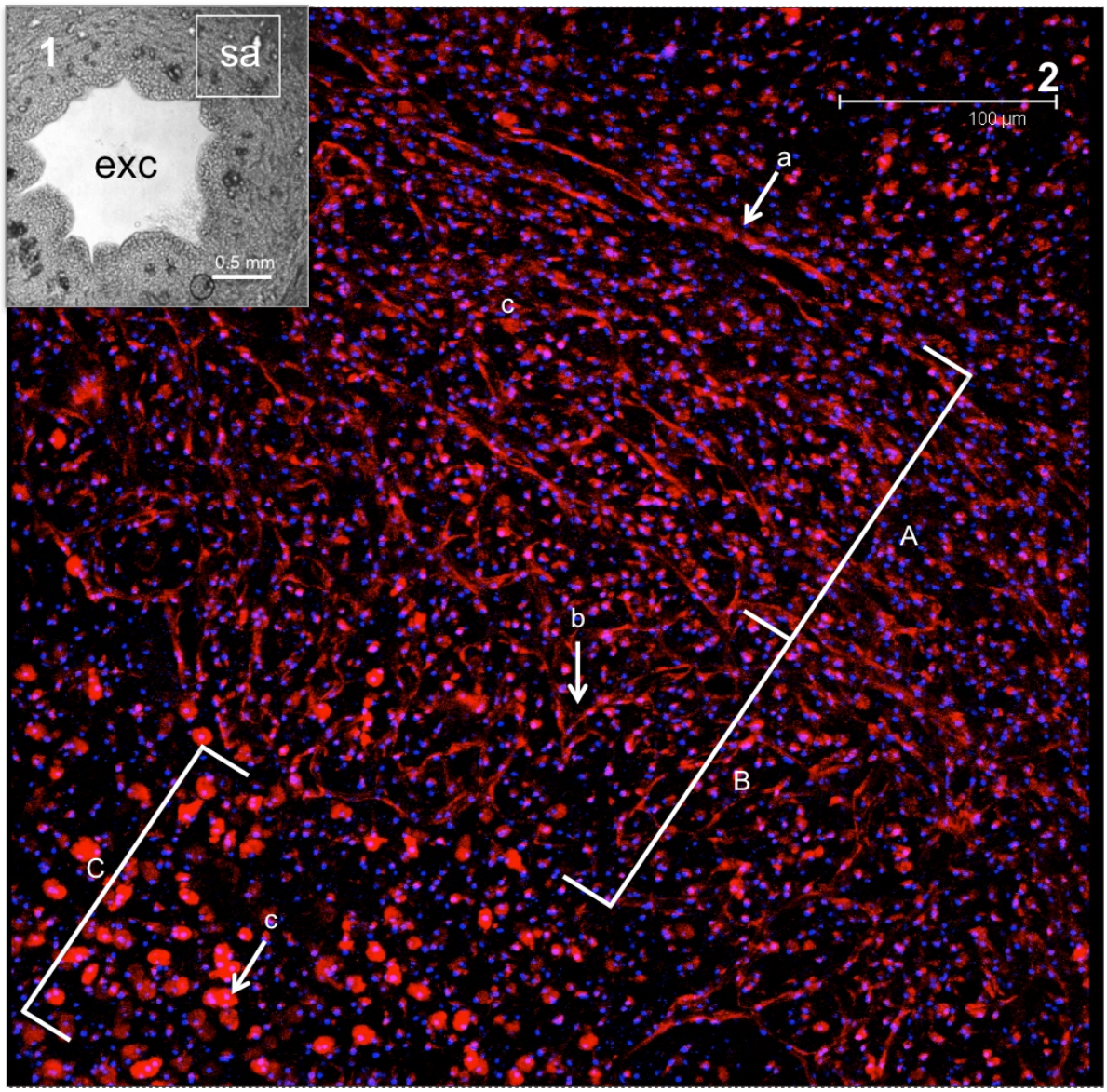

Figure 66. Bright field (**1**) and LSCM (**2**) Transversal sections of the oscular region. **1**. Transmission light images of the oscular region. **exc** = exhalant canal; **sa** = scanned area. **2**. Distribution of actin (rhodamine phalloidin, **red**) and Draq5 (nuclei, **blue**) in the nearby of the exhalant canal. **A** = area with circularly oriented actinocytes (**a**). **B** = area with radially oriented actinocytes (**b**). **C =** area with longitudinally oriented actinocytes (**c**).

TEM

Circularly oriented actinocytes appeared to be well organized to form thin bundles (fig. 67), each cell being packed to the adjacent onesby means of junctions quite comparable to typical adherens zonulae (fig. 68 A). Actinocytes showed an evident Golgi apparatus, an abundant rough endoplasmic reticulum (RER) and numerous mitochondria (fig. 68 B), and appear to be involved in a conspicuous phagocytic activity.

Figure 67. TEM longitudinal section of circular oriented actinocytes. Legend: **n** = nucleous; **fg** = phagosome; **red arrow** = actin filaments.

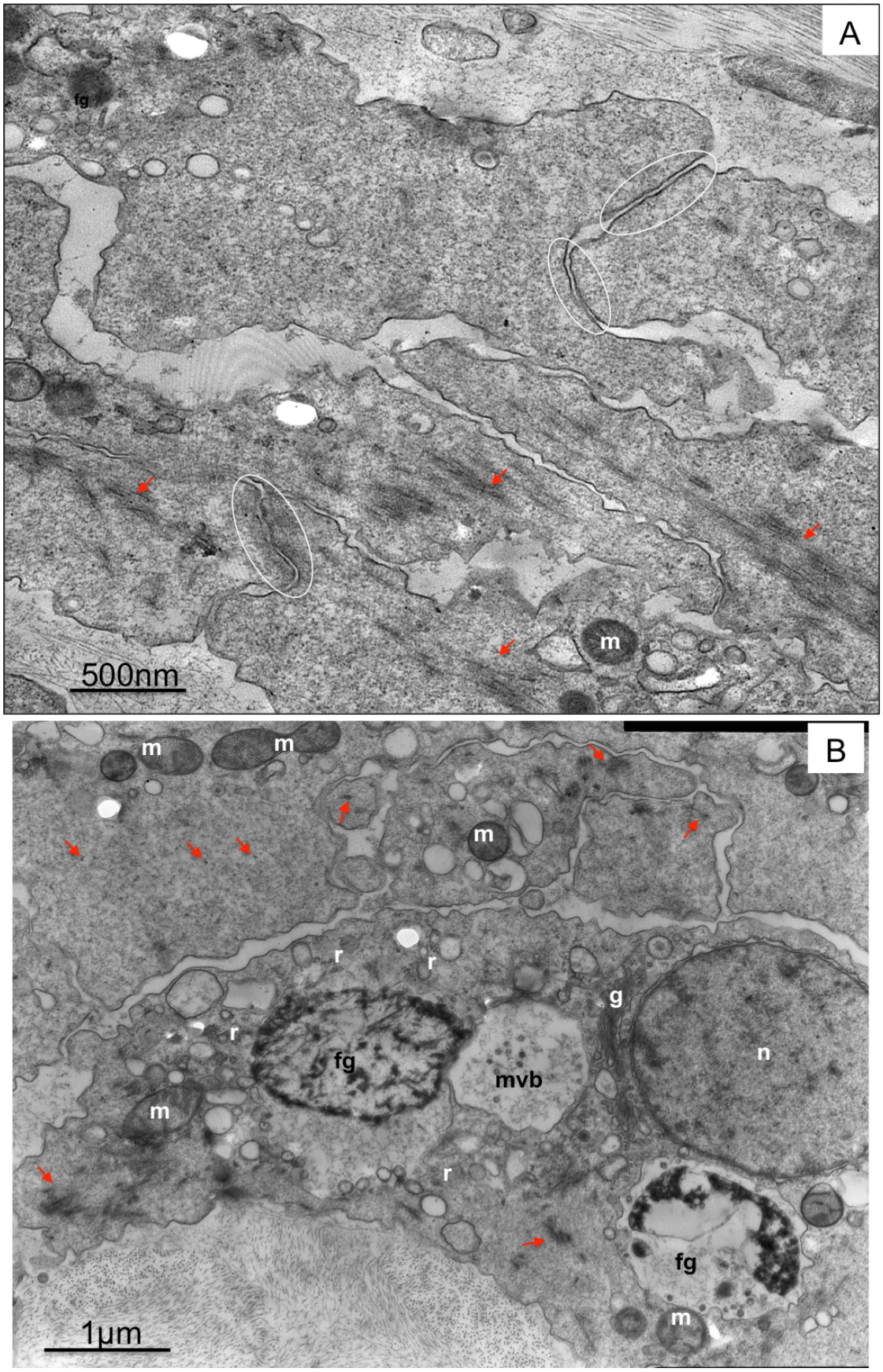

Figure 68. TEM micrographs of actinocytes. **A** detail of image 67 showing some zonulae adherens (white ellipses). **B** actinocyte showing a high phagocytosis activity. Legend: **red arrow** = actin filaments; **m** = mitochondria; **n** = nucleous; **r** = RER; **fg** = phagosomes; **g** = Golgi apparatus; **mvb** = multi vesicular bodies.

Longitudinal actinocytes arranged close to the exhalant canal were smaller in size and rarely associated together. These elements could be better identified as real myocytes since they are characterized by a sort of "contractile apparatus", defined by a number of actin filaments and scattered dense bodies (fig. 69, 70). The presence of presumptive myosin-like filaments could be also observed (fig. 70).

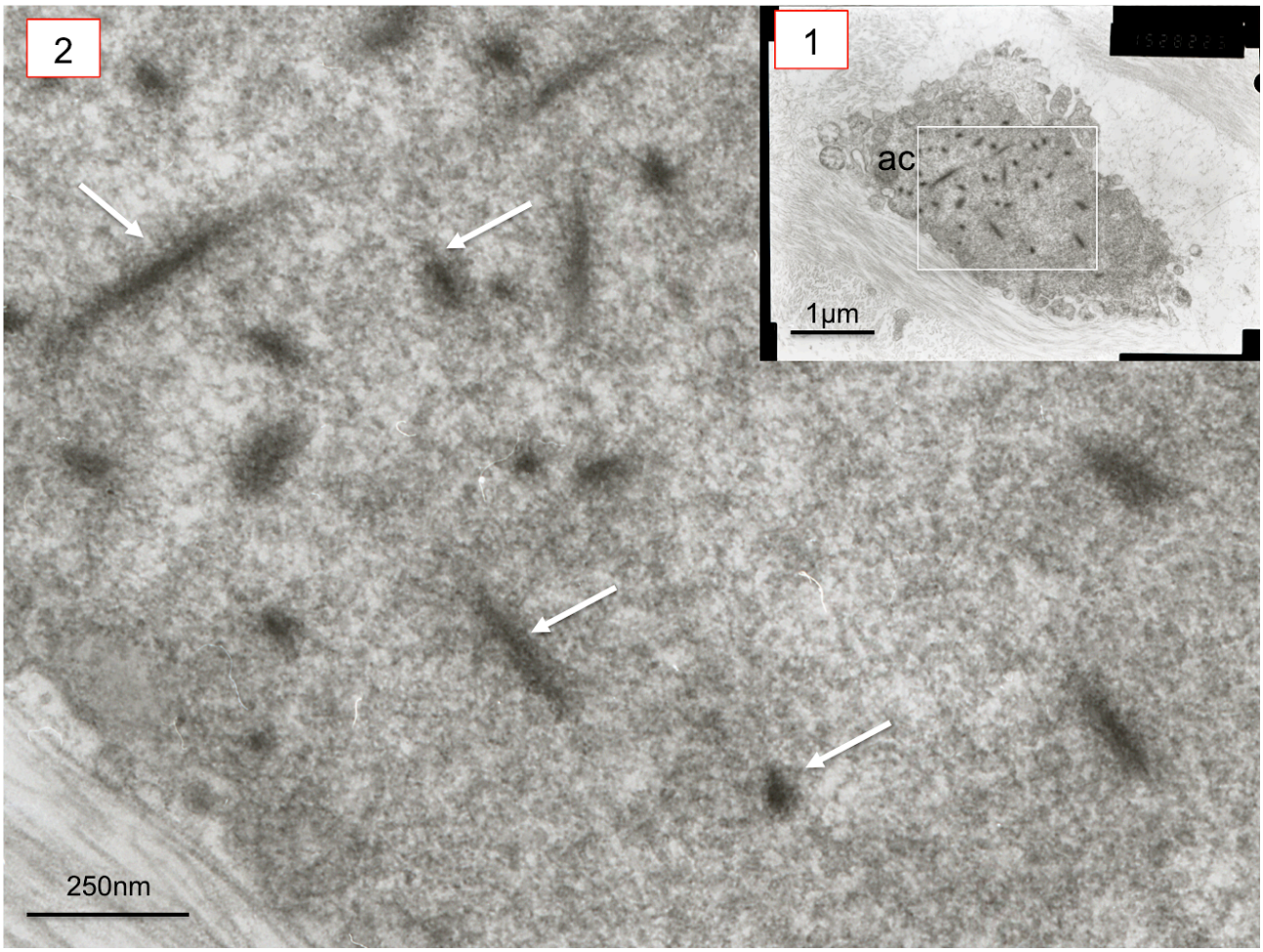

Figure 69. TEM micrograph of an actinocytes in cross section. **1** overview of the cell; **2** detail of the presumptive contractile apparatus. It is possible to observe a number of actin filaments and scattered dense bodies (**white arrows**) in different orientations. **ac** = actinocyte.

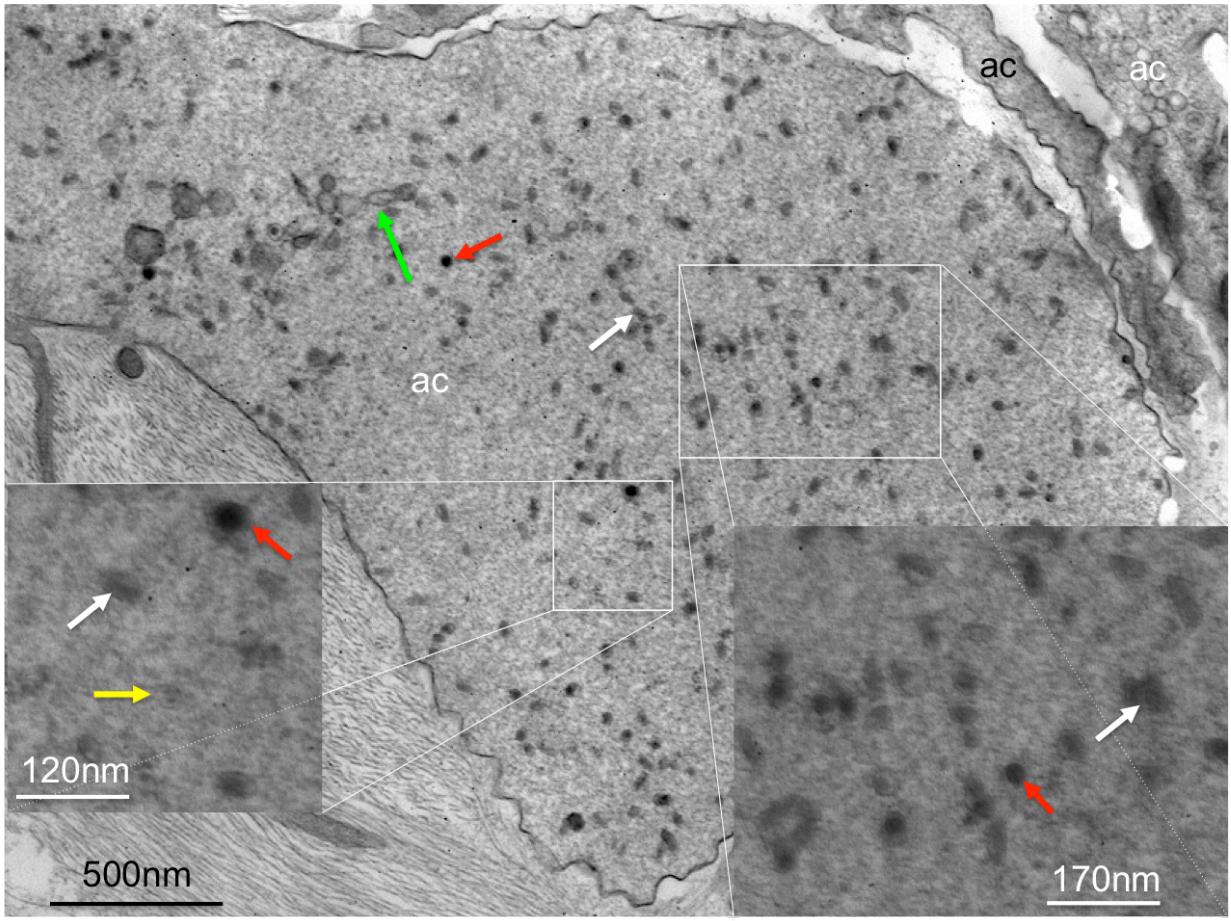

Figure 70. TEM cross section of actinocytes. It is possible to observe scattered dense bodies (**white arrows**), a relevant number of thin actin filaments (**yellow arrow**) and some thick myosin-like filaments (**red arrows**). Vacuoles = (**green arrow**); **ac** = actinocyte.

3.8 Reaction to mechanical stimulations

3.8.1 Analyses of the parameters derived from the deformation curves

The employment of the appropriate electronic force transducer shown in figure 11 allowed us to observe in detail the deformation curves induced by the rod shaped weight (fig. 12). The four parameters extracted from the curves were plotted against sponge thickness (fig. 71) and tested to check any possible correlations.

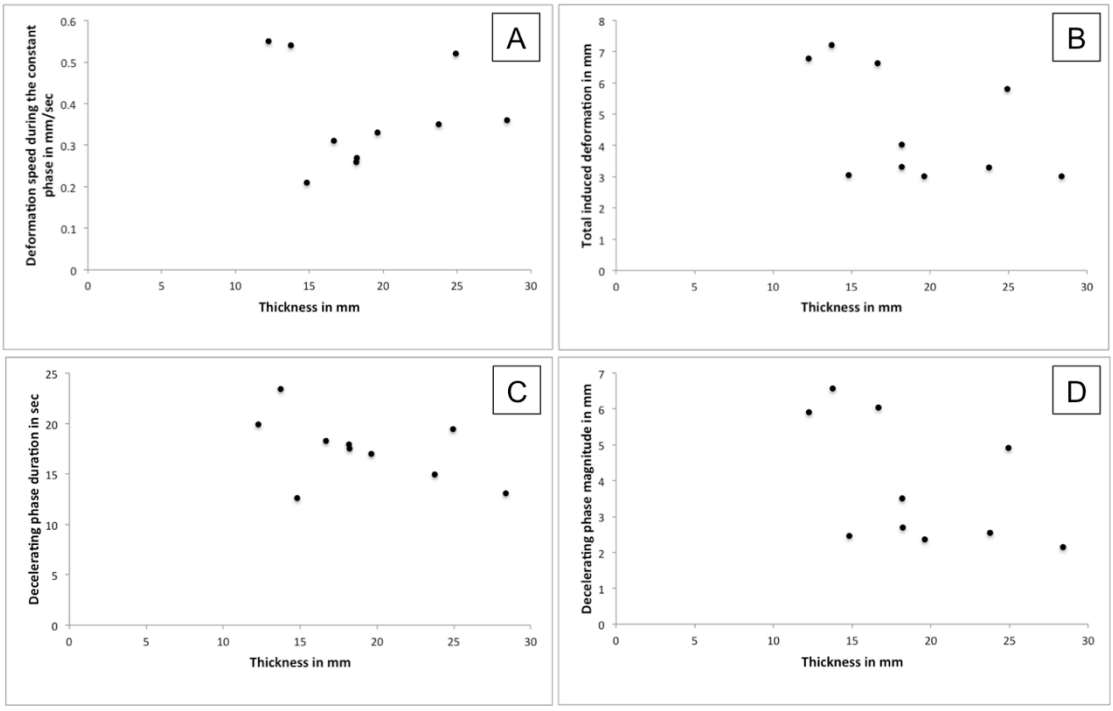

Figure 71. Scatter plots of sponge thickness and: speed during the constant phase (**A**); total induced deformation (**B**); decelerating phase duration (**C**); decelerating phase magnitude (**D**).

All the four parameters resulted to be independent from the sponge thickness (table 6). The speed during the constant phase deformation was chosen as the best parameter to describe the sponge state: in fact extracting these values from the curves was easier and much more rapid, and moreover it was the most independent of the four considered parameters (table 6).

Parameter	TI	CP	CPD	CPM
Number of XY Pairs	10	10	10	10
Pearson r	-0.4839	-0.07841	-0.4669	-0.5259
95% confidence interval	-0.8535 to 0.2098	-0.6748 to 0.5800	-0.8474 to 0.2307	-0.8681 to 0.1552
P value (two-tailed)	0.1565	0.8295	0.1737	0.1184
P value summary	ns	ns	ns	ns
Is the correlation signficant? (alpha=0.05)	No	No	No	No
R squared	0.2341	0.006148	0.2180	0.2766

Table 6. Summary of Pearson statistics. There were no correlations in each considered parameter. **TI** = total induced deformation; **CP** = constant deformation speed; **CPD** = decelerating phase duration; **CPM** = decelerating phase magnitude.

3.8.2 Checking the presence of a stiffening response following mechanical stimulations

The response to mechanical stimulation was previously verified by Parma (2007). However in his experiments the time elapsed between one stimulation and the subsequent one was not considered.

Here we analyzed the responses to mechanical stimulation of sponges at different time endpoints.

After 20 seconds there was no differences between stimulated and unstimulated samples (fig. 72).

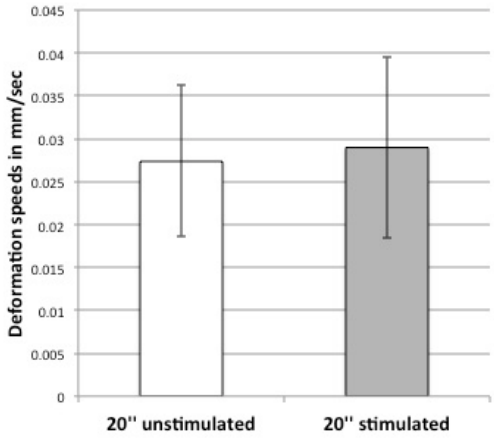

Figure 72. Mean deformation speeds measured 20 seconds after the treatments. There are no differences between unstimulated (**white column**) and stimulated (**grey column**) samples. ANOVA. Bars = standard deviations. N = 12.

After one minute from the treatments unstimulated samples were softer than stimulated ones (fig. 73).

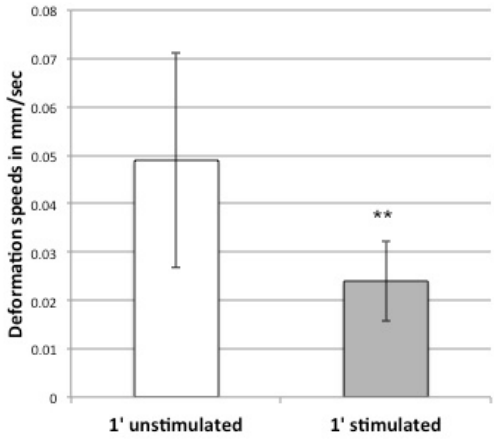

Figure 73. Mean constant deformation speeds measured 1 minute after the treatment. There is a statistically significant difference between unstimulated (**white column**) and stimulated (**grey column**) samples. ANOVA: ** = $p<0.01$; bars = standard deviations. N = 12.

Also 3 minutes after the treatments unstimulated sponges were softer than stimulates samples (fig. 74).

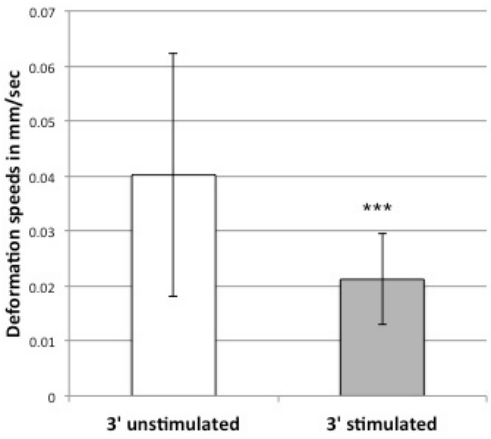

Figure 74. Mean constant deformation speeds measured 3 minutes after the treatment. There is a statistically significant difference between unstimulated (**white column**) and stimulate (**grey column**) samples. ANOVA: *** = $p<0.001$; bars = standard deviation. N = 12.

The procedure itself appeared to induce a temporary stiffening effect on unstimulated samples. After 1 and 3 minutes the sponges were softer (fig. 75).

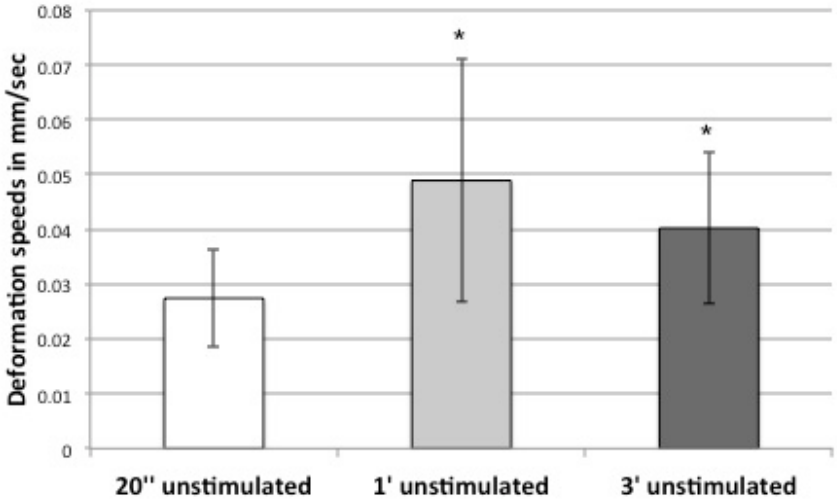

Graph 75. Mean deformation speeds of unstimulated specimens. There is a statistically significant difference between 20 seconds and 1 /3 minutes. **White column** = measurements after 20 seconds; **light grey** = measurements after 1 minute; **dark grey column** = measurements after 3 minutes. ANOVA: * = $p<0.025$; bars = standard deviation. N = 12.

Although there were no statistic differences between the three endpoints, it was possible to notice that stimulated sponges became stiffer as the time between stimulation and measurement increased (fig. 76).

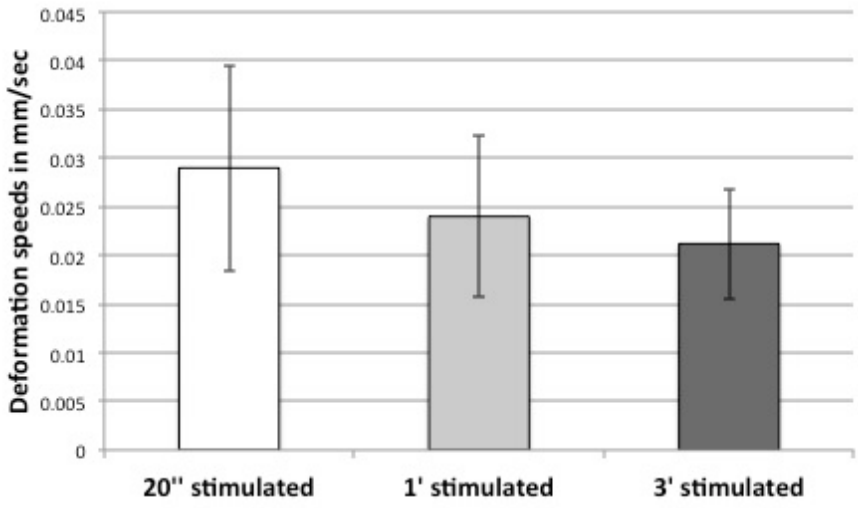

Figure 76. Mean deformation speeds of stimulated specimens. There are no statistically significant differences between 20 seconds and 1 or 3 minutes. **White column** = measurements after 20 seconds; **light grey** = measurements after 1 minute; **dark grey column** = measurements after 3 minutes. ANOVA. Bars = standard deviations. N = 12.

3.8.3 Checking the presence of a stiffening-signal transmission pathway

Previous experiments (Parma, 2007) showed that measuring sponge tensility with a procedure similar to that described above can induce stiffening only at low distance (0.5mm) from the stimulated/measured point: this led us to the conclusion that the measure itself induce stiffening in the nearby areas. In addiction, since no stiffening phenomena occurred at 4 cm distance, the stimulation magnitude did not appear to be enough to induce the sponge reaction.

Here we repeated the experiments employing a new equipment and varying both the parameters and the experimental conditions, namely the distances between the stimulation points, the amount of stimulation, the time between the different stimulations.

Measuring sponge tensility at 1 cm (fig. 77 point B) from a previously stimulated point (fig. 77 point A) revealed the capability of the sponge to stiffen adjacent regions when adequately stimulated. Other stimulations given at point B were not enough to induce a significant stiffening response at 4 cm distance (fig. 77 point C); however thus were enough to stiffen the sponge at 2 cm distance (fig. 77 point D). Although we observed a stiffening reaction at point B and D, those responses were significantly weaker if compared to what registered for vigorously manipulated sponges (fig. 77 point E).

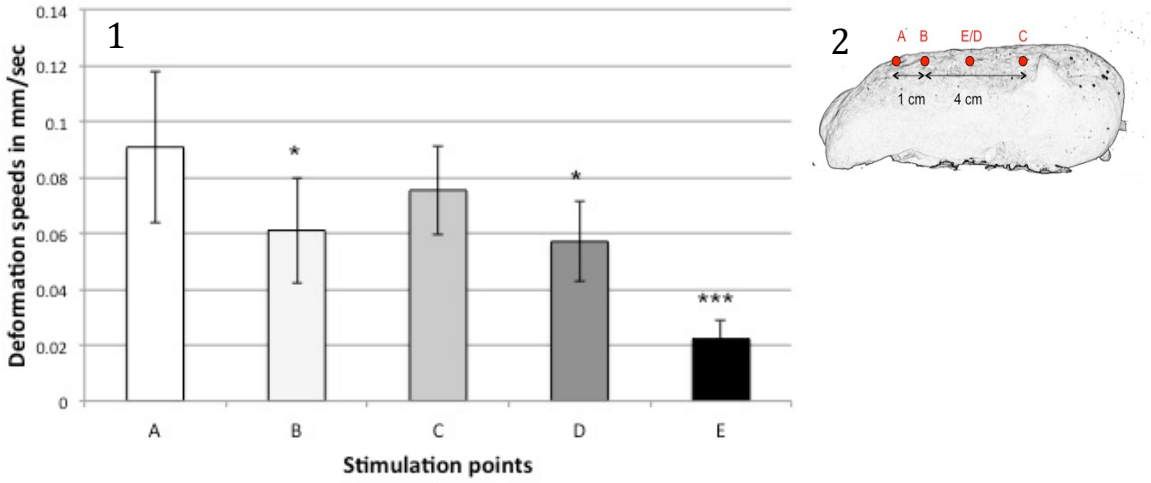

Figure 77. (**1**) Mean deformation speeds measures in different sponge areas (**2**). First stimulation/measurement on unstimulated sponge (**A**), at 1 cm from point A (**B**); at 5 cm form point A (**C**), at 3 cm from point A (**D**) and at point D after intense stimulation (**E**). There are statistically significant differences between point A and point B and D. Point E is statistically different from all the other points.
ANOVA: * = $p<0.025$; *** = $p<0.001$. Bars = standard deviations. N = 7.

3.8.4 Evaluating the possible role of the exopinacoderm in the signal transmission

Both sponges where the exopinacoderm was preserved and where the exopinacoderm continuity was altered maintained the capability to stiffen (fig. 78 A'; fig 79 A'). The magnitude of the given stimulation was, on the other hand, not enough to induce a stiffening reaction (at 1 cm about 1 minute after the stimulation) in both the experiments (fig. 78 B; fig. 79 B). Only sponges where the exopinacoderm continuity was preserved stiffen at 2 cm distance about 2 minutes after the stimulation (fig. 78 C).

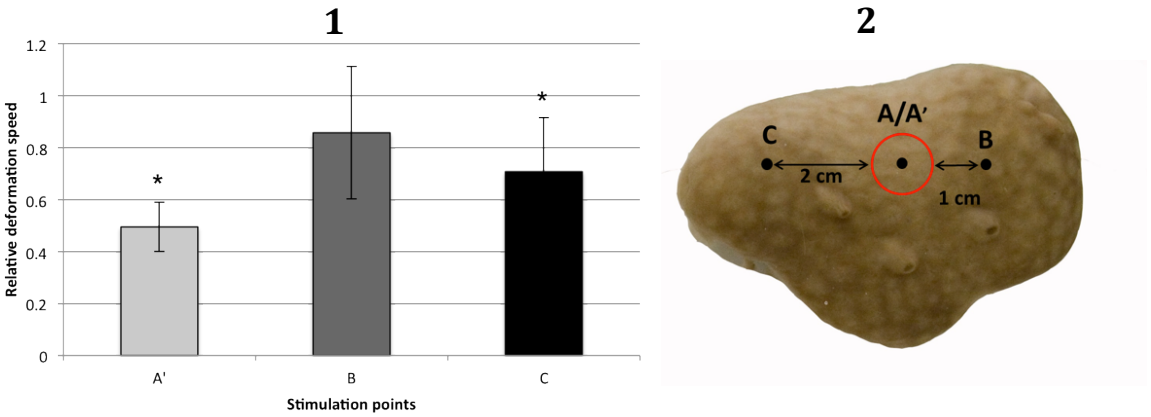

Figure 78. (**1**) Relative deformation speeds of intact specimens (deformation speed at points A',B,C/ deformation speed of points A). (**2**) scheme of the measured points . Point A' and point C were significantly stiffer than point A . Paired t-test; * = $p<0.025$. Bars = standard deviations. N = 6.

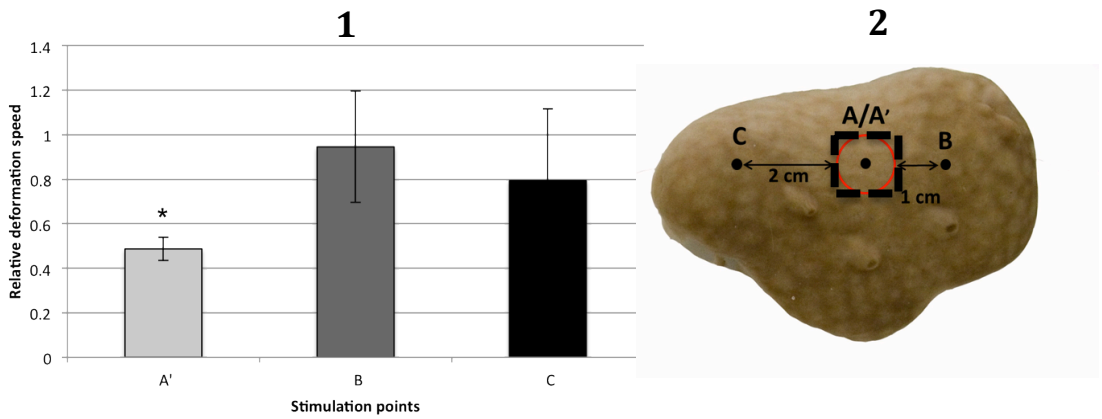

Figure 79. (**1**) Relative deformation speeds of specimens where the exopinacoderm continuity was alterated (deformation speed at points A',B,C/ deformation speed of point A). (**2**) scheme of the measured points. There is a significant stiffening only at point A'. Paired t-test; * = $p<0.025$. Bars = standard deviations. N = 6.

3.9 Biochemistry of mesohyl component

3.9.1 Testing the protein fraction on isolated ectosome samples

According to literature (Wilkie et al., 2006; Parma, 2007; Parma et al., 2007) isolated ectosome samples display less variability in different experiments. For this reason we decided to use isolated ectosome samples in RC to test the capability of the different extract to re-stiffen them and isolated ectosome samples partially destiffened (PD) to check the capability to re-stiffen them or to block the destiffening process.

Effect of tissue extract on RC samples

At the T0 endpoint all samples were in a well-destiffened state (fig. 80 T0). One hour after the exposure to the different media, it was possible to observe a significant increase of tensility (decrease of the bending magnitude) in ectosomes exposed to P40, P50, P60, P70 (fig. 80 T1). The increase of tensility was maintained also after 2 hours (fig. 80 T2).

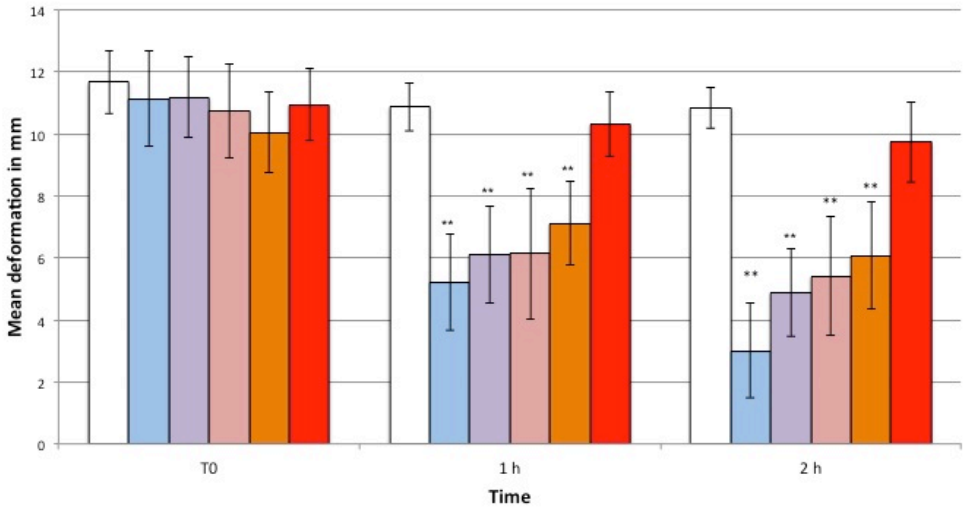

Figure 80. Mean observed bending of destiffned isolated beam-shaped ectosome before (T0) and after 1 and 2 hours in solutions containing 2 parts of ASW+1 part of: EBD (**control/white columns**); P40 (**blue columns**); P50 (**violet columns**); P60 (**pink colums**); P70 (**orange columns**) and P80 (**red columns**). One way ANOVA: ** = $p<0.01$. Bars = standard deviations. N = 5.

By comparing the relative bending, although non statistical differences were detected, it was possible to notice that the fraction P40 induced higher tensility changes: the relative bending induced by P40 was higher, both between T0 and T1 (fig. 81 A) and between T1 to T2 (fig. 81 B), than those induced by the other protein fractions.

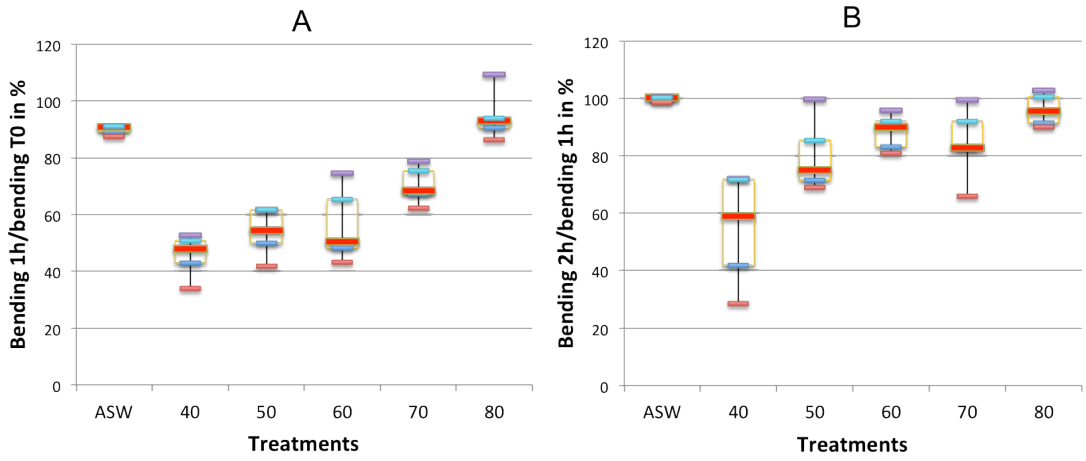

Figure 81. Boxplot of the relative occurred bending between T0 and 1h (**A**) and between 1h and 2h (**B**) of samples immersed in different solutions (data are the same of fig. 78). **ASW** = controls; **40** = P40; **50** = P50; **60** = P60; **70** = P70; **80** = P80.

3.9.2 Effect of tissue extract on PD samples

Exposing PD ectosome to P40 and P50 retarded the destiffening process (fig. 82). This retard was statistically significant after 3 hours where controls samples where softer than those exposed to P40 and P50 (fig. 82).

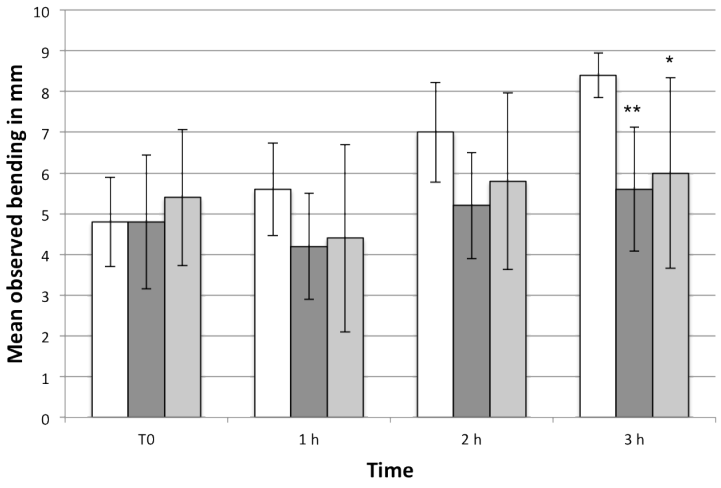

Figure 82. Mean occurred bending of partially destiffned isolated beam-shaped ectosome before (T0) and after 1, 2, and 3 hours in a solution containing 2 parts of ASW+1 part of: EBD (**control/white columns**); P40 (**dark grey columns**) and P50 (**light grey columns**). One way ANOVA: * = $p<0.05$; ** = $p<0.01$. Bars = standard deviations. N = 5.

3.9.3 Aggregation tests

The capability of P40 to aggregate collagen (i.e., to establish bonds between collagen fibrils) was tested according to Trotter and coworkers (1996). Aggregation test were generally performed in 24 multiwells plates at RT by mixing one of the collagen suspensions (CSs) with P40. Different experiments were conducted by changing the parameters to investigate the effects of P40 on isolated collagen fibrils.

Verifying the capability of P40 to aggregate collagen fibrils

The proteins present in the P40 fraction were able to aggregate collagen fibrils extracted from different according to Matsumura's protocols (fig. 83) in the presence of ions (ASW). The aggregation was faster (few seconds/minutes) when the solution containing proteins and collagen fibrils were shacked; the aggregation occurred within some hours when the solutions where not shacked (fig. 84).

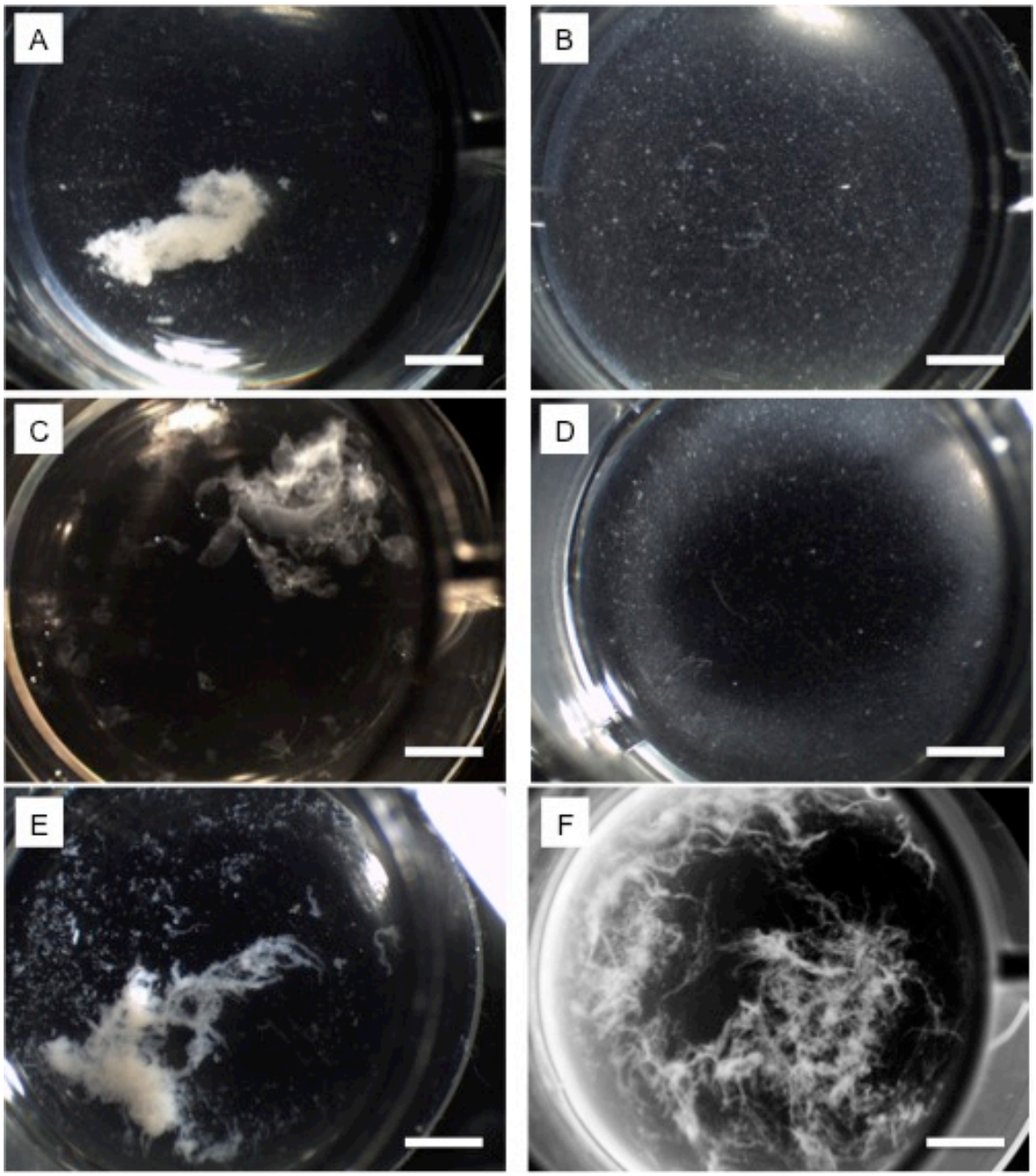

Figure 83. Aggregation assay: effects of P40 on different collagen extractions. **A** = ectosome collagen, extraction protocol A; **B** = ectosome collagen, extraction B; **C** = choanosome collagen, extraction protocol A; **D** = choanosome collagen, extraction protocol B; **E** = rat uterine cervix; **F** = echinoderm collagen (image colors were manipulated, real images was obtained with transmitted light). Bar = 3 mm.

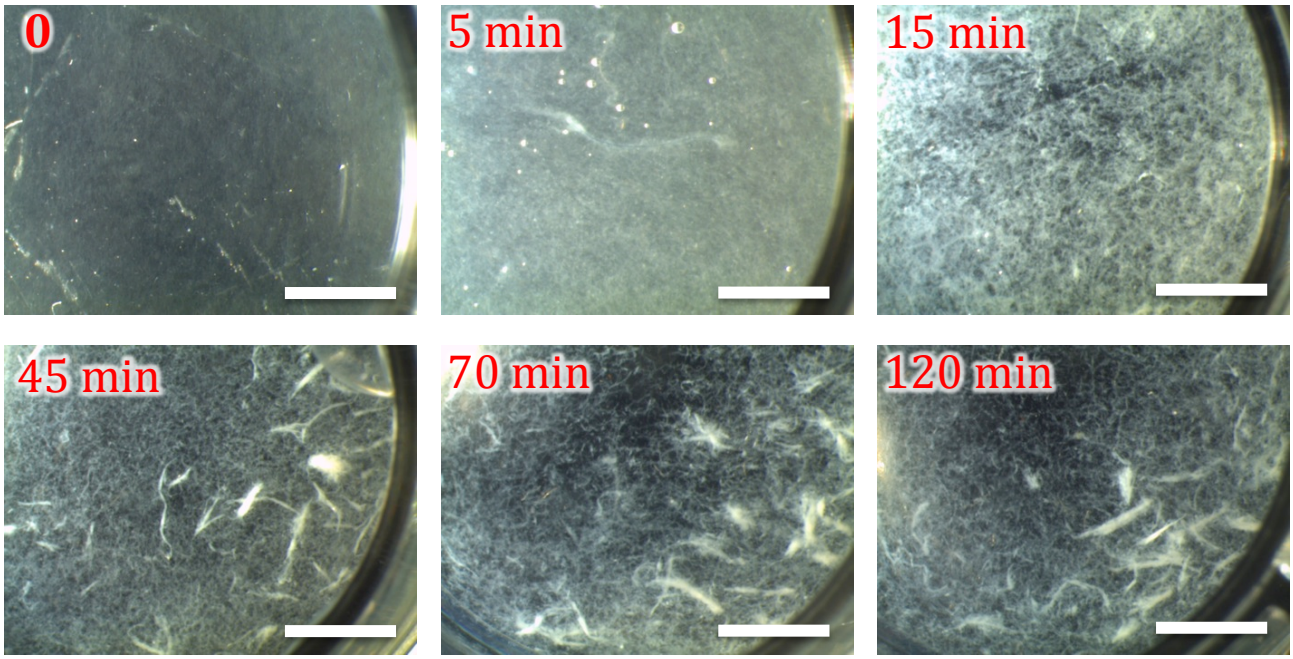

Figure 84. Effects of 250 µl of P40 added to 250µl ectosome collagen fibrils (in ASW). The plate was maintained stable in order to detect the aggregation behavior. Bar = 3 mm.

Verifying the possible dose dependent effects of P40

The apparent dose dependent effect of P40 on isolated collagen fibrils (fig. 85) was then checked by ImageJ software by desaturating and inverting the colors of the images of figure 81 (fig. 86 A) and then by measuring the integrated fluorescence (i.e the fibrils highlighted in white). As is possible to see in figure 86 B that there was a clear linear relation between P40 quantity and the integrated fluorescence.

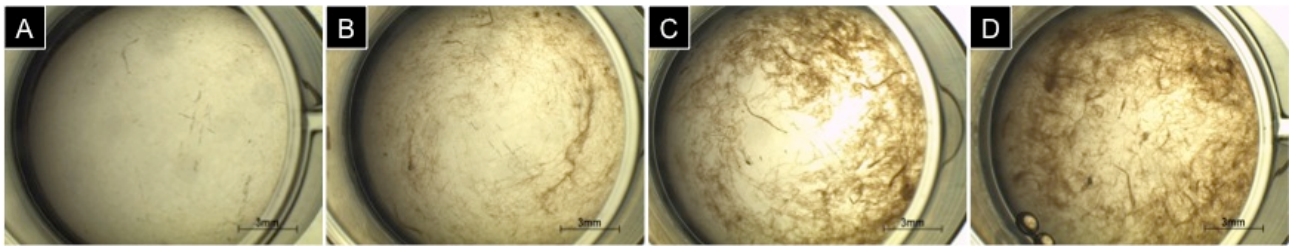

Figure 85. Aggregation assay: the dose/response effect of P40 on isolated collagen fibrils after 5 hours. Different amount of P40 or only dH_2O for the control were added to 250 µl of echinoderm CS in ASW (8mg/ml). **A** = control; **B** = 100µl of P40; **C** = 200µl of P40; **D** = 400µl of P40.

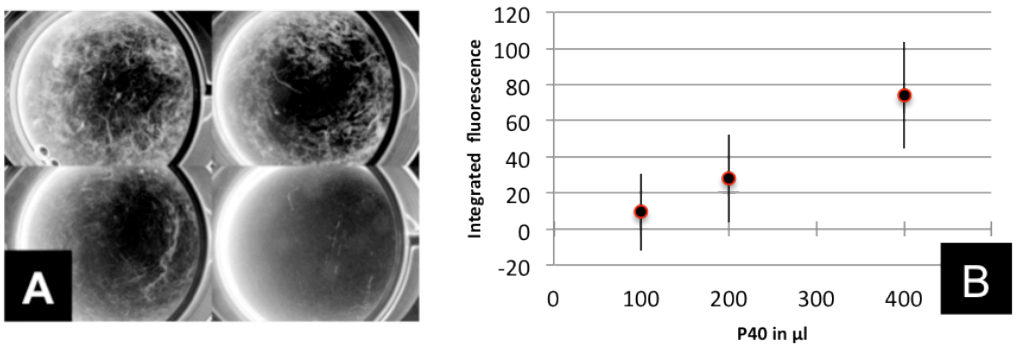

Figure 86. An estimation of the aggregated collagen has been performed by transforming the images of figure 81 into inverted black and white images (**A**) and measuring the integrated fluorescence (IF) with ImageJ software. The IF values have been then plotted against P40 quantities (**B**). Bars = standard deviation. N = 3.

Boling P40 at 100° for 5 minutes before mixing it with ectosome CS inhibited the aggregation of the fibrils (fig. 87 A). In contrast adding fresh P40 to the well induce a fast aggregation of the fibrils (fig. 87 B).

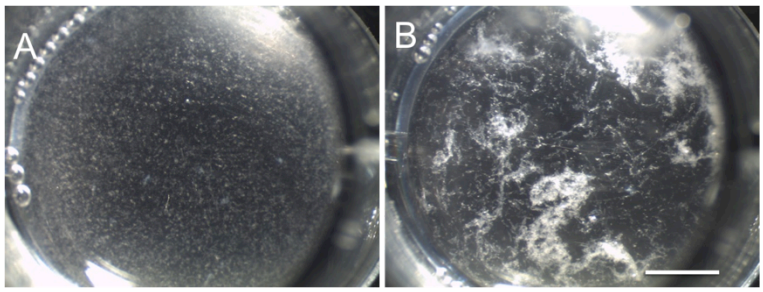

Figure 87. Aggregation assay: effect of boiled P40. 200 µl of ectosome CS in ASW were mixed with 200 µl of boiled P40 and shacked to accelerate the aggregation (**A**). After 30 minutes 200 µl of fresh P40 were added (**B**). Bar = 3mm.

Checking the role of different ions in the aggregation

All the previous aggregation tests were conducted in a medium containing different ions (those contained in the ASW). By testing the three most abundant ASW cations (Na_{+}, Mg_{2+}, Ca_{2+}), it was possible to demonstrate that the aggregation depended on divalent cations; in particular calcium ions induced the most evident aggregation (fig. 88) and that aggregation reaction occurred specifically between P40 and collagen. Magnesium cations induced some aggregation; moreover this aggregation was less abundant and stable than that obtained in the presence of calcium ions. In the absence of ions we had no aggregation at all.

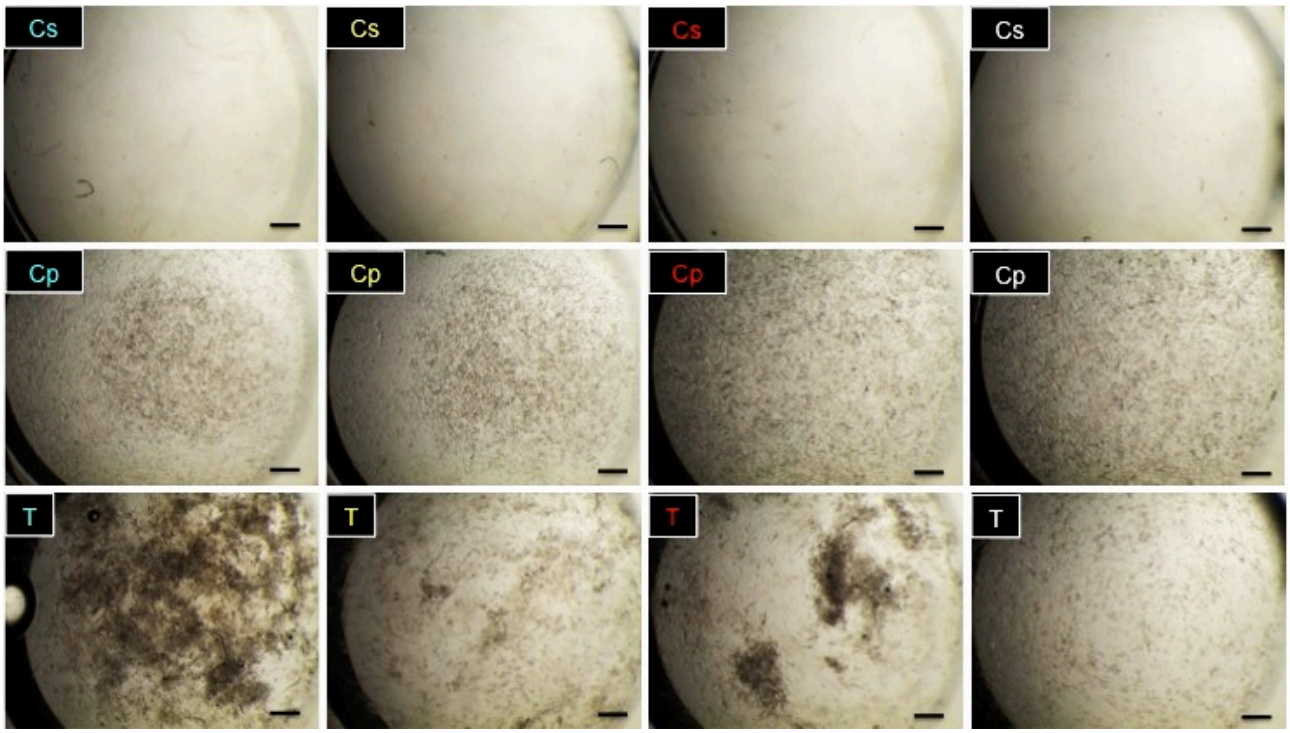

Figure 88. Aggregation assay: the role of different ions in the aggregation capability of P40. Concentrated solution containing $CaCl_2$ (blue), $NaCl_2$ (yellow), $MgCl_2$ (red) or dH_2O (white) have been added to the plates to reach a final concentration of 100 mM. **Cs** = 50 µl of ectosome collagen solution in dH_2O + 50 µl dH_2O; **Cp** = 50µl of P40 in dH_2O + 50 µl dH_2O; **T** = 50 µl of ectosome collagen solution in dH_2O + 50 µl of P40 in dH_2O. Bar = 1 mm.

3.9.4 Biochemical characterization of presumptive stiffening factor(s)

SDS-Page of the different fractions obtained via salting-out

The most effective protein solutions used in the tests (described at 3.9.2) were visualized in a 4-20% SDS-Page. Many proteins were present in the different fractions (fig. 89), since as expected the salting out is very inaccurate.

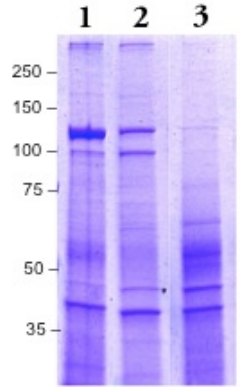

Figure 89. SDS-Page stained with brilliant blue Coomassie of P40 (**lane 1**), P50 (**lane 2**) and P60 (**lane 3**). Many proteins are present, although at different concentration, in all the three extracts.

Second purification step

A second purification step has been performed by using millipore Amicon tubes (molecular cut off 50 or 35KDa). Proteins contained in P40 fraction have been separated in protein bigger than 50KDa; between 50 and 35KDa and less than 35 KDa. The three protein fractions have been then resuspended in a same amount of dH_2O and tested with an aggregation assay with ectosome CS in the presence of Ca_{2+} ions. Our results showed that only proteins with a molecular weight bigger than 50KDa could induce aggregation (fig. 90).

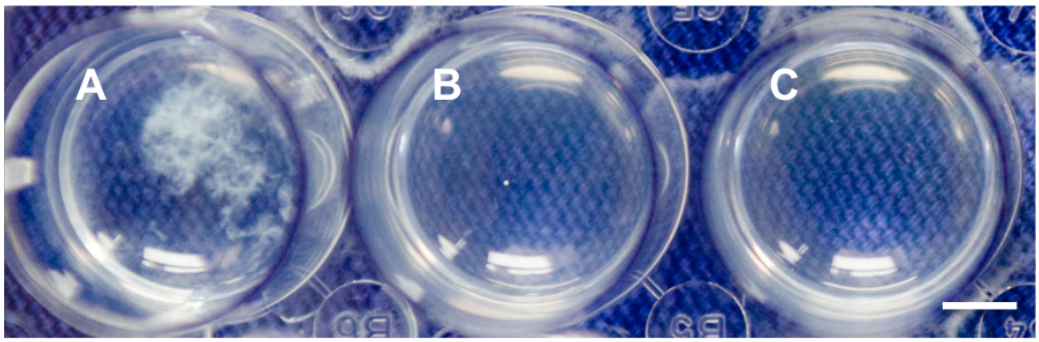

Figure 90. Aggregation assay: testing proteins of P40 separated on the bases of the molecular weight. 100 µl of ectosome CS were mixed with 100µl 0.1M $CaCl_2$ and 100 µl of:
A = proteins >50KDa; **B** = 50KDa>proteins>35KDa or **C** = 35KDa>proteins. Bar = 3mm.

3.9.4.1 Blue Native Page

Proteins separation

Proteins present in P40 did not separate well also when negatively charged with brilliant blue Comassie pre-staining in the presence of both 0.1 or 0.3 % Triton-X 100 (fig. 91 1, 2). Most of the proteins remained in the stalking gel; only three bands were detectable.

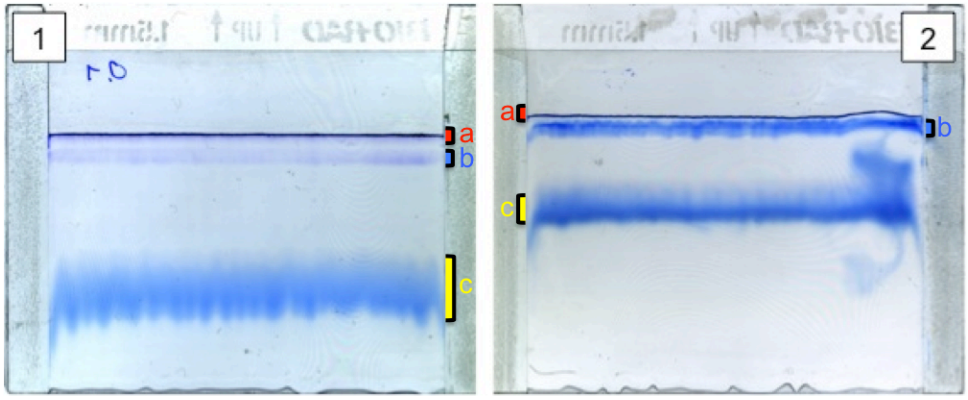

Figure 91. Blue Native electrophoresis of P40 pre-stained with brilliant blue Comassie and run in 0.1% (1) and 0.3% (2) Triton-X 100. Three bands were detectable, the first and more intense in the stalking (**a**), the second in the first part of the separating gel (**b**) band the third large band in the central part of the separating gel (**c**).

Aggregation assay

Part of the proteins recovered from the three bands were tested with a standard aggregation assay to check the capability to aggregate ectosome collagen fibrils. The most effective fraction (fig. 92, A) was the one that did not migrate in the gel; however proteins extracted from the second band were able to induce some aggregation (fig. 92 B). The third band did not induce any aggregation (fig. 92, C). It is possible to notice that the pre-staining procedure with Coomassie dye did not affect the aggregation capability.

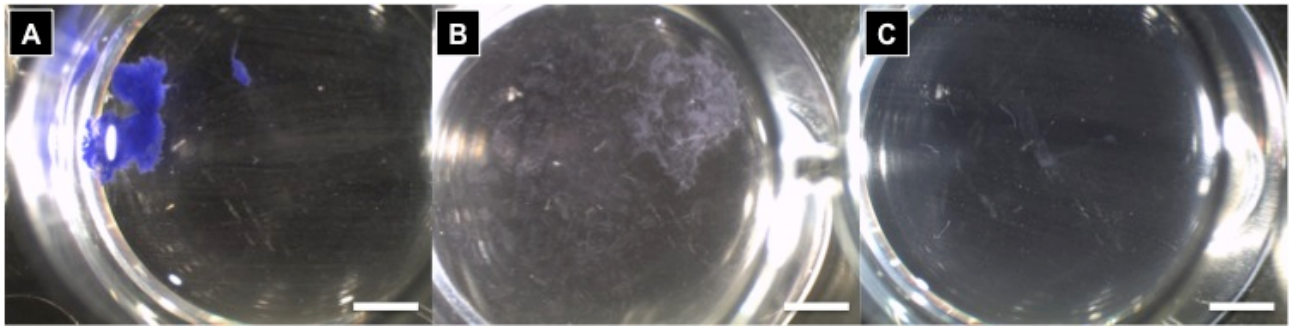

Figure 92. Aggregation assay: testing the proteins recovered from the gel. Although stained with Coomassie the proteins maintain the capability to aggregate ectosome collagen fibrils. The most effective fraction (**A**) was the one containing protein extracted from band **a**; some aggregation was detectable also in well **B** that contain protein from band **b**. Proteins extracted from band **c** did not induced aggregation (**C**).

SDS-Page

Running the proteins recovered from band a showed that many proteins were present in large amount (fig. 93 A) indicating that those proteins did not well separate also when stained with negative charges. In band b only few proteins, present also in band a, were present (fig. 93 B).

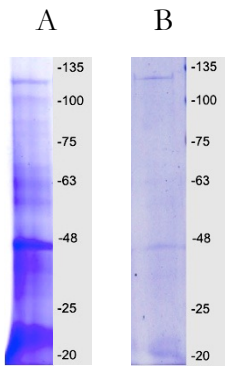

Figure 93. (**A**) SDS-Page of proteins recovered from band a and (**B**) band b.

Discussion

4.1 Reaction to mechanical stimulation

As far as we know *C. reniformis* is the only sponge where it has been experimentally proved the presence of a dynamic collagenous mesohyl able to stiffen after being manipulated (Wilkie et al., 2006). Unfortunately there is a total lack of specific investigations in other species. Stimulation/response events were reported to occur in the demosponges *T. willelma* and *E. muelleri*: both the sponges showing a contractile activity after localized stimulation (Nickel, 2004; Elliott & Leys, 2007). However in these animal models there are no data related to possible changes in the mechanical properties; it was only observed a stimulation/reaction phenomenon that may have some common physiological pathway with the phenomena recorded in *C. reniformis*.

Previous experiments carried out in our lab demonstrated the capability of isolated beam shaped samples of both ectosome and choanosome to stiffen after mechanical stimulations: in particular ectosomes samples reacted in a dose dependent manner (Parma, 2007). Moreover Parma (2007) reported that localized stimulations on the sponge surface were able to stiffen the adjacent regions (at 0.5 mm distance from previously stimulated points) but did not induce a significant stiffening reaction at 4 cm distance. That experiments was conducted with a basic equipment that could only record the total deformation induced by a rod shaped weight and there were no data related to possible influences given by the sponge thickness in the measured points.

With our new force transducer equipment we decided to repeat that experiment by changing some experimental parameters. With the new set up we could well describe the deformation process (fig. 12) and derive four parameters; by measuring with digital imaging techniques the thickness of the measured points we could also demonstrate the independence of these parameters from the sponge thickness (fig. 71, table 6). In order to describe the mechanical state of the sponge mesohyl we choose the deformation speed in the constant phase as the best parameter, in term of both greater independence from the sponge thickness and sampling convenience.

Our present data demonstrate that the reaction of the sponge *C. reniformis* to mechanical stimulations consists of at least two different processes: a passive shrinking and an active stiffening. The passive shrinkage is demonstrated by the observations that after being stimulated (compressed or cut) both whole sponges and isolated tissues recovery most of the volume/size along the axis mostly stimulated (fig. 24, 25, 53). Although the shrinking affects both the ectosome and the choanosome (despite some controversial results at 16°C), the main changes appear to involve the canal system (fig. 24, 53). The second active response involves both the stiffening of the sponge ECM and the contraction of the

large canals as indirectly demonstrated by the dimensional increase of both x and y axis during the return to RC (fig. 24).

The stiffening reaction lifetime influences the volume recovery of the sponges and depends on the amount of the stimulation. Light stimulations, such as water removal, induce a collapse of the sponge due to the gravity (fig. 51): this reduction in the vertical axis is soon recovered when the water was added again (movie 5, 6, 7). Moreover when a sponge is gently removed from the aquarium, thus inducing the collapse of the mesohyl, it is possible to record a transient stiffening reaction that fade quickly (fig. 75). On the other hand when the sponge is stimulated by stronger stimuli the stiffening reaction is much more stable (fig. 76) and some hours may be necessary to recovery its RC volume when heavily manipulated (fig. 23). These data suggest that the stiffening reaction prevents the recovery along the compressed axes that may occur only when the mechanical state of the sponge gradually return to its RC state.

Data obtained with the new biomechanical equipment finally demonstrate the presence of a conduction mechanism that is able to significantly stiffen region at 2 cm distance from previously stimulated areas (fig. 77). Although not statistically significant, it is interesting to notice (as in the case of the tests conducted by Parma, 2007) that the mean recorded deformation speeds at 4 cm distance from previous measurements were often lower than the undisturbed reference measures (fig. 77). It is possible to suggest that by increasing the localized stimulation magnitude it is possible to obtain a stiffening reaction also at greater distances or to induce the stiffening of the whole sponge. The recorded stiffening reactions (fig. 77, points B-D) after localized stimulations were quite low when compared to maximally stiffened sponge (fig. 77, point E), this result suggesting that our stimulations were rather low and far away to induce a great stiffening response of the sponge.

Although our experiments bring new information on the stiffening phenomenon a comprehensive explanation and description of the factors that play a role in the stiffening reaction has, however, not been achieved. Our experiments, combined with the data obtained by Parma (2007), suggest that the main factors involved in the signal propagation are the quantity/quality of the stimulation (i.e. the pressure magnitude, the number of the stimulations, the size of the stimulated area), the time occurring between the stimulation and the stiffening reaction, the distance between the stimulated area and the stiffening effect. Actually, in order to accurately describe the contribute of these factors, a lot of sponge specimens should be sacrificed; however thus may results in a overexploitation of the sponge populations in the collecting sites. For this reasons it should be important to try to farm *C. reniformis* specimens or to study the population structures in the field and in the collecting sites.

Our experiments demonstrate that another factor can affect the capability of the sponge to stiffen at distance, this factor being the exopinacoderm integrity. Although isolated beam shaped samples can react to local mechanical stimulations in the absence of exopinacoderm (Parma, 2007), our experiments

demonstrate that the exopinacoderm is involved in the signal propagation (fig. 78, 79). It is very likely that the exopinacocytes, which are a continuous cell layer directly in contact with the external environment, are involved in sensory activities and coordinations phenomena. Our investigations on the possible presence of mechanosensor structures show evidence of unexpected cell processes and expansions on the external surface of exopinacocytes (fig. 44): however the detailed fine structure and the correct functional interpretation of these processes are still unknown.

With regard to the paracrine signalling model (Ellwanger & Nickel, 2006), it is relevant the presence of numerous long processes at the exopinacocyte bases which are filled by of microtubules and small vesicles (fig. 45) and in contact with other cells in the mesohyl: this suggest that the signals can travel both on the surface and in the deeper layer where, after the release of signalling molecules, other cells may play different roles.

At the moment we cannot infer realistic hypotheses on the candidate-molecules involved in the signalling mechanism that induces the stiffening reactions at distance. Indeed it is likely that GABA is not involved since there are no evident differences in its distribution and no significant effects (increase in the viscosity) can be seen after GABA treatment. In contrast, the role of Glu is intriguing, even though not clear yet. We found some specific differences related to the Glu presence in the exopinacocytes: in particular Glu is localized only in the exopinacocytes of RC sponges (fig. 49). Moreover 2mM Glu can slightly increase the viscosity of isolated ectosome samples (fig. 64); it does not affect the recovery process from SC to RC (fig. 53), but can trigger a contraction event (fig. 60) on the whole sponge by generating high tensile forces, thus possibly affecting the viscosity.

4.2 Mesohyl mechanical properties

Collagenous tissues, when subjected to a constant tensile stress, respond whit a stereotyped response that consists of a primary and a secondary phase continuing until the rupture. In the primary phase the collagen fibrils reorient themselves in the direction of the tensile stress opposing a greater resistance, while the fibrils gradually align in the direction of the stress. The secondary phase is characterized by a rather constant elongation speed that depends on the interactions (bonds) occurring between the fibrils (i.e. friction forces) and within them (i.e. interfibrillar bonds). When the samples reach their maximum extension they start to rapidly elongate before to undergo rupture. Our data demonstrate that the sponge mesohyl, in particular the ectosome, does not respond to tensile stress as other collagenous tissues. In many ectosome samples we observed two different (sometimes three; fig. 29 b) constant phases, where the viscosity could be calculated within 30 minutes from the application of the tensile stress. However the observed different elongation patterns con be the results of the same process occurring with different time-scale: in this view it is possible that samples stretched by a lower force may anticipate the return to the RC tensility values by softening the ECM or directly undergo creeping

phenomena. The first hypothesis appears to be more likely since creeping phenomena are directly related to tensile stress magnitude (Parma et al., 2007). In contrast to other collagenous tissues, the first ectosome and choanosome viscosity values seemed to be totally unrelated to the applied stress (fig. 32 A, 34). This means that in this first phase the friction forces are independent from the applied stress, a very uncommon behaviour for a collagenous tissue. On the other hand the ectosome secondary viscosity values (fig. 32 B) were comparable to the behaviour of other collagenous tissues that usually creep under constant loads in a force dependent manner. Since in choanosome samples the occurrence of the secondary viscosity was less frequent, thus we could not calculate the secondary viscosity values.

It is important to remark that collagenous tissues when subjected to forced elongations undergo a typical response that consists again of three phases. In the first phase, called toe region, the samples elongate without opposing a great force due to the alignment of the collagen fibres in the direction of the elongation. When the fibres are aligned they start to resist to the forced elongation by generating higher forces: in this phase, where the stiffness is calculated, there is a quasi-linear relationship between stress and strain. When the samples reach their maximum elongation/force they undergo rupture; before the rupture it is often possible to observe a small region (plastic region) where the samples elongate without any force increase, or with a drastic force decrease due to rupture of many fibrils. In collagenous tissue both the stiffness and the breaking stress are related to the extension rate.

Data related to both ectosome and choanosome samples revealed again the strange and srtickling mechanical properties of the sponge mesohyl. In contrast to all the other collagenous tissues, sponge mesohyl samples showed a linear stress/strain pattern: we could not observe any toe region at low strain; neither some plastic deformation pattern at higher strain (fig. 36, 40). This pure elastic behaviour, together with the observed differences between the ectosome and the choanosome (fig. 43), has a great consequence on the sponge mechanical behaviour that follows a mechanical stimulation allowing the return of the sponge original dimension/shape after the stiffening effect end with a pure elastic recovery. In this light the higher stiffness of the ectosome give the major contribution to the recovery process. We must specify again that during the biomechanics tests, due to the lack of any "anaesthetic" agent, samples were probably in a stiffened condition: both the experimental procedures and the applied mechanical stress or strain can probably induce a stiffning response.

4.3 Contraction/expansion events

The presence of contraction/expansion events has been already demonstrated in other species belonging to both Calcarea, Demosponges and Homoscleromorpha (Nickel 2010; Bond, 2013). In particular extensive studies have been carried out on the freshwater sponge *E. muelleri* and the marine demonspoge *T. willelma*. These behaviours showed different pattern according to the species and possibly depending on the general anatomical architecture of each species: in the globular species *T.*

villelma the contractions are homogeneous (Nickel, 2004), whereas in the flattened species *E. muelleri* the contraction events are much more complex (Elliot & Leys, 2007). Our experiments demonstrate the occurrence of contraction/expansion events also in the sponge *C. reniformis*. For what concern the contraction and the expansion behaviour are concerned our time-lapse movies show that the contraction pattern is more comparable to that described in *T. villelma*. Specimens can contract homogeneously, or deform only parts of the body, or undergo a sort of contraction wave that starts in the lateral body region and ends in the oscular region (movie 1, 2, 3). Contrary to what observed in *T. villelma* and *E. muelleri* where a regular periodicity of the events was documented, there are no evident periodic contractions in *C. reniformis*.

The same specimen can show clear rhythmic contractions or no contractions at all in different days (movie 2a, 3). Moreover, when we monitor different undisturbed specimens in the aquaria it is possible to observe that while some sponges appear to contract synchronically others do not contract at all (movie 2). Although we had no evidences on the presence of a specific periodic contraction pattern within 9 hours, it is possible that the rhythm is rather more complex, including some resting periods, and that can take several hours before to start again. Our attempts to describe the contraction periodicity that eventually occurs within 48 h did not reveal any significant regular rhythm; with regards to this approach we should underline that the noise induced by temperature changes in the laboratory (with consequences on the sensitive components of the recording apparatus) may have introduced artefacts and hidden the natural pattern of contractions.

Another intriguing aspect related to these contraction phenomena is the possibility to induce/regulate them with neuroactive compounds (see Nickel 2010 for a detailed review). Data from literature show that many molecules commonly used in the upper metazoan nervous systems can induce contraction events and/or modulate their periodicity. We focused our attention on two of these molecules: GABA and Glu. While Glu has a strong capability to trigger the contraction events both in *T. willelma* (Ellwanger & Nickel, 2006) and *E. muelleri* (Elliot & Leys, 2010), GABA showed a completely different effect in the two species. In fact GABA induces and modulates contraction in *T. willelma* (Ellwanger & Nickel, 2006), whereas it does not induce any contraction in *E. muelleri*; in addition it can inhibit the sponge capability to contract also when Glu is added (Elliot & Leys, 2010). Our results demonstrate that both GABA and Glu can trigger contractions in *C. reniformis* (fig. 57, 58). There are no significant differences in the contraction magnitude (fig. 59) as reported for *T. willelma*. On the basis of the contraction magnitude Glu seems to induce faster responses and less durable contractions than GABA that, on the other side, appears to cause greater contractions (fig. 59).

However, we can guess that the two neuroagents may cause similar contraction behaviours only when the contraction magnitude is considered: indeed our data suggest that the two molecules can induce contractions by activating different mechanisms. This hypothesis is mainly based on the significant

differences observed when comparing the contraction events in term of generated forces (fig. 59). As far as we know our data are the first real measurements of the forces generated during the contraction events. In Contrast to the effects evaluated by measuring the contraction magnitude, the data related to the generated forces showed significant differences between GABA and Glu (fig. 62). In particular Glu induces higher contraction forces than GABA; moreover Glu seems again to induce faster and less durable responses than GABA. Indeed there are differences in the pattern of the curves: five minutes after the addition of Glu the contraction was evident, whereas it takes 10 minutes to detect a clear contraction when GABA was used. Both contractions reach the force peak after 15 minutes: however the force generated by Glu starts to fade soon (fig. 60), whereas the force generated by GABA remains extremely stable for 15 minutes more (fig. 61). These observations are not in contrast to what observed when the contraction events were considered in term deformation magnitude. Indeed the higher contraction magnitudes observed in the specimens exposed to GABA may be less powerful but more stable during the time, thus allowing the mesohyl to be much more deformed. On the other hand the relationship between the recorded stereotyped forces and the different contraction magnitudes is still unknown. One possible explanation may involve the different mesohyl/canals volume ratio that may vary significantly in the different specimens.

Our attempts to check the possible effect of the two molecules on the rhythm of the contraction/expansion events unfortunately did not give so far any information due to the lack of a clear natural rhythmicity.

Although the contraction events have been extensively studied in other species both the signalling pathway that control the phenomenon and the molecular bases that produce the contractions are still not clear (Renard at al., 2009; Nickel, 2010). It is now accepted that the contractions are given by a combination of pinacoderm/mesohyl contribution (Pavans de Ceccatty, 1986) that involves both the pinacocytes and the actinocytes. In this view it has been recently demonstrated with 3D synchrotron radiation-based x-ray microtomography techniques that during a contraction event volume changes occur only in the canal system, while the mesohyl remains stable; moreover the surfaces/volumes ratios were significantly different only for the pinacoderm (Nickel et al., 2011). The situation in *C. reniformis* is different since our data exclude the presence of actin filaments in the pinacocytes. In fact although some actin signal was detected in some pinacocytes (fig. 48 B), most of the cells were not labelled by rhodamine phalloidin (fig. 48, 49). On the other hand a strong actin signal was detected in presumptive spherolous cells and in other unidentified cells (fig. 48, 49). Thus this signal could be probably related to some protein with an actin-like dominium that binds rodhamine-phalloidin. For this reason we should consider the actual presence of actin filaments only in the actinocytes where TEM investigation clearly show their presence. As reported by Bonasoro et al. (2001) and confirmed by our present data, actinocytes are rare in the mesohyl but well concentrated around the large canals, especially in the

exhalant canals close to the osculum region (fig. 67). In the exhalant canals the arrangement of the actinocytes reaches its maximum extent and complexity being organized in three well-defined orientations. Actinocytes are longitudinally oriented, i.e. parallel to the axis of the canal, just few microns inside the canal itself; going deeper in the mesohyl they are arranged radially to the canal and in the third region actinocytes assume a circular disposition. In this third region the cells are often associated in small bundles (fig. 67) and present numerous cell junctions (fig. 68 A). Actinocytes also present remarkable ultrastructural differences. Longitudinal actinocytes, in particular, resemble smooth muscle cells and show evident cytoplasmic dense bodies, thin filaments and thick myosin-like filaments (fig. 69, 70); by contrast radial and circular actinocytes show only conspicous actin filament bundles (fig. 67).

The lack of actin filaments in the pinacoderm leads us to exclude a pinacoderm role in the contraction events that are instead probably due to the contraction of the actinocytes lining the canals. According to the "paracrine" signalling system propose in sponges (Ellwanger & Nickel, 2006) the activation of the actinocytes in the oscular region should occur following two different directions. The first pathway follows the direction of the water flow that passes through the sponges; the second one, possibly mediated by the pinacocytes processes, is directed towards the inner regions of the mesohyl. In this light we can hypothesize two different contraction patterns:

1- if the actinocytes of the three regions are sequentially activated by the same signalling pathway, going from the mesohyl closer to the canal region to the deeper mesohyl, we should expect a first length reduction of the canal, a subsequent increase of the canal lumen and a final canal contraction. Thus this pattern should generate a sort of peristaltic wave that end in the osculum region.

2- If different signalling pathways regulate the contraction of the different actinocytes present in the three regions, we should expect the possibility for the sponge to regulate both the canal length and diameter; in this second hypothesis the radial and circular actinocytes function as antagonist contractile effectors and should be activated in different moments. According to this second model the sponge can generate either a peristaltic wave or specifically control the canals diameter changing in this way the parameters that influence the water flow.

Indeed the observed differences in the actinocytes ultrastructure may result in different capability to contract: in this light we can hypothesize that GABA and Glu may act on the two different cell types thus generating different forces during the contraction events. We can guess that GABA, which is mainly detectable inside the radial/circular actinocytes (fig. 48), can control their activity while Glu controls the contraction of the parallel arranges and smooth muscle-like actinocytes (fig. 49 C, E). However this theory cannot explain the inhibitory effects of GABA in *E. muelleri* that is hard to conciliate with the observations conducted on *T. willelma* and *C. reniformis*.

Contrary to the other two animal models, localized stimulation induced by a glass pipette did not trigger any contraction events (data not shown) in *C. reniformis*.

4.4 Stiffening factor(s)

The capability to modulate the mechanical properties of collagenous tissue in a short time scale is well described in the echinoderm phylum (see Wilkie, 2005). In echinoderms it has been demonstrated that different ECM proteins that interact with the collagen fibrils are involved in the regulation of the ECM mechanical properties (Tipper & Trotter, 2003; Yamada et al., 2010). In the sponge *C. reniformis* the possible presence of stiffening factor(s) that can modulate the mechanical properties by interacting with the collagen fibrils was firstly hypothesized by Bonasoro et al. (2001) and later partially demonstrated by Wilkie et al. (2006). In particular Wilkie et al. (2006) demonstrated that the mechanical properties of the mesohyl are affected by the exposure to crude sponge extracts that were able to stiffen PD ectosome and choanosome. Although these experiments demonstrated that one or more stiffening factors were present, there were no information on its/their chemical nature. Our data confirm definitively the presence of at least one actin factor in the stiffening mechanism. Proteins contained in P40 fraction are able to re-stiffen RC isolated ectosomes (fig. 80, 81) and to inhibit the return to RC of SC isolated ectosomes (fig. 82). The inhibitory effects observed in figure 82 allow us to hypothesize that some enzymes, that can inactivate the presumptive stiffening factor, can be secreted in the ECM during the return from SC to RC. In this light the addiction of other exogenous substrate may delay the physiological process.

Our data demonstrate that one presumptive stiffening factor, contrary to what hypothesized by Wilkie et al. (2006), is a large protein with a molecular mass greater than 50 KDa (fig. 90). However it is possible that, like in echinoderms, more than one factor is involved in the regulation of the mechanical properties; for example a small (2.4 KDa) polypeptide was recently described as the responsible for the maximum stiffness state in *C. frondosa* (Yamada et al., 2010).

In terms of activity the dose dependent effect on isolated collagen fibrils (fig. 85) is independent from the time, suggesting that the stiffening factor is not an enzyme. Protein present in 400µl was probably not enough to aggregate all the collagen (2 mg) fibrils (fig. 86), since we did not reach the plateaux. 400µl of protein was extracted from 400mg of sponge, which is roughly composed by more than 30% collagen (Swatschek et al., 2002); this suggests that the stiffening reaction, and the subsequent release of the protein in the ECM, is given by changes of the mechanical properties of only part of the collagen present in the mesohyl.

Our aggregation test demonstrated that this low hydrophilic protein is able to interact with fibrillar collagens extracted from different phyla (fig. 83). The aggregation, which needs the presence of calcium ions in the media (fig. 88), is really fast when shacked and really stable among the time.

Our data suggest that, like in echinoderms, the stiffening factor-collagen interactions are likely mediated by collagen associated proteins (GAGs or PGs): aggregation tests with pure Sigma Bovine type I collagen had negative results (results not shown) whereas the aggregation tests on rat collagen (extracted according to Matsumura protocol) were positive (fig. 83). As far as we know this is the first animal stiffening factor which displays a clear capability to aggregates also vertebrate collagen. This capability is probably due to the presence of conserved bond sites among the phylogenetic tree.

The possibility to stabilize vertebrate fibrillar collagen, and possibly to control the mechanical properties of the tissue, may bring to a wide range of applications in the field of bioengineered materials. Moreover the double factor requirement (calcium ions plus stiffening factor) to trigger the aggregation is really important in terms of applications, since it should be possible to aggregate "*in situ*" 3D fibrillar collagen scaffolds by depositing collagen and stiffening factor(s) and then assembling these components according to the requirements simply by adding calcium ions. The protein complete characterization and sequencing is actually ongoing*. As stated above we could not report the obtained results in order to protect possible patent procedures at the moment in progress.

*In collaboration with Prof. Giovine (DISTAV, University of Genova) and Prof. Damonte (CEBR, University of Genova).

Conclusive remarks

This thesis was intended to study the coordinated phenomena occurring in the demosponge *C. reniformis*. In particular we focused our attention on the stiffening phenomena following mechanical stimulation and on the role of GABA and Glu in different aspects that require some coordination mechanisms. Before to approach these issues we carried out preliminary experiments in order to better describe different aspects of the *C. reniformis* biology.

In particular our results defined:

- the relaxing process that occurs after specimens were vigorously stimulated;
- the volumes/dimensions changes that occur during the tissue softening;
- the influence of water temperature on such process;
- the mechanical properties of both ectosome and choanosome;
- the presence of two different actinocytes phenotypes;
- the presence of contraction/expansion cycles.

For what concern the stiffening reaction following mechanical stimulation our data support the view that the stiffening of *C. reniformis* involves a combination of phenomena including dimensional compression of the sponge body and modification of the interactions between the collagen fibrils of the mesohyl mediated by a secreted stiffening factor. In particular the mechanical reaction after different types of mechanical stimulation implies:

- an initial passive response due to externally imposed compression, followed by an active response consisting of an increase in mesohyl stiffness;
- a rather slow propagation of the stiffening response through the surrounding stimulated region at a signal transmission speed of 1cm/min;
- a presumptive specific role of the exopinacoderm in signal transmission.

The biological significance of the stiffening phenomenon remains unclear. The physiological control of mesohyl stiffness may be related in part to regulation of the release of reproductive propagules. However, the adaptive advantage of the stiffening response to touch is more difficult to understand. Although some aspects related to the reaction of *C. reniformis* to mechanical stimulation have been resolved, many fundamental problems remain. In particular the molecular mechanisms that are the basis of the dynamic phenomena of sponge mesohyl need to be explored in detail. The ongoing characterization of the sponge stiffening factor(s) could throw more light on the evolutionary relationship between the mechanically adaptable collagenous tissues of sponges and echinoderms. At present, for what concern the similarities/differences between *C. reniformis* mesohyl and echinodems MCTs we can assert that despite the overall similarities in the behaviour of their connective tissues, and the obvious analogies in terms of morphology, physiology and biomechanics, there are significant

differences in some crucial aspects. In both phyla the histological and ultrastructural features are typical of fibrous connective tissue, which means that the characteristic component is an array of collagen fibrils in which different cell phenotypes are scattered. Nevertheless, an important difference can be found in the collagen fibrils themselves. Sponge fibrils are rarely organized into bundles and their mean diameter is significant lower than that of echinoderm. Since larger fibrillar bundles are usually formed as a result of crosslinking with different molecules, we could speculate that sponges lack some of these interfibrillar connections, which could have appeared later in animal evolution.

It is topical that in both echinoderms and sponges mutability is strongly affected by exogenous environmental factors (such as temperature, pH and ionic composition), although not always in the same way. For example decreasing temperature reduces mechanical resistance in starfish (Hidaka, 1983) but has the opposite effect in sponges (Fassini et al., 2012). On the other hand, [Ca_{2+}] variations exert similar effects both on sponges and echinoderms. In both animal models mutability is apparently based on a cell-mediated mechanism (Wilkie, 2005; Wilkie et al., 2006). In echinoderms the putative mechanical changes effector cells are the JLCs, on the other hand in sponges functionally analogous cells have not been identified. Although the most promising candidates are the gray cells, which share some features with echinoderm JLCs, no evidences of their involvement in the mechanical changes are present.

Independently from the effector cells, in both echinoderms and sponges the main mechanism governing mutability appears to be a variation in collagen interfibrillar cohesive forces.

Our results demonstrate that at least one sponge stiffening factor is significantly greater in respect to the proteins that regulate the MCTs mechanical properties; this aspect leads to speculate whether the sponge stiffening factor(s) is present also in echinoderms (but not yet discovered) or the evolution of dynamic connective tissues arose independently among the evolution.

Although our present data provide new information on the *C. reniformis* stiffening phenomenon, its biological significance is still not clear. Here we can guess that the physiological control of mesohyl stiffness may be involved in the creeping phenomena. In this view the possibility to stiffen the mesohyl can prevent/slow down the formation of propagules when the environmental conditions are not favorables.

Our investigations on the role of GABA and Glu suggest that the two neuroagents are not directly involved in the stiffening phenomena, but induce contraction events similar to those described in other marine demosponges. On the other hand our original biomechanical approach highlighted that, despite the similar recorded contraction magnitudes, the two chemicals induced different contraction forces. On the basis of these results we hypothesized that GABA and Glu act on different mechanisms leading to the activation of different actinocytes populations.

Finally we would like to underline the unexpected capability of the sponge stiffening factor(s) to aggregate collagens extracted from different animals; this capability representing an interesting aspect for biotechnological applications leading to the possibility to produce 3D scaffold with specific mechanical properties according to the specific cells requirements.

Acknowledgments

Institutions

I am grateful to the Area Marina Protetta of Isola di Bergeggi (SV, Italy) and Area Marina Protetta of Portofino for permission to collect experimental animals.

Student

I would like to thank all the students that help me during these 3 years of dense and hard work.

BSc students: Elisa Pratici; Francesca Pisanello; Alexandra Devos; Chiara Chiorboli.

MA students: Martina Persico; Francesco Lembo; Vasco Inzoli.

Professors and researchers.

I would firstly thank my tutor Prof. Francesco Bonasoro for gave me the freedom to expand my curiosity at 360° and to explore the aspects that more attracted my interest.

I would like also to thank Prof. Marco Giovine and his coworkers (Marina Pozzolini, Francesca Mussino, Annalisa Salis) for his great hail and for giving me the opportunity to characterize the stiffening factor in his lab.

Special thank goes to Prof. Daniela Candia and Prof. Iain C. Wilkie, two really important models that shape my human and scientific attitude.

Colleagues: in alphabetical order

Alice Barbaglio, Cristiano di Benedetto, Silvia Mercurio, Roberto Marotta, Michela Sugni. All of them taught me more than they though.

Supplement materials

Movie 1 http://www.youtube.com/watch?v=vXoigBO_Jxw

Movie 2 http://www.youtube.com/watch?v=ZNSR8pCs4ag&feature=youtu.be

Movie 2a http://www.youtube.com/watch?v=FZEmSwQdtRM&feature=youtu.be

Movie 3 http://www.youtube.com/watch?v=hq1rkn3zh7w&feature=youtu.be

Movie 4 http://www.youtube.com/watch?v=A7xx9MNz7hs&feature=youtu.be

Movie 5 http://www.youtube.com/watch?v=jLGe4-ViS7A&feature=youtu.be

Movie 6 http://www.youtube.com/watch?v=ftA5VdbafLs&feature=youtu.be

Movie 7 http://www.youtube.com/watch?v=okz5blNy6dE&feature=youtu.be

Paper 1 http://www.sciencedirect.com/science/article/pii/S0022098112002067

Paper 2 http://www.sciencedirect.com/science/article/pii/S0141113613001256

References

Aouacheria A., Geourjon C., Aghajari N., Navratil V., Deleage G., Lethias C., Exposito J. Y. 2006. Insights into early extracellular matrix evolution: spongin short chain collagen-related proteins are homologous to basement membrane type IV collagens and form a novel family widely distributed in invertebrates. Mol Biol Evol 23: 2288–302.

Bachmann S., Pohla H., Goldschmid A., 1980. Phagocytes in the axial complex of the sea urchin, Sphaerechinus granularis (Lam.). Cell and Tissue Research 213 (1): 109-120.

Bagby R. M. 1966. The fine structure of myocytes in the sponges *Microciona prolifera* (Ellis and Solander) and *Tedania ignis* (Duchassaing and Michelotti) J Morphol. 118 (2): 167-81.

Bagby R. M. 1970. The fine structure of pinacocytes in the marine sponge Microciona prolifera. Cell Tissue Res. 105: 579-594.

Barbaglio A., Tricarico S., Ribeiro A., Ribeiro C., Sugni M., Di Benedetto C., Wilkie I., Barbosa M., Bonasoro F., Candia Carnevali M.D. 2012. The mechanically adaptive connective tissue of echinoderms: its potential for bioinnovation in applied technology and ecology. Mar. Env. Res. 76: 108-113.

Barnes R. S. K., Hughes R. N. 1990. Introduzione all'ecologia marina. Piccin Nuova Libraria, Padova.

Bavestrello G., Arillo A., Cerrano C., Cattaneo-Vietti R., Cortesogno L., Gaggero L., Giovine M., Tonetti M., Sarà M. 1995. Quartz dissolution by the sponge *Chondrosia reniformis* (Porifera, Demospongiae). Nature 378: 374-376.

Bavestrello G., Benatti U., Calcinai B., Cattaneo-Vietti R., Cerrano C., Favre A., Giovine M., Lanza S., Pronzato R., Sara M., 1998a. Body polarity and mineral selectivity in the demosponge *Chondrosia reniformis*. Biological Bulletin. 195: 120-125.

Bavestrello G., Burlando B., Sarà M. 1998b. The architecture of the canal system of

Petrosia ficiformis and *Chondrosia reniformis* studied by corrosion casts (Porifera, Demospongiae). Zoomorphology 108: 161-166.

Bergquist P. R. 1978 Sponges. London: Hutchinson & University of California Press (Berkeley & Los Angeles).

Bidder G. P. 1937. The perfection of sponges. Proc. Linn. Soc. London 149: 119–147.

Birenheide R., Tamori M., Motokawa T., Ohtani M., Iwakoshi E., Muneoka Y., Fujita T., Minakata H., Nomoto K. 1998. Peptides controlling stiffness of connective tissue in sea cucumbers. Biological Bulletin 194: 253-259.

Bonasoro F., Candia Carnevali M.D., Wilkie I.C. 1995. The peristomial membrane of regular sea‐urchins: Functional morphology of the epidermis and coelomic lining in *Paracentrotus lividus* (Lamarck). Bolletino di zoologia 62 (2): 121-135.

Bonasoro F., Wilkie I.C., Bavestrello G., Cerrano C., Candia Carnevali M.D. 2001. Dynamic structure of the mesohyl in the sponge *Chondrosia reniformis* (Porifera, Demospongiae). Zoomorphology 121: 109–121.

Bond C., Harris A. K., 1988. Locomotion of sponges and its physical mechanism. J. Exp. Zool. 246: 271–284.

Bond C. 1992. Continuous cell movements rearrange ana- tomical structures in intact sponges. J. Exp. Zool. 263: 284–302.

Bond C. 2013. Locomotion and contraction in an asconoid calcareous sponge. Invertebrate Biology 132(4): 283–290.

Borchiellini C., Chombard C., Manuel M., Alivon E., Vacelet J., Boury-Esnault N. 2004. Molecular phylogeny of Demospongiae: implications for classification and scenarios of character evolution. Molecular Phylogenetics and Evolution 32: 823–837.

Borojevic R. 1966. Etude expérimentale de la differenciation des cellules des cellules de l'éponge au cours de son dévolopment. Dev. Biol. 17: 130-153.

Boury-Esnault N. and K. Rützler (eds), 1997. Thesaurus of Sponge Morphology. Smithsonian Contribution to Zoology, 596: 1-55.

Boury-Esnault N., Muricy G., Gallissian M., Vacelet J., 1995. Sponge without skeleton: a new Mediterranean genus of Homoscleromorpha (Porifera, Demospongiae). Ophelia 43: 23–43.

Boury-Esnault N. 1977 A cell type in sponges involved in the metabolism of glycogen. The gray cells. Cell Tissue Res. 175: 523-539.

Bretting H., Königsmann K. 1979. Investigations on the lectin producing cells in the sponge *Axinella polypoides*. Cell Tissue Res. 201: 487–497

Bretting H., Jacobs G., Donadey C., Vacelet J. 1983 Immunohistochemical studies on the distribution and the function of the Dgalactose- specific lectins in the sponge *Axinella polypoides* (Schmidt). Cell Tissue Res. 229: 551–571

Brusca R. C., Brusca G. J. 2002. *Invertebrates.* Sunderland, MA: Sinauer Associates.

Byrne M., 1985. The mechanical properties of the autotomy tissues of the holo- thurian Eupentacta quinquesemita and the effects of certain physicochemical agents. J. Exp. Biol. 117: 69-86.

Chapman E. R., 2002. Synaptotagmin: a $Ca(_{2+})$ sensor that triggers exocytosis? Nature reviews. Mol. Cell Biol. 3: 498-508.

Cluzel C., Lethias C., Garrone R., Exposito J. Y., 2004. Distinct maturations of N-propeptide domains in fibrillar procollagen molecules involved in the formation of heterotypic fibrils in adult sea urchin collagenous tissues. J. Biol. Chem. 279: 9811-9817.

Connes R. 1967. Structure et développement des bourgeons chez l'Esponge siliceuse *Tethia lincurium Lamark.* Recherhes experimentales et cytologiques. Arch. Zoolo. exp.

Gén. 108: 157-195.

Corriero G., Scalera Liaci L., Ruggiero D., Pansini M. 2000. The Sponge Community of a Semi-Submerged Mediterranean Cave. *Marine ecology*, Volume 21(1).

D'Alessio M., Ramirez F., Suzuki H. R., Solursh M., Gambino R. 1990. Cloning of a fibrillar collagen gene expressed in the mesenchymal cells of the developing sea urchin embryo. J. Biol. Chem. 265: 7050-7054.

De Vos L., Van de Vyver G. 1981. Étude de la contraction spontanée chez l'éponge d'eau douce *Ephydatia fluviatilis* cultivée in vitro. Ann. Soc. R. Zool. Belg. 111:21–31.

Diaz J. P. 1979. Variations, differenciations et fonctions des categories cellulaire de la demosponge d'eau saumaitres, *Suberites massa* Nardo, au cours du cycle biologique annuel et dans des conditions experimentales. Thèse. Univ. Sci. Tech. Languedoc. 1–332.

Elliott G. R. D., Leys S. P. 2010. Evidence for Glutamate, GABA and NO in coordinating behaviour in the sponge Ephydatia muelleri (Demospongiae, Spongillidae). J. Exp. Biol. 213: 2310-2321.

Elliott G. R. D., Leys S. P. 2007 Coordinated contractions effectively expel water from the aquiferous system of a freshwater sponge J. Exp. Biol. 210: 3736-3748.

Elliott G.R.D., Mac Donald T.A, Leys S.P. 2004. Sponge larval phototaxis: a comparative study. Boll . Mus. Ist. Biol. Univ. Genova 68: 291-300.

Ellwanger K., Nickel M. 2006. Neuroactive substances specifically modulate rhythmic body contractions in the nerveless metazoon Tethya wilhelma (Demospongiae, Porifera). Front. Zool. 27: 3-7.

Ellwanger K., Eich A., Nickel M. 2006. GABA and glutamate specifically induce contractions in the sponge *Tethya wilhelma*. J. Comp. Physiol. A Neuroethol. Sens. Neural. Behav. Physiol. 193 (1):1-11.

Emson R.H. 1966. The reactions of the sponge Cliona celata to applied stimuli. Comp. Biochem. Physiol. 18: 805–827.

Exposito J.Y., Boute N., Deleage G., Garrone R., 1995. Characterization of two genes coding for a similar four-cysteine motif of the amino-terminal propeptide of a sea urchin fibrillar collagen. European Journal of Biochemistry. 234: 59-65.

Exposito J. Y., Valcourt U., Cluzel C., Lethias C. 2010. The fibrillar collagen family. Int. J. Mol. Sci. 11: 407-426.

Fassini D., Parma L., Wilkie I. C., Bavestrello G., Bonasoro F., Carnevali M. D. C. 2012. Ecophysiology of mesohyl creep in the demosponge Chondrosia reniformis (Porifera: Chondrosida). J. Exp. Mar. Biol. Ecol. 428: 24-31.

Faulkner D. J. 2000. Marine natural products. Nat Prod Rep 17: 7–55.

Fell P. E. 1994. Porifera. In: Adiyodi KG, Adiyodi RG (eds) Reproductive biology of invertebrates, vol VI B. Asexual propagation and reproductive strategies. *Oxford and IBH Publishing*, New Delhi, pp 1–44.

Gaino E., Pronzato R. 1983. Etude en microscopie électronique du filament des formes étirées chez *Chondrilla nucula* Schmidt (Porifera Demospongiae) Annales des Sciences Naturelles, Zoologie, Paris. Vol.5: pp. 221-234.

Gaino E., Pansini M., Pronzato R., Cicogna F. 1991. Morphological and structural variations in Clathrina clathrus (Porifera, Calcispongiae). In: Reitner, J., Keupp, H. (Eds.), Fossil and Recent Sponges. Springer, Berlin Heidelberg, pp. 360-371.

Garrone R. 1978 Phylogenesis of connective tissue. Morphological aspects and biosynthesis of sponge intercellular matrix. Karger, Basel.

Garrone R., Huc A., Junqua S. 1975. Fine structure and physiochemical studies on the collagen of the marine sponge *Chondrosia reniformis* Nardo. J. Ultrastruct. Res. 52: 261–275.

Garrone R. 1974. Ultrastructure d'une gemmule armeé planctonique d'esponge clionidae. Arch. Anat. Micros. Morph. Exp. 63: 163-182.

Gazave E., Lapébie P., Renard E., Vacelet J., Rocher C., Ereskocsky A. V. 2010. Molecular phylogeny restores the supra-generic subdivision of homoscleromorph sponges (Porifera, Homoscleromorpha). PLoS ONE 5(12): e14290.

Gazave E., Lapébie P., Ereskocsky A. V., Vacelet J., Renard E., Càrdenas P., Borchiellini C. 2012. No longer Demospongiae: Homoscleromorpha formal nomination as a fourth class of Porifera. Hydrobiologia 687(1): 3-10.

Grant R. E. 1936. Animal kingdom. *In* The cyclopaedia of anat- omy and physiology. *Edited by* R.B. Todd. Sherwood, Gilbert and Piper, London. 107–118.

Harrison F. W., De Vos L. 1991 Porifera. In: Harrison FW, Ruppert EE (eds) Microscopic anatomy of invertebrates, vol 2. Wiley Liss, New York, pp 29–89.

Heinemann S., Ehrlich H., Douglas T., Heinemann C., Worch H., Schatton W., Hanke T. 2007. Ultrastructural studies on the collagen of the marine sponge *Chondrosia reniformis* Nardo. *Biomacromolecules*. 8(11):3452-7.

Hennebert E., Haesaerts D., Dubois P., Flammang P. 2010. Evaluation of the different forces brought into play during tube foot activities in sea stars. J. Exp. Biol. 213: 1162-1174.

Hidaka M., Takahashi K. 1983. Fine structure and mechanical properties of the catch apparatus of the sea-urchin spine, a collagenous connective tissue with muscle-like holding capacity. J. Exp. Biol. 103: 1-14.

Hidaka M., 1983. Effects of certain physico-chemical agents on the mechanical properties of the catch apparatus of the sea urchin spine. J. Exp. Biol. 103: 15-20.

Hooper D., Buchmann N., Degrange V., Dìaz S.M., Gessner M., Grime P. et al. 2002.

Species diversity, functional diversity and ecosystem functioning. In: Biodiversity and Ecosystem Functioning. (eds Loreau, M., Naeem, S. & Inchausti, P.). Oxford University Press, Oxford.

Jones W. C. 1962. Is there a nervous system in sponges? Biological Reviews 37: 1-50.

Jones W. C. 1957. The contractility and healing behaviour of pieces of Leucosolenia complicata. Q. J. Microsc. Sci. 98: 203–217.

Laport M. S., Santos O. C. S., Muricy G. 2009. Marine Sponges: Potential Sources of New Antimicrobial Drugs. Current Pharmaceutical Biotechnology 10 (1): 86-105.

Lawn I. D. 1982. Porifera. *In* Electrical conduction and behaviour in 'simple' invertebrates. *Edited by* G.A.B. Shelton. Clarendon Press, Oxford. pp. 49–72.

Leys S. P., Mackie G. O., Reiswig H.M., David W.S. 2007. The Biology of Glass Sponges. Academic Press. 145 pp.

Lazoski C., Solé-Cava A. M., Boury-Esnault N., Klautau M., Russo C. A. M., 2001. Cryptic speciation in a high flow scenario in the oviparous marine sponge *Chondrosia reniformis.* Mar. Biol. 139: 421-429.

Levi C. 1970. Les cellules des Esponges. Symp. Zool. Soc. London. 25: 353-364.

Leys S. P., Meech R. W. 2006. Physiology of coordination in sponges. Canadian Journal of Zoology 84: 288-306.

Leys S. P., Nichols S. A., Adams E. D. M. 2009. Epithelia and integration in sponges. Int. Comp. Biol. 49: 167-177.

Mackie G. O. 1979. Is there a conduction system in sponges? In: Biologie des Spongiaires. Editions du C.N.R.S. Lévi C & Boury-Esnault N., eds., pp. 145–152. C.N.R.S., Paris.

Maldonado M., Young C. M. 1996. Effects of physical factors on larval behavior, settlement and recruitment of four tropical demosponges. Marine Ecology Progress Series 130: 169-180.

Maldonado M., Durfort E. M., McCarthy E. D. A., Young C. M. 2003.The cellular basis of photobehavior in the tufted parenchymella larva of demosponges. Mar. Biol. 143: 427–441.

Marshall W. 1885. Coelenterata, Porifera, Tetractinellidae. In: Zoologische Wandttafeln der wirbellosen Thiere. Leuckart R, ed., Tafel XLVII. Th. Fischer, Kassel.

Matsumura T., 1974. Collagen fibrils of the sea cucumber, Stichopus japonicus: purification and morphological study. Connective Tissue Research 2: 117-125.

Matsuno A., Ishida H., Kuroda M., Masuda Y. 1988. Ultrastructures of contractile bundles in epithelial cells of the sponge. Zool. Sci. 5: 1212.

McMurray S. E., Henkel T. P., Pawlik, J. R. 2010. Demographics of increasing populations of the giant barrel sponge *Xestospongia muta* in the Florida Keys. Ecology 91: 560-570.

McNair G. T. 1923. Motor reactions of the freshwater sponge *Ephydatia fluviatilis*. Biol. Bull. (Woods Hole), 44: 153–166.

Milanese M., Chelossi E., Manconi R., Sara` A., Sidri M., Pronzato R. 2003. The marine sponge Chondrilla nucula Schmidt, 1862 as an elective candidate for bioremediation in integrated aquaculture. Biomolecular Engineering 20: 363-368.

Minchin E. 1900. Sponges. In: A Treatise on Zoology. Part II The Porifera and Coelentera. Lancester ER, ed., 1–178. Adam & Charles Black, London.

Motokawa T. 1982. Fine structure of the dermis of the body wall of the sea cucumber, *Stichopus chloronotus*, a connective tissue which changes its mechanical properties. *Galaxea* 1: 55-64.

Muricy G., Boury-Esnault N., Bézac C., Vacelet J. 1998. Taxonomic revision of the Mediterranean Plakina Schulze (Porifera, Demospongiae, Homoscleromorpha). Zoological Journal of the Linnean Society 124: 169-203.

Myllyharju J. 2003. Proly 4-hydroxylases, the key enzymes of collagen biosynthesis. Matrix Biology 22: 15-24.

Nickel M., Scheer C., Hammel J. U., Herzen J., Beckmann F. 2011. The contractile sponge epithelium sensu lato – body contraction of the demosponge Tethya wilhelma is mediated by the pinacoderm. J. Exp. Biol. 214: 1692-1698.

Nickel M. 2004. Kinetics and rhythm of body contractions in the sponge Tethya wilhelma (Porifera: Demospongiae). J. Exp. Biol. 207: 4515–4524.

Nickel M. 2006. Like a 'rolling stone': quantitative analysis of the body movement and skeletal dynamics of the sponge Tethya wilhelma. J. Exp. Biol. 209: 2839– 2846.

Nickel M. 2010. Evolutionary emergence of synaptic nervous systems: what can we learn from the non-synaptic, nerveless Porifera? Invertebrate Biology 129(1): 1–16.

Pansini M., Pronzato, R. (1982) Distribuzione ed ecologia dei Poriferi nella grotta di Mitigliano (Penisola sorrentina) *Boll. Mus. Ist. Biol*. Univ. Genova, 50 (Suppl.) 287-293.

Pansini M., Manconi R., Pronzato R. 2011. Porifera I: Calcarea, Demospongiae (partim), Hexactinellida, Homoscleromorpha. In Fauna d'Italia, Calderini ed. Bologna. ISBN-978-88-506-5395-9.

Parker G. H. 1910. The reactions of sponges, with a consideration of the origin of the nervous system. J. Exp. Zool. 8: 765–805.

Parma L., Fassini D., Bavestrello G., Wilkie I. C., Bonasoro F., Candia Carnevali M. D. 2007. Ecology and physiology of mesohyl creep in *Chondrosia reniformis.* Porifera Research: Biodiversity, Innovation & Sustainability. Proceedings of the 7th International Sponge Symposium, Rio de Janeiro, Brasil.

Pavans de Ceccatty M., Garrone R. 1971. Fibrogenèse du collagène chez l'Eponge *Chondrosia reniformis* Nardo (Démosponge Tétractinellidae). Origine et evolution des lophocytes. CR. Acad. Sci. Paris 273: 1957– 1959.

Pavans de Ceccatty M. 1974a. Coordination in sponges: the foundations of integration. Am. Zool. 14: 895–903.

Pavans de Ceccatty M. 1974b. The origin of the integrative systems: a change in view derived from research on coelenterates and sponges. Perspect. Biol. Med. 17: 379-390.

Pavans de Ceccatty M. 1959. Les structures cellulaires de type nerveux chez Hippospongia communis LMK. Ann. Sci. Nat. Zool. Biol. Anim. 12: 105–112.

Pavans de Ceccatty M. 1981. Demonstration of actin filaments in sponge cells. Cell. Biol. Int. 5: 945–952.

Pavans de Ceccatty M. 1986. Cytoskeletal organisation and tissue patterns of epithelia in the sponge *Ephydatia mülleri*. J. Morphol. 189: 45–65.

Pozzolini M., Bruzzone F., Berilli V., Mussino F., Cerrano C., Benatti,U., Giovine M., 2012. Molecular characterization of a nonfibrillar collagen from the marine sponge Chondrosia reniformis Nardo 1847 and positive effects of soluble silicates on its expression. Marine Biotechnology 14: 281-293.

Pronzato R. 2004. A climber sponge. Boll. Mus. Ist. Biol. Univ. Genova 68: 549-552.

Renard E., Vacelet J., Gazave E., Lapiébe P., Borchiellini C., Ereskovsky A. V. 2009. Origin of the neuro-sensory system: new and expected insights from sponges. Integrative Zoology 4: 294-308.

Ribeiro A. R., Barbaglio A., Benedetto C. D., Ribeiro C. C., Wilkie I. C., Carnevali M. D. C., Barbosa M. A. 2011. New insights into mutable collagenous tissue: correlations between the microstructure and mechanical state of a sea-urchin ligament. PLoS ONE 6, e24822.

Ribeiro A.R., Barbaglio A., Oliveira M. J., Ribeiro C. C., Wilkie I. C., Candia Carnevali M. D., Barbosa M. A. 2012a. Matrix metalloproteinases in a sea urchin ligament with adaptable mechanical properties. PLoS ONE 7, e49016.

Ribeiro A. R., Barbaglio A., Oliveira M. J., Santos R., Coelho A. V., Ribeiro C. C., Wilkie I. C., Carnevali M. D. C., Barbosa M. A. 2012b. Correlations between the biochemistry and mechanical states of a sea-urchin ligament: a mutable collagenous structure. Biointerphases 7.

Saitta B., Buttice G., Gambino R. 1989. Isolation of a putative collagen-like gene from the sea urchin Paracentrotus lividus. Biochemical and Biophysical Research Communications 158: 633-639.

Sarà M., Vacelet J. 1973. Ecologie des Démosponges. In: Grassé PP (ed) *Traité de zoologie, Anatomie, systématique, biologie: Spongiaires*. Masson, Paris 3: 462–576.

Schmidt O. 1866. Zweites Supplement der Spongien des Adriatischen Meeres enthaltend die Vergleichung der Adriatischen und Britischen Spongiengattungen. Verlag von Wilhelm Engelmann, Leipzig. 23 pp.

Sciscioli M., Ferri D., Liquori G. E., Lepore E., Santarelli G. 2000. Lectin histochemistry and ultrastructure of microgranular cells in *Cinachyra tarentina* (Porifera, Demospongiae). Acta histochem. 102: 219-230.

Sidri M., Milanese M., Brummer F. 2005. First observations on egg release in the oviparous sponge *Chondrilla nucula* (Demospongiae, Chondrosida, Chondrillidae) in the Mediterranean Sea. Inv. Biol. 124 (2): 91–97.

Simpson T. L. 1984) *The cell biology of sponges*. Springer, Berlin Heidelberg New York.

Sollas W. J. 1888. Report on the Tetractinellida collected by H.M.S. Challenger during the years 1873–1876. Report on the scientific results of the voyage of H.M.S. Chal-lenger 25: 1–458.

Srivastava M., Simakov O., Chapman J., et al. 2010. The *Amphimedon queenslandica* genome and the evolution of animal complexity. Nature 466: 7307.

Sugni M., Fassini D., Barbaglio A., Biressi A., Di Benedetto C., Tricarico S., Bonasoro F., Wilkie I. C., Candia Carnevali M. D. 2013. Comparing dynamic connective tissue in echinoderms and sponges: Morphological and mechanical aspects and environmental sensitivity. In press. http://dx.doi.org/10.1016/j.marenvres.2013.07.010

Swatschek D., Shatton W., Kellermann J., Müller W. E. G., Keuter J. 2002. Marine sponge collagen: isolation, characterization and effects on the skin parameters surface-pH, moisture and sebum. Eur. J. Pharm. 53 (1): 107-113.

Storch V., **Welsch U**. 2008. Biologia e sistematica animale. Delfino Antonio ed. Roma.

Szulgit G. K., Shadwick R. E. 1994. The effects of calcium chelation and cell perfo- ration on the mechanical properties of sea urchin ligaments. In: David, B., Guille, A., Féral, J.P., Roux, M. (Eds.), Echinoderms Through Time. Balkema, Rotterdam, pp: 887-892.

Takahashi K. 1967 The catch apparatus of the sea-urchin spine. II. Response to stimuli. J. Fac. Sci. Univ. Tokyo, Sect 4, 11: 121-130.

Tamariz E., Grinnell F., 2002. Modulation of fibroblast morphology and adhesion during collagen matrix remodeling. Molecular Biology of the Cell 13: 3915-3929.

Tamori M., Takemae C., Motokawa T. 2010. Evidence that water exudes when holothurian connective tissue stiffens. J. Exp. Biol. 213: 1960-1966.

Tipper J., Lyons-Levy G., Atkinson M., Trotter J. 2003. Purification, characterization and cloning of tensilin, the collagen-fibril binding and tissue-stiffening factor from Cucumaria frondosa dermis. Matrix Biol. 21: 625–635.

Trotter J. A., Koob, T.J. 1989. Collagen and proteoglycan in a sea urchin ligament with mutable collagenous properties. Cell Tissue Res. 258: 527-539.

Trotter J. A., Koob, T. J. 1995. Evidence that calcium-dependent cellular processes are involved in the stiffening response of holothurian dermis and that dermal cells contain an organic stiffening factor. J. Exp. Biol. 198: 1951-1961.

Trotter J. A., Lyons-Levi G., Luna D., Koob T.J., Keene D.R., Atkinson M.A. (1996). Stiparin: a glycoprotein from sea cucumber dermis that aggregates collagen fibrils. Matrix Biol. 15: 99-110.

Uriz M. J., Turon X., Mariani S. 2008. Ultrastructure and dispersal potential of sponge larvae: tufted versus evenly ciliated parenchymellae. Mar. Ecol. 29: 280–97.

Vacelet J. 1966. Les cellules contractiles de l'éponge cornée Verongia cavernicola Vacelet. C. R. Acad. Sci. Paris 263: 1330–1332.

Vacelet J. 1967. Les cellules à inclusions de l'Eponge cornèe *Verongia cavernicola* Vacelet. J. Microscopie 6: 237-240.

Hooper J. N. A., Van Soest, R. W. M. 2002. *Systema Porifera: A Guide to the Classification of Sponges*, Kluwer/Plenum, New York.

Vogel S. 1977. Current-induced flow through living sponges in nature. *Proc. Natl. Acad. Sci.* U S A. 74 (5): 2069-71.

Warburton F. E. 1966. The Behavior of Sponge Larvae. Ecology 47: 672–674.

Wessel G. M., Marchase R. B., McClay D. R., Developmental Biology. Volume 103 (1): 1235-245.

Wilkie I. C., Candia Carnevali, M. D., Bonasoro, F. 1992. The compass depressors of *Paracentrotus lividus* (Lamarck) (Echinodermata: Echinoidea): ultrastructural and mechanical aspects of their variable tensility and contractility. Zoomorphology 112: 143-153.

Wilkie I. C., Candia Carnevali M. D., Andrietti F. 1993. Variable tensility of the peristomial membrane of the sea urchin *Paracentrotus lividus* (Lamarck). Comparative Biochemistry and Physiology - Part A, 105: 493-501.

Wilkie I. C., Candia Carnevali M. D., Andrietti F. 1994. Microarchitecture and mechanics of the sea- urchin peristomial membrane. *Boll. Zool.* 61: 39-51.

Wilkie I. C. 2005. Mutable collagenous tissue: overview and biotechnological perspective. *In:* Matranga V (ed). *Echinodermata. Progress in molecular and subcellular biology, vol. 39*. Springer, Berlin. pp. 219-248.

Wilkie I. C., Parma L., Bonasoro F., Bavestrello G., Cerrano C., Candia Carnevali M. D. 2006. Mechanical adaptability of sponge extracellular matrix: evidence for cellular control of mesohyl stiffness in *Chondrosia reniformis* Nardo. J. Exp. Biol. 209: 4436-4443.

Wilkie I. C., Barbaglio A., Maclaren W. M., Carnevali M. D. C., 2010. Physiological and immunocytochemical evidence that glutamatergic neurotransmission is involved in the activation of arm autotomy in the featherstar Antedon medi- terranea (Echinodermata: Crinoidea). J. Exp. Biol. 213: 2104-2115.

Wilkie I. C., Emson R. H. 1987. The tendons of Ophiocomina nigra and their role in autotomy. Zoomorphology 107: 33-44.

Wilkie I. C., 1983. Nervously mediated change in the mechanical properties of the cirral ligaments of a crinoid. Marine Behaviour and Physiology 9: 229-248.

Wilkie I. C., 1988. Design for disaster: the ophiuroid intervertebral ligament as a typical mutable collagenous structure. In: Burke, R.D., Mladenov, P.V., Lambert, P., Parsley, R.L. (Eds.), Echinoderm Biology. Balkema, Rotterdam, pp. 25-38.

Wilkie I. C. 1996. Mechanical properties of the peristomial membrane of the cidaroid sea-urchin Stylocidaris affinis. Journal of Zoology, London 238: 557-569.

Wilson H. V. 1910. A study of some epitheloid membranes in monaxonid sponges. J. Exp. Zool. 9: 536–571.

Witting I., Braun H. P., Schägger H. 2006. Blue native Page. Nature Protocols **1**: 418-428.

Yahel G., Whitney F., Reiswing H. M., Medrano D. I., Leys S.P. 2003. In situ feeding and metabolism of glass sponges (Hexactinellida, Porifera) studied in a deep temperate fjord with a remotely operated submersible. Limnol. Oceanogr., 52(1): 428–440.

Yamada A., Tamori M., Iketani T., Oiwa K., Motokawa T., 2010. A novel stiffening factor inducing the stiffest state of holothurian catch connective tissue. J. Exp. Biol. 213: 3416-3422.

Yamada S., Sugahara K., Özbek S. 2011. Evolution of glycosaminoglycans: comparative biochemical study. Communicative & Integrative Biology 4: 150-158.

Zanetti G. 2002. Dinamismo strutturale nella spugna *Chondrosia reniformis* (Porifera, Demospongiae): osservazioni in habitat. Tesi di Laurea, University of Milan, Italy.

Zilberger C., Solè-Cava A. M., Klautau M. 2006. The extent of asexual reproduction in sponges of the genus Chondrilla (Demospongiae: Chondrosida) from the Caribbean and the Brazilian coasts. J. Exp. Mar. Biol. Ecol. 336: 211–220.